LOW COST, EFFICIENT, HYBRID SOLAR CELLS

Instituto de Ciencia Molecular

Universitat de València

Memoria presentada por Olga Malinkiewicz para aspirar al grado de Doctor en Nanociencia y Nanotecnología

Dirigida por:

Dr. Hendrik Jan Bolink

Dr. Hendrik Jan Bolink, Investigador de la Universidad de Valencia en el Instituto de Ciencia Molecular (ICMol) certifica que la memoria presentada por la licenciada Olga Malinkiewicz con el título "Low cost, hybrid solar cells" corresponde a su Tesis Doctoral y ha sido realizada bajo su dirección, autorizando mediante este escrito la presentación de la misma.

En Valencia, a 27 de abril del 2017

Dr. Hendrik Jan Bolink

TABLE OF CONTENTS:

RESUMEN EN ESPAÑOL……. 7

INTRODUCTION……..... 25

Cyanine dyes as donors …….…. 30

Hybrid organic-inorganic perovskite …….……. 33

BI-LAYER SOLAR CELLS BASED ON CATIONIC DYES …… 39

1. **Development of the lab-scale coating technique, for neat bilayer film formation……... 41**
2. **Devices …….. 46**
    a. **Solution processed devices …….. 47**
    b. **Partially evaporated devices …….. 48**
3. **Summary …….. 49**

PEROVSKITE SOLAR CELLS …… ……..... 61

1. **Development of perovskite evaporation technique ……..... 63**
2. **Devices ……... 68**
    a. **Device architecture …….…… 68**
    b. **Large area devices ……... 74**
    c. **Flexible and Semi-transparent cells …….. 74**
    d. **Radiative efficiency …….…… 74**
3. **Summary …….. 75**

GENERAL CONCLUSIONS……. 91

OUTLOOK …….. 95

LIST OF PUBLICATIONS ……... 101

REFERENCES …… 105

ACKNOWLEDGEMENTS……. 113

RESUMEN EN ESPAÑOL

RESUMEN EN ESPAÑOL:

Actualmente, existen diversas estrategias para producir energía limpia mediante fuentes renovables, pero es la explotación directa de la energía del Sol la que se presenta como una solución ideal, siendo la mayor fuente de energía verde en la Tierra. La potencia de la energía solar que llega a la Tierra cada año es del orden de 86000 TW (Terawatt, 10^{12} Watt). Esto representa 4800 veces la demanda energética anual del mundo, estimada en 18 TW. Además, todos los depósitos de energía fósil reconocidos (petróleo, carbón y gas) contienen todos juntos tan sólo una cantidad de energía equivalente a la recibida del Sol durante 56 días. Esta situación muestra claramente la necesidad de aprovechar esta gran reserva de energía limpia con el fin de satisfacer la creciente demanda energética del planeta.

Las tecnologías fotovoltáicas (FV), que convierten la energía del Sol directamente en electricidad, han sido desarrolladas desde hace muchos años. Al fin del año 2009, la capacidad FV instalada en el mundo fue mayor que 23 GW. En 2012, los 100 GW fueron alcanzados, y hacia el final de 2015 se instalaron 227 GW de FV a nivel global. Esta es una cantidad capaz de producir al menos 300 terawatts hora (TWh) de electricidad cada año, siendo un indicativo de la impresionante evolución de esta tecnología. El silicio cristalino es la principal tecnología FV que domina el mercado (87%). Sin embargo, la prevaleciente tecnología FV basada en silicio presenta inherentes desventajas que impiden la deseada inclusión de la energía solar en la vida cotidiana. Esta tecnología tan sólo puede ser implementada en forma de paneles rígidos, de gran área y con un coste relativamente alto, lo que limita su aplicación principalmente a granjas solares de nivel industrial y a tejados de edificios. Una alternativa es la tecnología de películas delgadas, la cual se basa en la deposición de capas extremadamente finas de materiales fotosensibles sobre sustratos de bajo coste como vidrio, acero inoxidable o plástico. Las células

solares de películas delgadas basadas en silicio y otros semiconductores inorgánicos (como por ejemplo los CIGS, CdTe), muestran una eficiencia de conversión de energía alta (PCEs), mayores a 20 %. Sin embargo, sufren de un costo de producción relativamente alto debido a las condiciones de procesamiento de las mismas. Este hecho motivó el desarrollo de nuevos tipos de células FVs, con potencial para reducir los costes de fabricación, siendo la fotovoltaica orgánica (FVO) el mejor ejemplo. Los dispositivos de FVO incorporan pequeñas moléculas orgánicas semiconductoras (basadas en carbono) o polímeros para convertir la energía solar incidente en electricidad. Estas tecnologías difieren significativamente de los dispositivos FVs inorgánicos en su principio de funcionamiento, como así mismo en sus métodos de producción. La FVO está basada en capas orgánicas delgadas con grosores del orden de decenas a centenas de nanómetros, pudiendo ser fabricadas mediante impresión, evaporación en vacío o mediante técnicas compatibles con *roll-to-roll*. Estas estrategias de producción tienen el potencial para la fabricación de dispositivos fotovoltaicos en masa y a bajo coste, lo que representa un contraste importante con respecto a la fotovoltaica basada en silicio cristalino la cual conlleva asociada un alto coste y un elevado consumo energético. La FVO puede ser fácilmente integrada en dispositivos electrónicos, incluso en textiles y otros elementos estructurales flexibles debido a sus métodos de producción. Una ventaja intrínseca que los semiconductores orgánicos ofrecen es que a través de ingeniería molecular es posible sintetizar materiales orgánicos con propiedades ópticas, eléctricas y mecánicas deseadas. Desde finales de los años ochenta, las eficiencias de las células solares orgánicas han ido creciendo constantemente desde menos de un 1 % hasta alrededor del 11 % hacia finales del 2015. La continua mejora en eficiencia ha sido principalmente motivada por un entendimiento más profundo de los principios físicos que gobiernan el funcionamiento de estas células, como así mismo al desarrollo de nuevas arquitecturas moleculares para una mayor eficiencia de conversión y a la

optimización de las nanoestructuras y su procesamiento. Las continuas mejoras en funcionamiento y la demostración del potencial de fabricación en grandes cantidades han posicionado a las FVO como un contendiente serio en lo que se refiere a las soluciones energética FVs del futuro.

La idea de utilizar moléculas orgánicas como materiales absorbentes de luz proviene de la simple observación de los sistemas fotosintéticos presentes en las plantas, los cuales usan sistemas moleculares para el almacenamiento de la luz y su conversión en energía química útil. Los primeros experimentos a comienzos del año 1958, consistieron en la incorporación de colorantes orgánicos bioinspirados como porfirinas, ftalocianinas, merocianinas o clorofilas, entre dos capas metálicas con una función de trabajo alta. Estas primeras células solares no excedieron eficiencias del 1 %. Una importante contribución fue introducida para Ching W. en 1968 mediante la publicación de un trabajo en el que se describía un diseño de dos capas exhibiendo una eficiencia de conversión de energía de alrededor del 1%. Las propiedades fotovoltaicas de este dispositivo estaban determinadas por la interfaz entre dos materiales orgánicos evaporados térmicamente, uno de ellos absorbiendo luz y generando un estado excitado como donante de electrones y el otro actuando como un aceptor capaz de atraer los electrones fotoexcitados. Este principio de operación basada en la transferencia de carga fotoinducida entre donante y aceptor es el mecanismo fundamental presente en todas las subsecuentes células solares orgánicas. El diagrama correspondiente a la formación de un excitón y el proceso de extracción de carga común en todas las células solares orgánicas y ejemplos de laboratorio de células solares flexibles se halla representado en la figura 1 de esta tesis.

El siguiente desarrollo importante en el campo de la FVO tuvo lugar en 1992, cuando Sariciftci et al. descubrieron la transferencia de carga altamente eficiente entre un polímero

semiconductor y un fullereno de tipo Buckminster (C_{60}), siendo este último el más prominente aceptor de electrones empleado actualmente en el campo de la FVO. Este avance sentó las bases para la fabricación en grandes cantidades de células solares orgánicas mediante procesos basados en disolución (tales como *roll-to-roll*). El fullereno C_{60} puede ser evaporado térmicamente para la fabricación de células solares basadas en procesos en vacío. Por otro lado, para su procesamiento en disolución, el C_{60} debe ser derivatizado debido a su baja solubilidad. El más popular de estos derivados es el PCBM ([6,6]-phenyl C61-butyric acid methyl ester). Estas dos estrategias de procesamiento representan así mismo la demonstración seminal de los dos tipos de tecnologías FVOs más exitosas en la actualidad: células solares orgánicas evaporadas en vacío y células solares orgánicas de tipo fullereno-polímero preparadas mediante procesos en disolución.

Colorantes basados en cianinas como donantes en FVO

Los colorantes basados en cianinas son una clase interesante de materiales para aplicaciones en FV, principalmente debido a su alto coeficiente de absorción y a su bajo coste. Estos sistemas no son nuevos para la industria, puesto que fueron utilizados y siguen aplicándose hasta la fecha para incrementar el rango de sensibilidad de emulsiones fotográficas y como absorbentes en soportes CD-R y DVD-R, proveyendo sus colores azules y verdes característicos. Recientemente, estos colorantes encontraron aplicación en biotecnología (etiquetado, análisis) y en dispositivos opto-electrónicos. En los colorantes basados en cianinas, las transiciones ópticas ocurren típicamente en el rango de pocos eV, solapándose adecuadamente con el espectro solar. El ancho de banda del espectro de absorción de las cianinas es menor en comparación con los semiconductores inorgánicos (figura 2 de esta tesis doctoral). Aunque una banda de absorción estrecha es una desventaja en términos de almacenamiento de flujo solar, múltiples absorbentes apilados y conectados en serie pueden ser diseñados para expandir el

rango de absorción. Los niveles de energía de las cianinas pueden ser fácilmente modificados mediante la elección de la longitud del puente de polimetino, puesto que su *bandgap* puede ser disminuido mediante el incremento del número de enlaces doble, desplazando así la absorción hacia longitudes de onda más largas.

Aparte de sus excelentes coeficientes de absorción, los colorantes basados en cianinas tienen conductividades decentes permitiendo el transporte de carga en las capas orgánicas. Sus conductividades electrónicas provienen de una carga deslocalizada en el puente de polimetino entre dos átomos de nitrógeno (ilustrado en la figura 3 de esta tesis doctoral). Los portadores de carga se desplazan mediante un mecanismo de *hopping* entre estados localizados. Las movilidades de estos portadores de carga son por tanto bajas, con valores típicos menores a 10^{-5} cm^2/Vs. Esta baja movilidad de los portadores de carga establece una limitación en el grosor de las capas activas que pueden ser utilizadas en una célula solar, debido a una mayor pérdida por recombinación al incrementar dichos grosores. Es particularmente interesante que las cianinas son conductores iónicos intrínsecos en términos de conductividad. Cada molécula de colorante basado en cianina es acompañada por un contra ion móvil. Estos iones pueden difundirse, por ejemplo, hacia las capas adyacentes construyendo así un importante espacio de carga capaz de alterar los niveles de energía en las hetero-uniones.

En este contexto, los dispositivos basados en una arquitectura plana y simple son la mejor plataforma para investigar y entender los mecanismos de funcionamiento de este tipo de sistemas. En estas arquitecturas, huecos y electrones son separados espacialmente reduciendo al mínimo la probabilidad de recombinación en el dispositivo. Mientras que las células de Tang fueron preparadas mediante métodos de evaporación, los colorantes basados en cianinas son sales que no pueden ser evaporadas. Por otro lado, las capas preparadas mediante deposición desde disolución tales como *spin-coating* no garantizan una uniformidad suficiente para la

creación de interfaces bicapa de alta calidad. El estrés inducido por las fuerzas de rotación genera una uniformidad pobre en los bordes de las muestras, con un impacto directo en la uniformidad del grosor de las capas. Adicionalmente, una alta cantidad de disolución precursora sobre el sustrato y las fuerzas de cizalladura pueden alterar la planaridad de las interfaces fabricadas.

El primer objetivo de esta tesis doctoral fue el desarrollo de una técnica de recubrimiento desde disolución, a escala de laboratorio, para la fabricación de bicapas de alta calidad, denominada técnica de recubrimiento de menisco. El recubrimiento de menisco puede ser una alternativa atractiva al método de *spin-coating* por numerosas razones. En primer lugar, debido al uso de cantidades extremadamente pequeñas de disolución precursora. Además, esta técnica garantiza una escalabilidad directa de los resultados obtenidos en el laboratorio mediante el empleo de *slot-die coaters* industriales, como así mismo una buena uniformidad de las capas orgánicas en grandes áreas. En particular, presenta una serie de características interesantes para el sector académico que no son proporcionadas por el método de *spin-coating* tradicional. Un ejemplo de ello es el control que puede ser alcanzado en el gradiente de grosores de las muestras. A pesar de todas estas ventajas, hay pocos trabajos publicados empleando la técnica de recubrimiento de menisco en electrónica orgánica. El acceso a la teoría de esta interesante técnica se encuentra limitada en comparación con otras tecnologías de recubrimiento más ampliamente desarrolladas. La implementación de esta técnica fue extremadamente exitosa para la deposición de materiales de bajo peso molecular (tales como el [6,6]-phenyl C61-butyric acid methyl ester (PCBM)), generando dispositivos con un funcionamiento superior en comparación con aquellos preparados mediante la técnica de *spin-coating*. El recubrimiento por menisco fue implementado exitosamente en varias células solares

con bicapas de alta calidad de aceptores basados en fullerenos y donantes basados en colorantes de cianina.

El control sobre el espacio de carga iónico permite la regulación del flujo de carga electrónica y la implementación de funcionalidades únicas en dispositivos opto-electrónicos orgánicos. **Por lo tanto, el segundo objetivo de esta tesis doctoral, fue el estudio de la influencia de los iones en el funcionamiento de las células solares basadas en cianinas.** Fue demostrado que los iones móviles tienen un gran impacto en la energética de las células solares.

Perovskitas híbridas orgánicas-inorgánicas

Mientras que la FVO puede presentar ventajas en lo que se refiere a su costo, abriendo así un amplio rango de excitantes posibilidades (tales como variedad de colores o semi-transparencia), también tiene desventajas tales como su pobre estabilidad térmica y mecánica. Adicionalmente, mientras que el transporte eléctrico en materiales orgánicos ha mejorado en los últimos veinte años, la movilidad se encuentra fundamentalmente limitada por las débiles interacciones de van der Waals entre las moléculas orgánicas (en contraposición con las más intensas fuerzas iónicas y covalentes halladas en los sistemas inorgánicos extendidos). Además, nuevamente debido a la limitada extensión de los orbitales en las moléculas orgánicas, la energía de unión de los excitones es mayor que la energía térmica, lo que conlleva que sólo puedan disociarse en cargas libres en una interfaz donante-aceptor. Dicha interfaz donante-aceptor requiere un offset en la energía de los niveles de los orbitales de estas moléculas lo que consume parte de la energía potencial disponible en el sistema. Por contra, debido a sus orbitales o bandas extendidas, los semiconductores inorgánicos tienen una menor energía de unión en los excitones, en comparación con la energía térmica a temperatura ambiente, lo que supone que pueden ser fácilmente disociados en cargas libres manteniendo una energía potencial alta. Por lo tanto, las

eficiencias halladas en la FVO son significativamente menores en comparación con las células inorgánicas.

Lo que parece ser una solución ideal es un material que combine la robustez y la alta eficiencia de las células solares inorgánicas con el fácil procesamiento y bajo coste de producción de los materiales orgánicos. Algo que parecía poco probable de suceder, se hizo recientemente realidad con el redescubrimiento de las perovskitas basadas en haluros como importantes absorbentes en células solares. Las perovskitas híbridas orgánica-inorgánicas ofrecen una combinación inusual de buena solubilidad en un rango amplio de disolventes polares comunes con unas características semiconductoras apropiadas. En los últimos tres años, el funcionamiento de las células basadas en perovskita ha mejorado rápidamente hasta alcanzar eficiencias tan altas como 22.1 %, siendo reportada recientemente por el Korea Reseach Institute of Chemical Technology (KRICT) en colaboración con la Ulsan National Institute of Science and Technology (UNIST). En este contexto, otro resultado muy importante en el campo fue publicado por el grupo del profesor M. Grätzel de la EPFL (Suiza), en el cual se mostraron células con una eficiencia de conversión de energía solar a electricidad (PCE) de hasta 21.1 % con un nivel de reproducibilidad record. Dichas células fueron fabricadas mediante una arquitectura n-i-p empleando una formulación de perovskita basada en la mezcla de cationes.

Las propiedades únicas de las perovskitas basadas en haluros provienen de la combinación de constituyentes orgánicos e inorgánicos en un solo sistema, en forma de un *composite* a escala molecular. Esta característica en las perovskitas híbridas permite superar las limitaciones cuando los dos tipos de materiales son utilizados por separado. Por ejemplo, los materiales inorgánicos (típicamente caracterizados por interacciones iónicas y covalentes) ofrecen el potencial para una movilidad electrónica alta, un amplio rango de *band gaps*, una sustancial resistencia mecánica y una estabilidad térmica remarcable. Por otra parte, las moléculas

orgánicas que generalmente interactúan a través de interacciones más débiles (puentes de hidrógeno e interacciones de Van der Waals), proporcionando la posibilidad de una diversidad estructural, altos coeficientes de absorción en los rangos de longitud de onda del visible, propiedades mecánicas plásticas y bajas temperaturas de procesamiento.

En las pervoskitas basadas en haluros, todos estos aspectos son combinados en un solo material híbrido que durante su deposición (por ejemplo, mediante *spin-coating* o co-evaporación) forman sistemas cristalinos auto-ensamblados. Los cristales tienen la ventaja adicional de que pueden ser caracterizados estructuralmente mediante difracción de rayos X (DRX), dando la posibilidad de correlacionar las características estructurales con unas propiedades específicas en el material. Por lo tanto, las medidas de DRX son una herramienta muy útil para el desarrollo y optimización de estos materiales.

Las perovskitas basadas en haluros no son materiales nuevos en el campo de la opto-electrónica. A finales de los años noventa, fueron extensivamente estudiadas en los laboratorios de IBM por David Mitzi como un material activo para diodos y transistores. Sin embargo, debido a su inestabilidad frente a la humedad no fueron consideradas como materiales viables para FV. En células solares fueron utilizadas relativamente tarde, en 2009. Un grupo japonés, liderado por el Prof. Miyasaka, fue el primero en emplear perovskitas basadas en $CH_3NH_3PbI_3$ desde disolución, como un sensibilizador en estructuras mesoscópicas de dióxido de titanio (TiO_2) en arquitecturas DSSC, alcanzando una PCE de 3.8%. Desafortunadamente, estas células sufrían de importantes problemas de estabilidad. El electrolito líquido (empleado como transportador de huecos), actuaba disolviendo la perovskita y produciendo así una rápida degradación de las células. Tres años más tarde, la eficiencia de las células solares basadas en perovskita fueron dramáticamente mejoradas por el grupo del Prof. Kanatzidis. En sus trabajos emplearon una perovskita basada en estaño ($CsSnI_3$) en sustitución del electrolito líquido. Este trabajo supuso

el primer ejemplo de una arquitectura DSSC sólida estable, con eficiencias mayores al 10%. Un gran avance tuvo lugar poco después cuando el equipo de la Universidad de Oxford liderado por el Prof. Henry Snaith, inspirándose en el trabajo del Prof. Miyasaka, reemplazó en electrolito líquido por un polímero sólido (spiro-OMeTAD), eliminando la causa de la rápida degradación de las células de perovskita de Miyasaka. Adicionalmente, el concepto de haluros mezclados (combinando iones de ioduro y cloruro) fue empleado por primera vez, incrementando la formación de las capas y la estabilidad del material bajo iluminación constante. Las células fueron preparadas completamente a partir de métodos de disolución, alcanzando eficiencias de alrededor del 10 % en uno de los primeros intentos. La perovskita basada en plomo $CH_3NH_3PbI_3$ no requirió dopaje (como en las células de Kanatizidis) y demostraron ser un excelente conductor de electrones. Este resultado supuso un tremendo éxito, lo que atrajo la atención de la comunidad científica hacia la investigación de este tipo de células solares.

Con respecto a la preparación de este material, las perovskitas laminadas son fácilmente preparadas mediante *spin-coating* desde disolución debido a su solubilidad en disolventes orgánicos convencionales tales como gamma-butirolacton (GBL) o dimetilformamida (DMF), entre otros. Mediante *spin-coating* desde disolución, es posible la preparación de capas delgadas de perovskitas laminadas con buenas propiedades ópticas y ordenación estructural. Esta excelente procesabilidad ha sido empleada para la fabricación de capas delgadas de perovskita de alta calidad aplicables en electrónica y dispositivos ópticos. Sin embargo, la técnica de *spin-coating* presenta dificultades a la hora de ofrecer un control preciso en el grosor de las capas como así mismo en su morfología. Además, esta técnica no es compatible con estrategias basadas en procesos en seco para la fabricación de capas semiconductoras y dispositivos en condiciones de vacío. **Por tanto, el tercer objetivo de esta tesis doctoral fue**

el desarrollo de una estrategia para la preparación de capas de perovskita, proveyendo no sólo un control preciso en el grosor de las mismas sino también exhibiendo una buena compatibilidad con un procesado en vacío. En el contexto de esta tesis, el trabajo se enfocó en el desarrollo de un método de crecimiento auto-organizado de capas de perovskita laminadas, denotado como método de deposición en vacío. La co-evaporación de diferentes precursores fue empleada con el fin de obtener capas delgadas de perovskitas del tipo $CH_3NH_3PbI_3$ (MAPI). Esta técnica es por ejemplo utilizada ampliamente en la fabricación de pantallas OLED y en FVO, donde las capas activas consisten de más de un componente (Alq_3 y NPB como ejemplos). En la técnica de co-evaporación, el grosor de la capa puede ser modificado desde unos pocos nanómetros hasta un micrómetro con una precisión del orden de 5 nm, siendo preciso la utilización de condiciones de alto vacío. Otra ventaja del proceso de evaporación con respecto al procesado desde disolución es la capacidad de preparar capas multi-apiladas de películas delgadas en grandes áreas. El proceso de evaporación dual de perovskita es compatible con un procesado seco, como el empleado en la preparación de películas semiconductoras y dispositivos en vacío. Aunque finalmente una célula de multi-unión formada íntegramente por perovskita debería ser accesible, las células solares basadas en perovskita han alcanzado actualmente funcionamientos que son suficientes para incrementar las eficiencias absolutas de células de silicio altamente cristalino y aquellas basadas en (di)selenurio de indio y galio. Adicionalmente, debido a que la deposición desde vapor de las capas de perovskita es totalmente compatible con métodos de procesamiento convencionales para la fabricación de células solares de silicio, la infraestructura necesaria para la escalabilidad de este proceso ya se encuentra disponible. Además, el alineamiento del *bad gap* en perovskitas híbridas proporciona una oportunidad para fabricar células en tándem de perovskita/silicio y perovskita/CIGS con eficiencias mejoradas. En este sentido, la co-evaporación puede

potencialmente permitir la fabricación de este tipo de dispositivos en un sólo proceso, en base al hecho de que la deposición en vacío es comúnmente utilizada en el campo de las tecnologías fotovoltaicas con capas delgadas. La co-evaporación de perovskitas híbridas orgánica-inorgánicas fue extensivamente estudiada y desarrollada, desembocando en la formación de películas altamente reproducibles, cristalinas y compactas. El uso de esta técnica permitió la preparación de dispositivos en grandes áreas, logro que fue descrito por la revista Nature Photonics como "un significativo *milestone* en la investigación de la fotovoltaica basada en perovskita". Aunque pueden ser potencialmente ligeros y flexibles, hasta la fecha la mayoría de las células solares altamente eficientes basadas en este material hacen uso de una capa compacta de TiO_2, la cual requiere de procesos de sinterización con altas temperaturas (alrededor de 500 ºC). Este hecho se traduce en un proceso de fabricación más complejo que excluye las aplicaciones que hacen uso de sustratos flexibles. Como consecuencia, estrategias de producción tales como el *roll-to-roll* (R2R) resultan irrealizables, siendo este método una de las potenciales ventajas e interés en términos de la transferencia de esta tecnología al ámbito industrial. Adicionalmente, el empleo de TiO_2 estaría fuertemente ligado a la aparición de efectos de histéresis, uno de los principales problemas de las células solares basadas en perovskita. **Considerando todo esto, el objetivo final de esta tesis doctoral fue el desarrollo de una arquitectura de dispositivo basado en perovskita libre de óxido, el cual no muestre histéresis y sea compatible con sustratos flexibles.**

Capas de pervoskita fueron intercaladas entre dos transportadores de carga delgados, poliarilamina (poly-TPD, material tipo-p) y [6,6]-phenyl C61-butyric acid methyl ester (PCBM, material tipo-n). Esta novedosa arquitectura libre de óxido presenta eficiencias tan altas como los dispositivos estándar basados en TiO_2. Debido a que el proceso de fabricación no requiere de altas temperaturas de sinterización es totalmente compatible con el empleo de sustratos

flexibles. Una excelente calidad en las capas de perovskita y la eliminación de la capa de óxido conllevan una desaparición del efecto de histéresis. La combinación de un excelente control en las capas y una reproducibilidad alta presente en una arquitectura simple permitió diversos estudios de interés, entre los que se pueden citar:

- Influencia de diferentes materiales transportadores de electrones y de huecos en el funcionamiento de los dispositivos,
- Comparación de electrodos con diferentes funciones de trabajo,
- Efecto del grosor de la capa de perovskita,
- Eficiencia radiativa de las células de perovskita.

Fue así mismo posible la descripción de los efectos sobre la eficiencia de la célula asociados a un incremento del área activa. Este trabajo desembocó en la producción de una patente de aplicación (nº EP13183813), como así mismo a la publicación de numerosos artículos y contribuciones a conferencias internacionales.

Conclusiones

En vista de las bajas eficiencias obtenidas en células basadas en cianinas (en comparación con aquellas basadas en perovskita), es posible predecir que este tipo de sistemas no llegarán a desempeñar un rol importante dentro del sector energético. Sin embargo, los estudios en este tipo de células tales como los movimientos iónicos dentro del dispositivo o el posible origen de la forma en S de las curvas de medida, pueden ser directamente transferibles al campo de las perovskitas. En general, un incremento tan elevado de las eficiencias en células solares de perovskita no hubiera sido posible sin los estudios previos llevados a cabo en células orgánicas y del tipo DSSC. Todo lo desarrollado durante décadas para las células orgánicas y DSSC, aceleró significativamente el proceso de evolución de las células de perovskita. No es una coincidencia que la línea asociada a las perovskitas en la gráfica del NREL sea casi una

continuación de la asociada a células orgánicas y DSSC. Tanto la síntesis como el estudio de diferentes materiales transportadores de carga, así mismo como el desarrollo y descripción de los mecanismos de transporte de carga para este tipo de dispositivos, fueron transferidos al campo de las perovskitas, resultando en la obtención de eficiencias récord mayores al 20% en tan sólo pocos años. Este ejemplo muestra claramente que existe todavía un nicho (y una necesidad) para el estudio de nuevos materiales como los colorantes basados en cianina y su correspondiente desempeño en células solares orgánicas. El conocimiento adquirido en estos sistemas simples puede ser más tarde empleado para un mejor entendimiento de sistemas más complejos tales como los basados en perovskita.

Si bien se posicionan como clara candidata para revolucionar el campo de la FV, la tecnología basada en perovskita se encuentra limitada esencialmente por dos factores, que requieren de una mayor dosis de esfuerzo en investigación, antes de que pueda ser aplicada en el mercado: estabilidad y contenido en plomo. La perovskita más comúnmente utilizada con fórmula $CH_3NH_3PbI_3$ presenta una tendencia a descomponerse bajo exposición a la humedad, en ioduro de plomo y ioduro de metilamonio principalmente, perdiendo las propiedades opto-electrónicas. Adicionalmente, dicha degradación es acelerada por la exposición a la luz y al oxígeno, como así mismo al tratamiento térmico. Los problemas relacionados con la degradación de las perovskitas y la estabilidad de las células basadas en las mismas deben de ser urgentemente abordados con el fin de obtener largos tiempos de vida con altas eficiencias, que garanticen la transferencia de esta tecnología desde el laboratorio a la industria. Una de las estrategias prometedoras para subsanar este problema es la basada en el diseño composicional de las perovskitas. Recientemente, formulaciones con mezclas de cationes empleando formamidina (FA) y cesio (Cs) mostraron mejoras prometedoras en este campo. El catión de formamidina, debido a su mayor tamaño comparado con el metilamonio, y al combinarse con

un elemento inorgánico como el cesio desembocaron en la mejora significativa de las estabilidades frente a luz y humedad de las capas. Células solares empleando la formulación $Cs_{0.05}$ $(MA_{0.17}$ $FA_{0.83})_{0.95}$ $Pb(I_{0.83}Br_{0.17})_3$ alcanzaron una PCE estable del 21.1 % con una excelente estabilidad a largo plazo operando durante 250 horas.

Por otro lado, la estabilidad de la perovskita puede ser garantizada mediante la encapsulación. Introduciendo una capa adicional con propiedades de barrera (por ejemplo, Al_2O_3) puede efectivamente protegerse las capas de perovskita sensibles a la humedad, extendiendo el tiempo de vida de los dispositivos.

En lo que se refiere al bajo coste de la tecnología, este punto es cuestionable si una estabilidad de larga duración es requerida. Sin embargo, tras su uso estos dispositivos baratos pueden ser reemplazados por otros nuevos. En este sentido, el impacto en el medioambiente se establece como una de las mayores limitaciones.

La perovskita MAPI contiene una fracción significativa de plomo, correspondiendo a alrededor de 0.35 g/m^2 para capas con un grosor de 300 nm. Mediante unos apropiados procesos de sellado y reciclaje tras la vida útil, módulos solares basados en este material son previsibles. Ha sido demostrado que el plomo proveniente de dispositivos degradados puede ser recuperado y empleado en la producción de nuevas células solares basadas de perovskita. Otra solución posible para subsanar esta problemática es el reemplazo del Pb, siendo esta opción la más deseado con diferencia. De hecho, el empleo de perovskitas con Pb es problemático bajo la actual legislación de la UE, pudiendo ser este un factor limitante en la futura comercialización y aceptación pública de este producto. Algunas pruebas han sido llevadas a cabo para la fabricación de dispositivos libres de plomo. La primera prueba de reemplazamiento de plomo en perovskitas fue llevado a cabo con estaño (Sn). Los dispositivos basados en esta estrategia alcanzaron eficiencias de alrededor del 5.73 %. Sin embargo, la perovskita basada en estaño es

altamente inestable debido a la tendencia del Sn^{2+} a oxidarse en Sn^{4+}. Otra desventaja de esta estrategia es el hecho de que los compuestos de estaño no son tampoco inertes para la salud humana, presentado niveles similares de toxicidad.

Mientras la mayoría de la comunidad está enfocada en el contenido de plomo, existe otro aspecto igualmente importante. La producción de materiales de perovskita en grandes áreas requerirá de una tecnología basada en disolución con el fin de ser viable para su comercialización. El procesamiento en disolución actual emplea disolventes que no son ecológicos que muestran un potencial peligro para la salud humana como el DMF o tóxicos como los basados en clorinas. En este sentido, su utilización a gran escala se encuentra simplemente excluido.

INTRODUCTION

INTRODUCTION:

Nowadays, there are a few approaches to produce clean energy from renewable sources, but what seems almost like an ideal solution is the direct exploitation of the sun's energy, which is the greatest source of clean energy for the Earth. The power of the Sun's energy reaching the Earth every year is around 86 000 TW (Terawatt, 10^{12} Watt). This is about 4800 times more than the current world's yearly demand for energy, estimated to be 18 TW[1]. Furthermore, all of the recognized fossil fuel deposits (oil, coal and gas) contain altogether only as little energy as the one that reaches the Earth from the Sun within 56 days. This situation clearly shows the need of taking profit of this big reservoir of clean energy in order to fulfil Earth's rising energy demand.

Photovoltaics (PV) technologies, which convert Sun's energy directly into electricity, have been developed since many years. At the end of 2009, the world's cumulative installed PV capacity was more than 23 GW. In 2012, the 100 GW mark was reached and by the end of 2015 , 227 GW of PV had been installed globally — an amount capable of producing at least 300 terawatt hours (TWh) of electricity every year,[2] which is an indication of the impressive evolution of this technology. Crystalline silicon is the main PV technology that dominates the market (87%). However, the currently prevailing silicon PV technology has inherent drawbacks that prevent it from desired widespread application of solar power in everyday life. The dominating PV technology can only be implemented as rigid, large-area, relatively costly panels, which limits its application primarily to industrial-level power farms and on-the-roof panels. An alternative is Thin Film technology, which is made by depositing extremely thin layers of photosensitive materials onto a low-cost backing such as glass, stainless steel or plastic. Thin film solar cells based on silicon and other inorganic semiconductors (like for expample CIGS, CdTe) exhibit high power conversion efficiencies (PCEs) of >20%[3] but they suffer from relatively high production cost due to tedious processing conditions.

This triggered the development of new types of PV cells, having the potential to radically diminish manufacturing costs, being organic photovoltaics (OPVs) the best example. OPV devices are made of organic (carbon-based) semiconducting small molecules or polymers for converting incident sunlight into electrical power. They differ significantly from inorganic photovoltaic (PV) devices in the physical principles of their operation, as well as in their methods of production. OPVs are based on organic thin films of tens to a few hundreds of nanometers and can be fabricated using printing, vacuum evaporation, and roll-to-roll compatible techniques. These fabrication strategies offer the potential for ultra-low cost mass-producible photovoltaic devices[4,5]. This is in contrast with the costly and energy-intensive fabrication of traditional crystalline silicon-based photovoltaics. OPV can be easily integrated into consumer electronics devices, even textiles and other mechanically flexible structural elements due to their production methods. An intrinsic advantage that organic semiconductors offer is that through molecular engineering, organic materials with custom-tailored optical, electrical, and mechanical properties can be synthesized. Since the late 1980s, organic solar cell efficiencies have consistently risen from <1% to around 11% as of the end of 2015. The continuous improvement of efficiency has been driven by a deeper understanding of the physics governing the operation of OPVs, as well as to the development of new molecular architectures for more efficient solar energy conversion and the optimization of nanostructures and processing. With continued performance improvements and successful demonstrations of high-volume production, OPV is now being accepted by many as a serious contender in future PV energy solutions. The inspiration of using organic molecules as light absorbing materials comes from the simple observation of photosynthetic systems in plants which use molecular systems to harvest light and convert it into useful chemical energy[6]. Early experiments, starting in 1958, focused on sandwiching bio-inspired organic dyes such as porphyrins, phthalocyanines[7], merocyanines[8] or chlorophylls[9,10] between two metals with a large work function offset. These

early cells did not exceed efficiencies of 1%. A significant breakthrough came in 1986, when Ching W. Tang published a 2-layer design demonstrating a power conversion efficiency of about 1%[11].The photovoltaic properties of this device were determined by the interface between two thermally evaporated organic materials, one absorbing light and generating an excited state as electron donor and the other acting as an acceptor pulling away the photoexcited electron. This donor-acceptor photoinduced charge transfer principle is the fundamental mechanism that all subsequent organic solar cell designs relied on. The scheme of the exciton formation and charge extraction process that is common to all organic cells and laboratory examples of flexible solar cell is depicted in Figure 1.

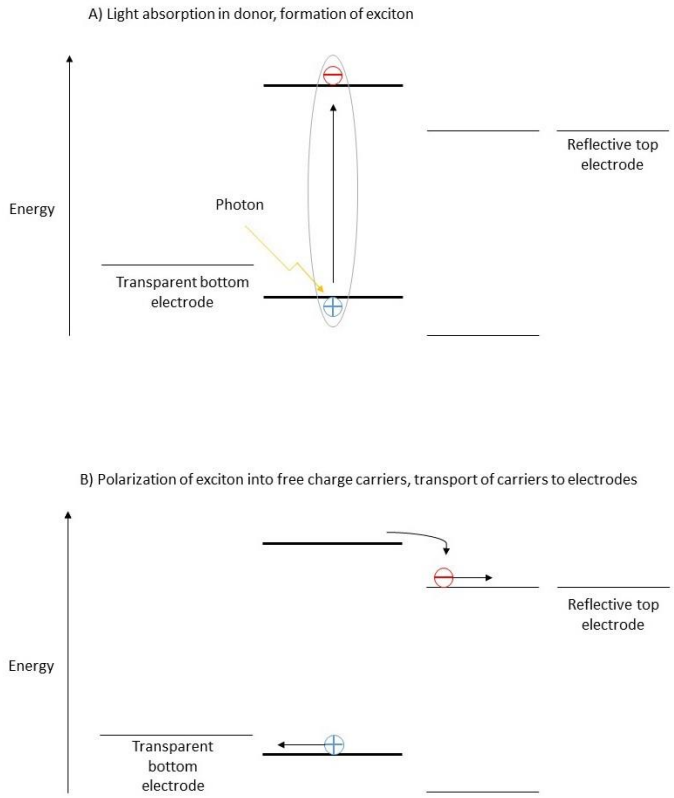

Figure 1 ***Schematics of the donor-acceptor photoinduced charge transfer mechanism.***

The next important development in the OPV story came in 1992, when Sariciftci et al. discovered the highly efficient photoinduced charge transfer between a semiconducting

polymer and Buckminsterfullerene (C_{60})[12], being the most prominent electron acceptor used in OPVs nowadays. This step paved the way for high-volume solution-processable (as roll-to-roll) organic solar cells. The C_{60} fullerene can be readily thermally evaporated for vacuum-processed cells. On the other hand, for solution processing C_{60} must be derivatized due to its limited solubility. The most popular of such derivatives is PCBM ([6,6]-phenyl C61-butyric acid methyl ester).

These two processing strategies also represent seminal demonstrations of the two distinct types of OPV technologies that are most successful today: vacuum-processed evaporated organic solar cells and solution-processed polymer-fullerene organic solar cells.

Cyanine dyes as donors for OPV

Cyanine dyes are an interesting class of materials for photovoltaic applications, mainly due to their high absorption coefficient and low-cost[13]. They are not new to industry, as they were used and still applied up to the date, to increase the sensitivity range of photographic emulsions and as absorbers in CD-R and DVD-R media, providing their characteristic bluish and greenish colour[14]. More recently these dyes found applications in biotechnology (labelling, analysis) and in optoelectronic devices[15,16]. In cyanine dyes, optical transitions are typically in the range of few eV, which overlaps well with the solar spectrum. The absorption spectrum bandwidth of cyanines is narrower when compared to conventional inorganic semiconductors (Figure 2).

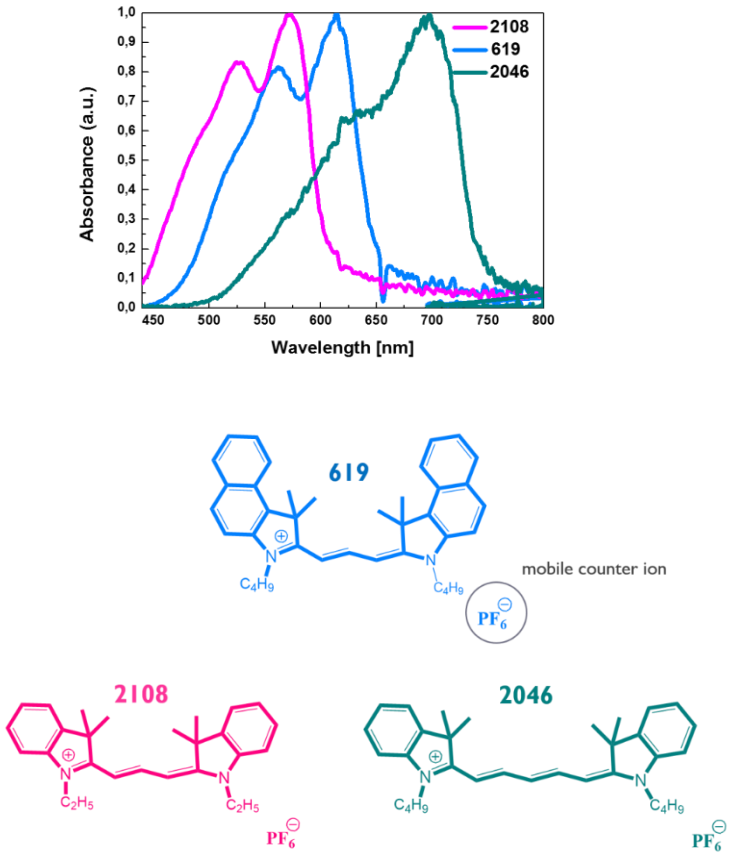

Figure 2 Absorption spectra of the cyanine dyes and their corresponding chemical structures.

Although a narrow absorption band is a disadvantage in terms of harvesting solar flux, multiple absorbers in stacks connected in series can be engineered to expand the absorption range. The energy levels of the cyanines can be easily tuned by a choice of the polymethine bridge length as their bandgap can be decreased with increasing the number of double bonds, shifting the absorption towards longer wavelengths.

Apart from the excellent absorption coefficients, cyanine dyes have decent conductivities which allow charge transport within the organic layer. Their electronic conductivity arises from a delocalized charge on the polymethine bridge between two nitrogen atoms as it is conceptually shown on figure 3[17].

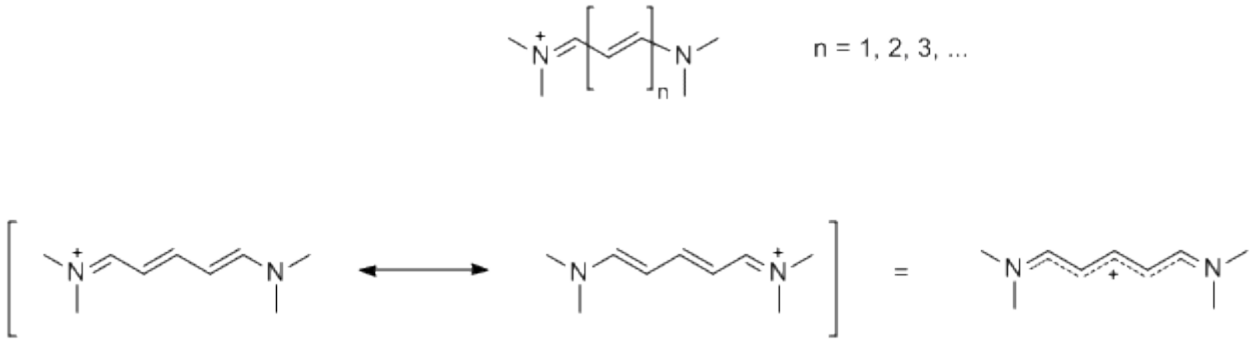

Figure 3 Polymethine bridge between two nitrogen atoms with delocalized charge.

Charge carriers move around by a hopping mechanism between localized states. The charge-carrier mobilities are, therefore, inherently low, with typical values of $<10^{-5}$ cm^2/Vs[5,18]. This low charge-carrier mobility puts a constraint on the thickness of the active layer that can be used in a solar cell, due to a higher recombination loss when increasing the layer thickness. What is particularly interesting about cyanine dyes is that, in terms of conductivity, they are intrinsic ionic conductors[19,20]. Each molecule of the cyanine dye is accompanied by a mobile counter ion. These ions can diffuse, for example, into adjacent layers and build up important space charge that alters energy levels at heterojunctions[21,22].

In this context, simple and planar device architectures are the best platforms for investigating and understanding the working mechanisms of this type of devices[23]. In these architectures, holes and electrons are spatially separated from each other and recombination probability within the device is reduced to minimum. While Tang's cells were prepared by evaporation method,[23] cyanine dyes are salts and cannot be evaporated. On the other hand, layers prepared by wet solution-coating processes such as spin-coating does not guarantee sufficient uniformity of the films to create neat bi-layer interfaces. The stress induced by the spinning motion causes poor uniformity on the edges of the samples, with a direct impact on the uniformity of the layer thickness over the substrate. Additionally, a large amount of precursor solution on the substrate and the sheering forces may alter the planarity of the fabricated interfaces.

The first objective of the Thesis is to develop a lab-scale coating technique, for neat bilayer preparation from solution, referred as meniscus coating technique[24]. The control over the ionic space charge allows the regulation of the flow of electronic charge carriers and the implementation of unique functionalities to organic optoelectronic devices. **Hence, the second objective of the thesis, is to study the influence of the ions on the cyanine solar cell performance.**

Hybrid organic-inorganic perovskites

Whilst organic photovoltaics may have cost advantages opening up a wide range of other exciting possibilities (like variety of colours or semi-transparency), they also have their drawbacks, such as poor thermal and mechanical stability[4]. In addition, while the electrical transport in organic materials has improved over the last twenty years, the mobility appears to be fundamentally limited by the weak van der Waals interactions between organic molecules (as opposed to stronger covalent and ionic forces found in extended inorganic systems)[25]. Additionally, again due to the limited extension of orbitals in organic molecules the exciton binding energy is much higher than the thermal energy, implying they can only dissociate in free carriers at a donor accepter interface. Such a donor-accepter interface requires an offset in energy levels of the orbitals of these molecules which takes up part of the available potential energy of the system. In contrast inorganic semiconductors, due to the extended orbitals or bands, have a exciton binding energy lower than the thermal energy at room temperature which implies that they are readily dissociated in free carriers maintaining the high potential energy. Hence the efficiency of OPV is significantly reduced comparing to inorganic cells.

What seems to be an ideal solution is the material that would combine robustness and high efficiency of inorganic solar cells, together with easy processing and low manufacturing costs of organic materials[26]. Something that would seem unlikely to happen, recently became reality

with the halide perovskite re-discovery as a great absorber in solar cells[27–29]. Hybrid organic-inorganic perovskites offer an unusual combination of good solubility in a wide range of common polar solvents and desirable semiconducting characteristics[26,30,31]. In the three years since, the performance of perovskite-based solar cells has improved rapidly to reach efficiencies as high as 22.1 %, being recently reported by the Korea Research Institute of Chemical Technology (KRICT) in collaboration with the Ulsan National Institute of Science and Technology (UNIST)[3]. In this context, another very remarkable result was published by the group of Prof. M. Grätzel at EPFL (Switzerland) where cells with solar-to-electrical power conversion efficiency (PCE) up to 21.1 % and record-level reproducibility were fabricated in a n-i-p architecture with a triple mixed cation perovskite formulation[32].

The unique properties of the halide perovskites arise from combining organic and inorganic constituents in one, single molecular-scale composite (figure 4) [33,34]. This feature in hybrid perovskite allows to overcome the limitations when the two kinds of materials are used separately. For example, inorganic materials (typically characterized by covalent and ionic interactions) offer the potential for high electrical mobility, a wide range of band gaps, substantial mechanical hardness, and thermal stability. On the other hand, organic molecules which generally interact through weaker interactions (hydrogen bonding and van der Waals interactions) provide the possibility of structural diversity, high absorption coefficients in visible wavelength range, plastic mechanical properties and low temperature processing.

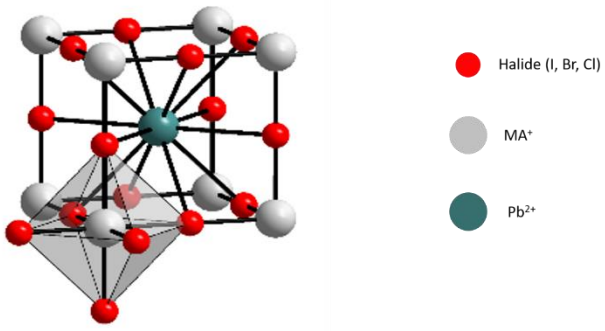

Figure 4 The structure of hybrid perovskite

In halide perovskites, all of these aspects are combined in one hybrid material which during deposition (e.g. by spin-coating or co-evaporation) form self-assembled, crystalline systems[26]. Crystals have the additional advantage that can be structurally characterized using X-ray technique, giving the possibility to correlate structural features with a specific material properties. Thus, XRD measurement is a very useful tool for the development and optimization of this material.

Halide perovskites are not new materials in the field of optoelectronics. In the late nineties, they were extensively studied in IBM laboratories by David Mitzi[31] as an active materials for diodes and transistors. However, due to its moisture instability they were not pursued as viable PV materials. In solar cells they were used relatively late, in 2009. A group from Japan, led by prof. Miyasaka was the first to use solution-processed methylammonium lead iodide ($CH_3NH_3PbI_3$) perovskite as a sensitizer on mesostructured titania dioxide (TiO_2) in DSSC architecture, achieving a power conversion efficiency (PCE) of 3.8%[27]. Unfortunately, these cells suffered from major stability issues. Liquid electrolyte (used as hole transporter), was dissolving perovskite material causing fast degradation of the cells. Three years later efficiency of the perovskite based solar cells was dramatically improved by group of prof. Kanatzidis. He used a tin based ($CsSnI_3$) perovskite material in substitution of the liquid electrolyte. This work supposed the first solid state DSSC ever made with efficiency exceeding 10%[28]. Real breakthrough came soon after, when Oxford University team led by prof. Henry Snaith, inspired by prof. Miyasaka work, replaced the liquid electrolyte by a solid polymer (spiro-OMeTAD), eliminating the cause of the fast degradation of the perovskite in Miyasaka's cells[29]. Additionally, the concept of mixed halides (mixing of chlorine and iodine ions) was used for the first time, enhancing the layer formation and material stability under continues light illumination. The cells were fully prepared by solution process methods, reaching efficiencies

of about 10% efficiency in one of the very first attempts[29]. The lead based $CH_3NH_3PbI_2Cl$ perovskite did not require doping (like in Kanatizidis' cell) and proved to be an excellent electron conductor. This result supposed a tremendous success, which brought the attention of the scientific community into the research of this type of solar cells.

Regarding the preparation of this material, layered perovskites are easily spin-coated from solution due to their solubility in conventional organic solvents such as gamma-butyrolactone (GBL) or dimethylformamide (DMF) among others. By spin-coating from solutions, it is possible to prepare thin films of the layered perovskites with good optical quality and oriented layered structure[29,32,35]. This excellent film processability has been used for the fabrication of high-quality layered perovskite thin films with applicability for electronic and optical devices. However, the spin-coating technique has difficulty in the precise control of film thicknesses and film morphologies. In addition, this technique is not compatible with dry processing routes for the preparation of semiconductor films and devices in vacuum conditions. **Thus, the third objective of the Thesis is the development of an strategy for perovskite film preparation, which not only provides precise control of film thicknesses but also exhibits a good compatibility with dry processing.**

Even though perovskites can be potentially lightweight and flexible, to date most of the reported high-efficiency perovskite solar cells make use of a TiO_2 compact layer which requires a high-temperature (around 500°C) sintering process[36,37]. This is translated into a more complex fabrication process which excludes applications based on the use of flexible substrates. As a consequence, production strategies such as Roll-to-Roll (R2R) processing turns to be impeded, being this one of their main potential advantages and interest in terms of transfer to industry of perovskite technology. Additionally, TiO_2 might be strongly related to a hysteresis effect, one of the main problems of the perovskite based solar cells. **Considering all this, the final**

objective of this Thesis is the development of an oxide free perovskite device architecture, that shows no hysteresis and is compatible with flexible substrates.

BI-LAYER SOLAR CELLS BASED ON CATIONIC CYANINE DYES

BI-LAYER SOLAR CELLS BASED ON CATIONIC CYANINE DYES

1. Development of a lab-scale coating technique, for neat bilayer film formation.

Meniscus coating can be an attractive alternative to spin coating for several reasons. Firstly, it uses extremely small amounts of precursor solution. Moreover, this technique guarantees a direct scalability of the results obtained in the lab to industrial slot-die coaters and a good uniformity of the organic layers over large areas. It presents a couple of specially attractive features for the academic sector that are not available via traditional spin-coating method. One example is the control that can be achieved over the thickness gradient on the sample. In this context, it is worthy to mentioned the work of F. Nickel in which this technique was applied for special mapping of the photocurrents for fast and efficient material screening and rapid layer thickness optimization in polymer solar cells[39]. Despite of all these advantages, there are only few works published on the use of meniscus coating technique in organic electronics. The access to the theory of this interesting technique is limited compared to other well developed coating technologies. B. Park et al. were in 2009 the first who used the meniscus concept for fabricating lab-scale optoelectronic devices (OPV, OLEDs and LECs)[40]. The authors have shown that by utilizing the downstream meniscus of the solution, which can be controlled by adjusting experimental parameters of the gap height and the carrying speed, the process can produce high quality thin films. A schematic illustration of the meniscus coating process developed by Park is shown in Fig. 5.

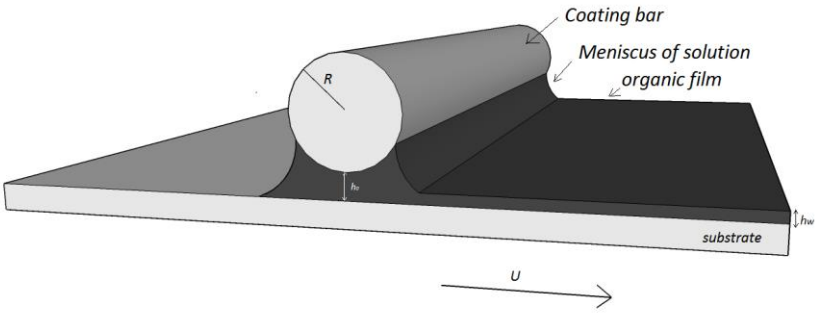

Figure 5 . A schematic representation of the principle of the meniscus coating technique

As shown in the figure 5, a cylindrical coating barrier hangs continuously at a specific height (h_0) above a rigid or flexible substrate that is lying upon a carrying stage that transports the substrate horizontally. The coating process proceeds in the following four major steps:

(1) A substrate is attached to the carrying stage and the coating barrier is placed at the front edge of the substrate.

(2) Then, an organic solution is introduced into the empty space between the barrier and the substrate by capillary action. Due to the surface tension of the liquid, a uniform downstream meniscus of the solution is formed between the substrate and the bar.

(3) The substrate is transported horizontally at a given constant velocity while maintaining the shape of the downstream meniscus. A thin solution layer of the downstream meniscus is then spread and formed evenly on the substrate. The wet film thickness is described by the complex Landeau Levich relation, given by equation 1:

$$h_{\text{wet}} = k\sqrt{\mu}U/\rho g(C_a)^{1/6} \qquad \textit{(equation 1)}$$

where k is a system dependent constant, ρ is the density of the solution, g is the gravitational constant, μ is the solution viscosity, U is the translation speed, and C_a is the capillary number.

The capillary number is given by $\mu U / \gamma$, where γ is the surface tension. In practice it simplifies to:

$$h_{\text{wet}} = K \frac{(\mu U)^{0.66}}{(\rho g)^{0.5} \gamma^{0.167}} \quad \textit{(equation 2)}$$

Thus, for a given coating solution, the wet film thickness is a function of only one mechanical variable, the translation speed as the gap is usually fixed at a constant height above the substrate.

(4) The wet film that has been spread on the substrate is dried and its thickness is given by equation 3

$$h_{dry} = \omega \, h_{wet} \qquad \textit{(equation 3)}$$

where ω represents the solid volume fraction of the coating solution. A heater may be used to assist the evaporation of the residual solvent in the wet film on the substrate. When this process is carried out, it is possible to obtain a substrate that is coated with a solid organic film of uniform thickness. The work of Park et al.[40] showed the potential of meniscus coating for producing high quality organic semiconductor thin films. Precisely speaking, the authors used an inverted meniscus concept named as "horizontal dipping" or "H-dipping" technique. Both meniscus and the dipping technique are based on capillary forces that are used for the adhesion of the solution to the substrate.

In the frame of this Thesis, a lab-scale meniscus coating process was developed, similar to the Park's work. The main difference was that instead of a round coating bar, a rectangular one (further called "blade") was implemented in a simple commercial ERICHSEN coating system. The "blade" was not hanging above the substrate (like in a Park et al. work) but was

assembled directly on the supporting stage as it is shown on figure 6. This was done to eliminate variables in the distance to the substrate and make this method more reproducible.

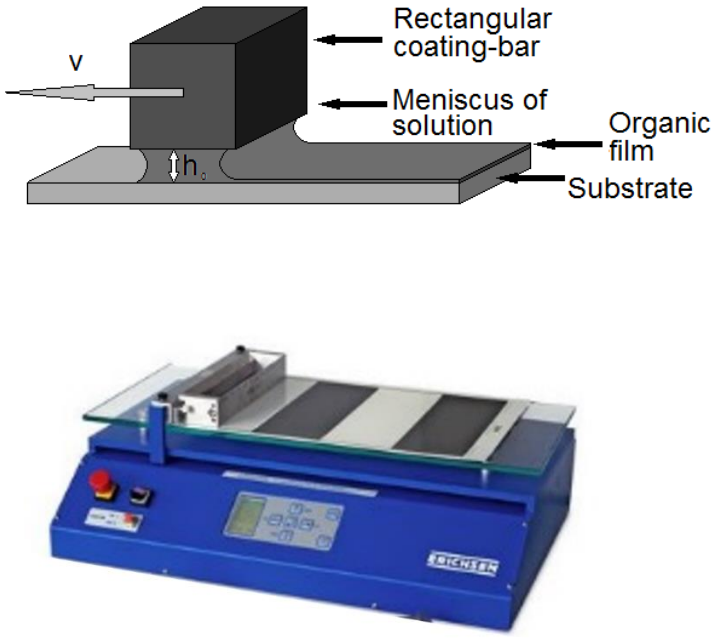

Figure 6. The scheme of the meniscus coating technique with rectangular coating bar and experimental set-up

In opposition to the system developed by Park, the "blade" was translated by the moving arm above the substrate, which was fixed to the supporting stage. That allows an easy exchange of the coating "blades" (no mounting necessary) with different gap heights, facilitating maintenance and cleaning of the system. Although meniscus coating may resemble the blade coating method, these two techniques are in fact very different. In the the doctor-blade (or wire-bar) coating process a wet film is formed with a thickness of the order of the gap size in the blade and is independent of the translation speed of the substrate. This is so called "metered" process because the thickness of the film is imposed externally and does not depend much on the capillary trapped solution in the meniscus. The wet film thickness is determined by the gap size and because of that it is very difficult to obtain sub-micron thicknesses, as this would require a very low solid content, that is usually difficult to dry uniformly as a result of the very

low viscosity. On the other hand, meniscus coating is a "pre-metered" process, where the thickness of the coated film is determined by the velocity of the blade and does not depent a lot on the gap height. In this way, the films can be as thin as few nanometers, being at the same time very reproducible.

Another useful property of the meniscus coating is the extremely small amount of solvent that are needed to coat substrates. In the case of meniscus coating process, the solvent evaporates fast (usually within one second) due to the very low wet film thickness. This fast drying limits negative interaction with previously deposited layers and facilitates the formation of multi-layer devices as well as neat bi-layer interfaces. Because the solution deposition process only uses capillary and gravitational forces, meniscus coating is especially suitable for small molecules and dispersed solutions which are very difficult to spin coat homogenously on the substrate due to centrifugal forces (appearing during spin-coating). When considering a mass production line, the substrate is less susceptible to particle contamination from falling debris because the substrate is placed above the coating apparatus in order to feed the meniscus as larger amounts of solution are necessary with respect to the laboratory trials. Although there are many others known, well developed and currently explored film-forming techniques for large scale applications (e.g. billboard advertisements), many of them require large amounts of material (e.g. screen printing). The primary advantage of meniscus or capillary coating is that material efficiencies are approximately 95 % of the fluid supplied[41]. Additionally, currently most of the commercial coating technologies are not accurate enough to form ultra-thin organic layers (e.g. blade coating), and many of them are unsuited for the small scale laboratory quick trials (e.g. ink-jet). On the contrary, the meniscus coating technique is compatible with slot-die coating which is scalable industrial coating method which is used on both small and large area devices.

The implementation of this technique was extremely successful for the deposition of small molecular weight materials (such as [6,6]-phenyl C61-butyric acid methyl ester (PCBM)), leading to a superior performance devices containing these films with respect to the devices processed by spin-coating technique.

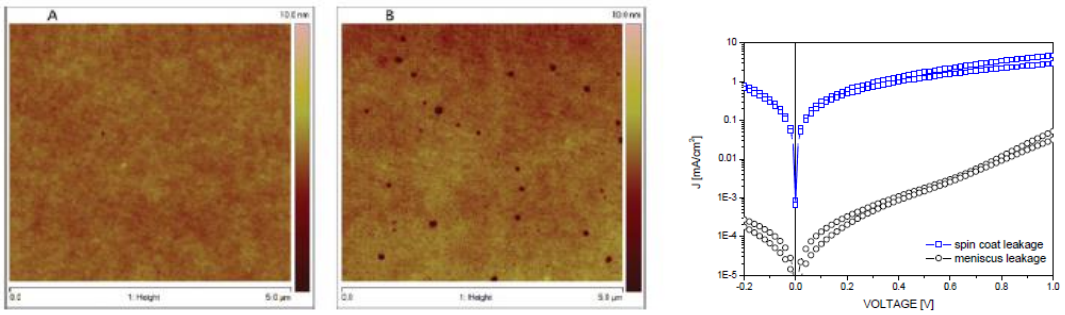

Figure 7. AFM picture of PCBM layer prepared by meniscus coating (A) vs spin coating (B) and the leakage current of the PCBM based device prepared by meniscus (A) and spin-coating (B). In both cases PCBM layer thickness was 50nm.

At last but not least, another important advantage of the meniscus coating technique over spin-coating is a very low material usage. For example in the work of T. Goos et al. only few millilitres of solution were sufficient to prepare more than fifty devices, exhibiting a very good reproducibility[53]. This enabled the study of a very interesting group of ionic polymers and the influence of their ionic group on the device performance. The results of this study however are outside the scope of this Thesis.

2. Devices

In this chapter we describe the development of bi-layer solar cells making use of the meniscus technique. We developed various bi-layer solar cells, using cationic cyanine dyes as the electron donor and a functionalized fullerene derivative as the electron acceptor. In the following this work will be summarized.

a. Solution processed devices:

In order to fabricate the devices, where both donor and acceptor are processed from solution, the finding of orthogonal solvents for both materials turns to be crucial. While cyanines are easily soluble in many benign polar solvents, PCBM is not presenting this behaviour and is soluble only in aromatic solvents. In the experiments performed in this thesis, the most convenient approach was to deposit the cyanine layer onto the PCBM film[52]. In this device configuration, light passes in first instance through the electron acceptor layer, in opposition to the majority of the organic photovoltaic architectures. That order implies an inverted flow of charges in the device, establishing the ITO electrode as the electron collecting contact. As ITO has a high level of free charges and is therefore both a good electron and hole contact. Therefore, to guarantee an electron selectivity at this contact, it needs to be covered with a thin layer of ZnO, which is an excellent hole blocking material. On the other hand, a MoO_3/Ag top electrode was employed as the hole selective contact in the device. The whole device architecture is presented in figure 8.

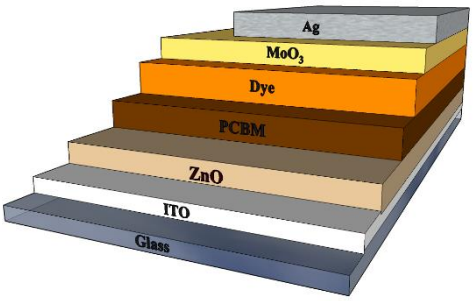

Figure 8. Device architecture of a solution processed device.

In a planar device architecture, the thickness of the active layers is limited by the exciton diffusion length in the organic materials. This was verified to be around 40 nm and 30 nm for PCBM and the dye layer, respectively. It was not a trivial task to prepare a working device with an active layer thickness below 100nm. All the devices prepared by spin-coating showed very

high leakage current, low FF and most of them were shorted. AFM measurements confirmed presence of many pinholes in the spin coated PCBM layer, which was identified as the reason for the low power conversion efficiency.

This problem was overcome by using the meniscus coating technique for the device fabrication. Meniscus method is particularly suitable for the deposition of small molecular weight materials, like $PCBM_{60}$ (Phenyl-C61-butyric acid methyl ester) as mentioned extensively in Chapter 2.2.1 of this thesis. Using meniscus coating we were able to achieve ultrathin, pinhole free layers of PCBM. The devices prepared by this technique showed exceptionally high voltages (1V) and decent FF despite the ultra-low thicknesses of the active layers[52]. These results were published in RSC Advances journal which is inserted in this thesis on page 21.

b. Partially evaporated cyanine dye based solar cells.

What is most interesting about cyanine dyes is the presence of the mobile counter ion, which can move after applying the electric filed, changing the energetics of the solar cell.

In order to study the effect of the cyanine dye counter ion on the device performance, we change solution processed PCBM to evaporated C60 fullerene[54]. In this way, we could be sure that any effect we observed was coming from the ionic nature of the cyanine dyes and not from e.g. thickness variation of the acceptor layer. Because solubility was no longer an issue we decided to go back to the most frequently used device configuration. For the p-type contact we used standard ITO/PEDOT and for the n-type contact we used BCP/Ba:Ag.

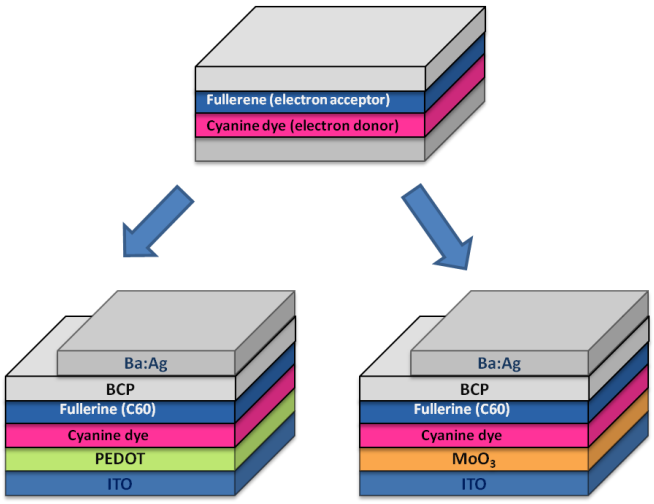

Figure 9. Device architectures

First interesting finding was that some of the devices represent S-shape J-V curve while others not. The appearance of the S-shape was strongly correlated with the band-gap of the dye that was used as a donor. The S-shape was present, whenever the bandgap of the dye exceeded the energy difference between contact electrodes. We could easily eliminate this effect by increasing the build in voltage of the cell by substituting PEDOT with MoO_3 contact.

The second finding was that the use of a dye with a small perchlorate ClO_4 counter-ion, always lead to cells with low fill factors, regardless of the band gap of the dye, whereas the dyes with the larger PF_6 counter-ion showed high fill factors and good device performances.

These results were published in Advanced Energy Materials journal which is inserted in this thesis on page 26.

3. Summary.

In summary meniscus coating was successfully implemented in various neat bi-layer solar cells with fullerene acceptor and cyanine dye donor. The cells exhibit a high open circuit voltage. It was also demonstrated, that the ions have a large impact on the energetics of the solar cells[55].

RSC Advances

Cite this: *RSC Advances*, 2012, **2**, 3335–3339

www.rsc.org/advances

PAPER

Meniscus coated high open-circuit voltage bi-layer solar cells

Olga Malinkiewicz, Martijn Lenes, Hicham Brine and H. J. Bolink*

Received 12th January 2012, Accepted 12th January 2012
DOI: 10.1039/c2ra20075a

Neat bi-layer solar cells of a fullerene acceptor and a cyanine dye donor were prepared using meniscus coating. Meniscus coating is very material efficient and leads to high quality pinhole-free films. The cells exhibit high open circuit voltages of 1 volt, only 0.8 eV below the band gap of the cyanine dye. This is one of the smallest differences reported for organic solar cells and illustrates an almost optimal donor–acceptor energy level alignment.

Introduction

The field of organic photovoltaics (OPV) has been receiving considerable attention ever since the invention of the bi-layer type solar cell by Tang in 1986.[1] There, a sandwich structure consisting of two materials with a band-edge offset was used to split up strongly bound excitons into free carriers leading to the first reasonably efficient organic solar cell. Throughout the years a steady increase in efficiency has been obtained using this type of solar cell by optimizing energy levels, electrode materials, carrier mobilities and absorption coefficients leading to power conversion efficiencies of over 3%.[2] Higher device efficiencies are generally reported for bulk heterojunction (BHJ) devices, formed by phase separated donor and acceptor molecules.[3] Although pioneered for polymeric donor materials, BHJs have also been prepared using evaporated materials.[4,5] This when used in combination with doped transport layers has led to a device efficiency of 8.3%.[6,7] BHJ solar cells are still dominated by polymeric donor materials in combination with a small molecular weight solution processable fullerene derivative.[8,9] One drawback related to the use of polymers is their complex synthesis and associated difficult purification. Alternatively, small molecular weight materials can also be used as donors and have led to promising solution processable BHJ devices.[10,11] The high efficiencies obtained with BHJ architectures exist due to a much larger donor–acceptor interface enabling thicker films. These structures, however, are at the same time difficult to control as they depend critically on the dimensions and extension of each of the two phases which is altered by the choice of solvent, processing conditions and annealing of the film. This holds especially for small molecule based BHJs which often show a very fine intermixing of donor and acceptor greatly increasing recombination losses. Therefore, there is still an interest to prepare planar donor–acceptor junctions as it allows for a better understanding of the device mechanisms.[2,12–14] Additionally, it serves as a platform to screen materials in a more straightforward way as the device performance can be considered a minimum achievable value. Planar devices are usually prepared by vacuum deposition as this ensures a well-defined interface between the two layers. Partial solution processed devices have also been reported in which the first material, usually the donor is processed from solution and the second material is deposited on top *via* vacuum sublimation.[15] Recently, neat double layer devices were prepared using a film transfer method that revealed interesting device physics.[16] It is in general not trivial to obtain a bi-layer device of only small molecular weight materials using solution processing.

Here we demonstrate solution processed neat bi-layer inverted solar cells using cationic cyanine dyes as the electron donor and a functionalized fullerene derivative as the electron acceptor. Cyanine dyes are interesting candidates for use in solar cells because of their very high absorption coefficients (10^5 M^{-1} cm^{-1}) allowing a large number of photons to be absorbed in extremely thin layers.[15,17–19] Secondly they are soluble in polar solvents and exhibit good film forming properties. This enables their solution based processing on top of a film consisting of a functionalized fullerene soluble in aromatic solvents. Lastly, they are commercially available in a great number of varieties enabling fine-tuning of energy levels and physical properties.

Results and discussion

For this study two dyes, 1-ethyl-2-[3-(1-ethyl-3,3-dimethyl-1,3-dihydro-indol-2-ylidene)-propenyl]-3,3-dimethyl-3*H*-indolium hexafluorophosphate (**D1**) and 3-butyl-2-[3-(3-butyl-1,3-dihydro-1,1-dimethyl-2*H*-benzo[*e*]indol-2-ylidene)-propenyl]-1,1-dimethyl-1*H*-benzo[*e*]indolium perchlorate (**D2**), were used as donors (Fig. 1 left). The acceptor used in this study, [6,6]-phenyl-C_{61}-butyric acid methyl ester (PCBM) is a functionalized fullerene which is one of the most studied materials in OPV because of its high carrier mobility, appropriate energy levels for forming a type II heterojunction with most available donor materials, and high solubility.

The cationic cyanine dyes dissolve well in polar solvents, such as 2,2,3,3-tetrafluoro-1-propanol (TFP). Unfortunately, they also dissolve, albeit only at low concentrations, in the aromatic solvents (toluene, chlorobenzene) used to process PCBM.

Instituto de Ciencia Molecular, Universidad de Valencia, PO Box 22085, ES-46071, Valencia, Spain. E-mail: henk.bolink@uv.es

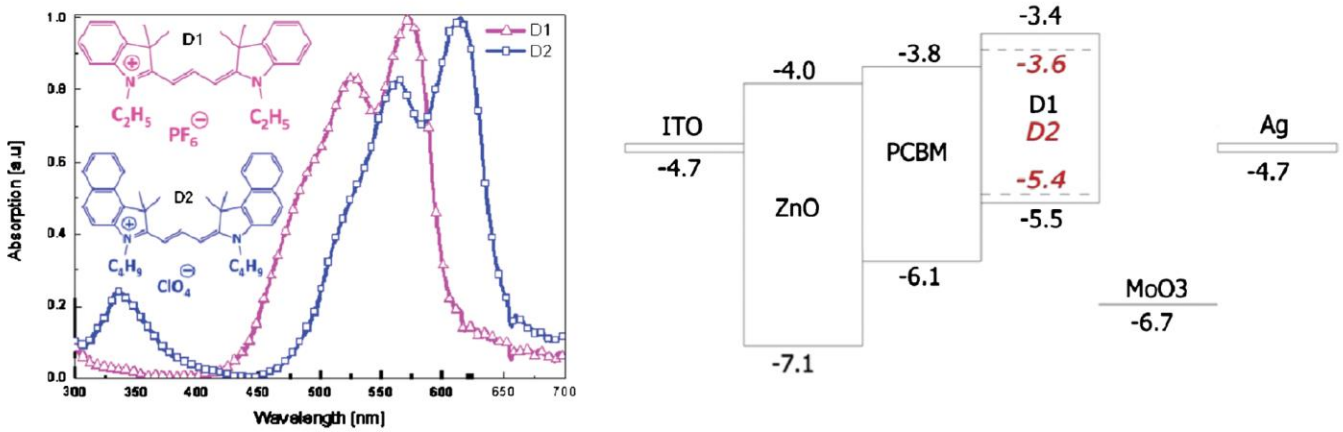

Fig. 1 Chemical structure of the cyanine dyes and their thin film absorption spectra (left) and energy of the work function, valence and conduction band and molecular orbitals for the electrodes, metal oxides and organic molecules, respectively (right).

Therefore, it is not possible to obtain neat bi-layers by processing PCBM on top of the cyanine dye based film, as a fraction of the dye would dissolve and mix with the PCBM layer. PCBM, however, is completely insoluble in TFP and therefore it should be possible to deposit the cyanine dyes on top of the PCBM layer. Hence an inverted device structure is required for this solution processed bi-layer solar cell. In order to achieve efficient charge collection buffer layers are used, ZnO in between the ITO and the PCBM layer and molybdenum trioxide (MoO_3) in between the metal and the cyanine dye layer (Fig. 1 right). The use of MoO_3 offers advantages over the more commonly used PEDOT:PSS as hole injection/extraction layer due to the deep lying HOMO levels of the cyanine dyes.[13] Secondly the ZnO/active layer/MoO_3 device architecture has been proven to be a stable configuration offering high performance and lifetimes in inverted photovoltaic and light emitting devices.[20]

We have employed a non-standard method to deposit the small molecular weight materials based films referred to as meniscus coating.[21] In our lab-scale method we use capillary forces to place the drop of solution containing the small molecular weight molecules in between the substrate and the bottom of a flat blade (3 by 20 mm). Because the distance between the blade and the substrate is small (0.2 mm) the drop is maintained within the gap creating the so called meniscus. This meniscus is stretched when moving the blade over the substrate leaving behind a thin film of the small molecular weight material (Fig. 2).

The resulting dry film thickness is primarily determined by the drawing speed of the blade and its distance to the substrate.[22] This is different from blade coating where the solution is pushed by the blade leaving behind a thick wet film (the thickness depending on the height of the blade used).

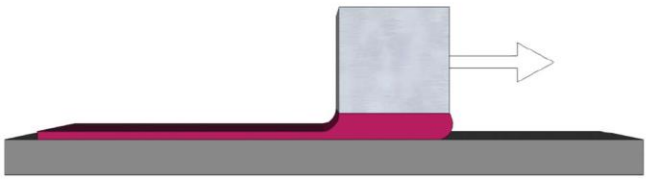

Fig. 2 Schematic of the meniscus coating technique employed.

A solution (30 μl) containing 0.24 mg of PCBM in chlorobenzene was used to coat a 50 nm thick PCBM film on an ITO/ZnO substrate 3 cm wide and 12 cm long, the drawing speed of the blade was 20 mm s^{-1}. The resulting PCBM layer is very uniform and shows a rms of around 2 nm from AFM analysis (Fig. 3A). To compare this PCBM film quality with spin coated ones, PCBM layers were also prepared by spin coating from a chlorobenzene solution using concentrations of 20 and 30 mg ml^{-1}. By varying the rotation speed of the spin coater, PCBM films with a thickness of 50 nm could be obtained for both concentrations. These spin coated layers also appear quite homogeneous with an rms below 3 nm (Fig. 3B) yet show a considerable amount of pinholes penetrating through the layer. Such pinholes are highly undesirable since they will result in the generation of shorts and hinder the formation of a neat bi-layer. These pinholes were present in all the spin coated films prepared and not observed in any of the meniscus coated films.

After preparing the PCBM layer by meniscus coating and a short drying period (20 s) the dye layer is applied using meniscus coating. In order to create a neat bi-layer the solvent of the dye should not dissolve the underlying PCBM layer. The integrity of the PCBM layer upon exposure to TFP by the meniscus coating was verified by comparing the absorption spectrum of the film before and after exposure (Fig. 4). From these measurements it was established that the coating procedure does not change the underlying PCBM layer and a neat PCBM/dye solution processed bi-layer is formed. The solution processed bi-layer

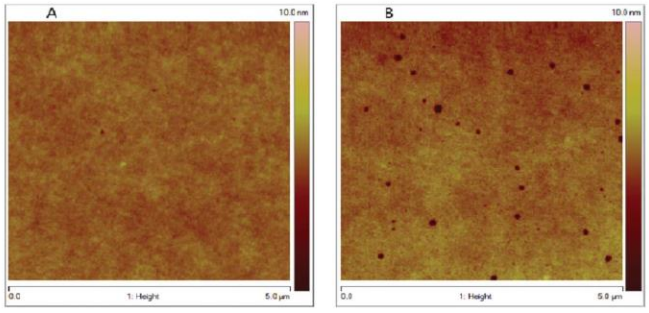

Fig. 3 Atomic force microscope images of A: PCBM film coated using meniscus coating and B: PCBM film coated using spin coating.

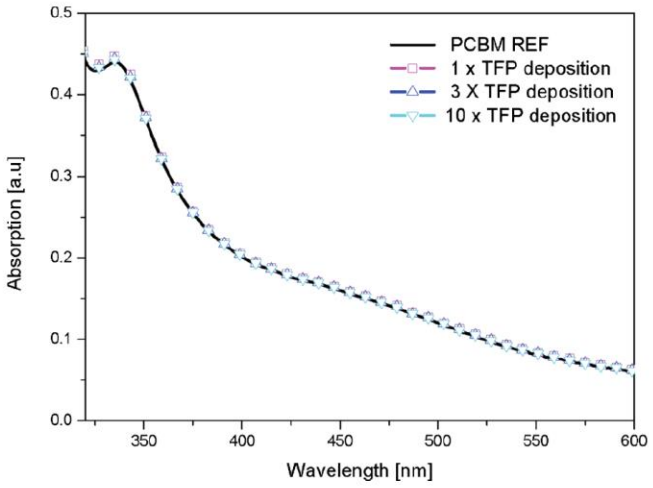

Fig. 4 Thickness profiles and absorption spectra of PCBM films exposed to TFP solutions.

architecture was completed to a photovoltaic cell by thermally evaporating the MoO_3 and Ag layers. An additional benefit of meniscus-coating above spincoating is the very low material usage as most of the solution is used for the film formation. In contrast, with spincoating typically only 5% of the material ends up in the film. To prepare a 50 nm thick layer on our 30 by 30 mm substrates using spincoating 6.7 mg PCBM was needed whereas with meniscus coating we employed only 0.24 mg.

To identify the optimum performance, solar cells with different layer thicknesses of the PCBM and **D1** were prepared. The layer thicknesses used were 45, 50 and 70 nm for the PCBM layer and 30, 40 and 30 nm for the dye layer. These layers were integrated in the following devices A, B and C, having PCBM and **D1** layer thicknesses of 45 and 30 nm, 50 and 40 nm, and 70 and 30 nm, respectively. We note that meniscus coating allows to accurately prepare films with varying thicknesses. The *J*–*V* curves obtained for these devices under white light illumination are depicted in Fig. 5.

The absorption spectra of the devices resemble the layer thickness, that is, the device with the thinnest layers has the lowest absorption. Interestingly, the maximum current density is obtained for the device with the thinnest layers of PCBM and cyanine dye (45 and 30 nm, respectively). This is likely due to the limited exciton diffusion length in the materials, meaning that while the thicker dye layer is able to absorb more photons, the additionally generated excitons do not reach the donor–acceptor interface and hence do not contribute to the device current. For practical reasons it is difficult to go to a thinner cyanine dye layer which might be required to reduce the recombination losses and hence lead to higher fill factors. The performance for these cells is summarized in Table 1.

For this reason layer thicknesses of 45 nm for the PCBM and 30 nm for the cyanine dye layers were selected for further device analysis using both dyes, **D1** and **D2**.

The typical absorption spectra of both the bi-layer devices are depicted in Fig. 6. The absorption in the visible region is governed by the cyanine dyes. Both devices show similar absorption intensities yet the absorption spectrum of the device employing **D2** is red-shifted by approximately 50 nm in accordance with the absorption spectra of the pure dyes and

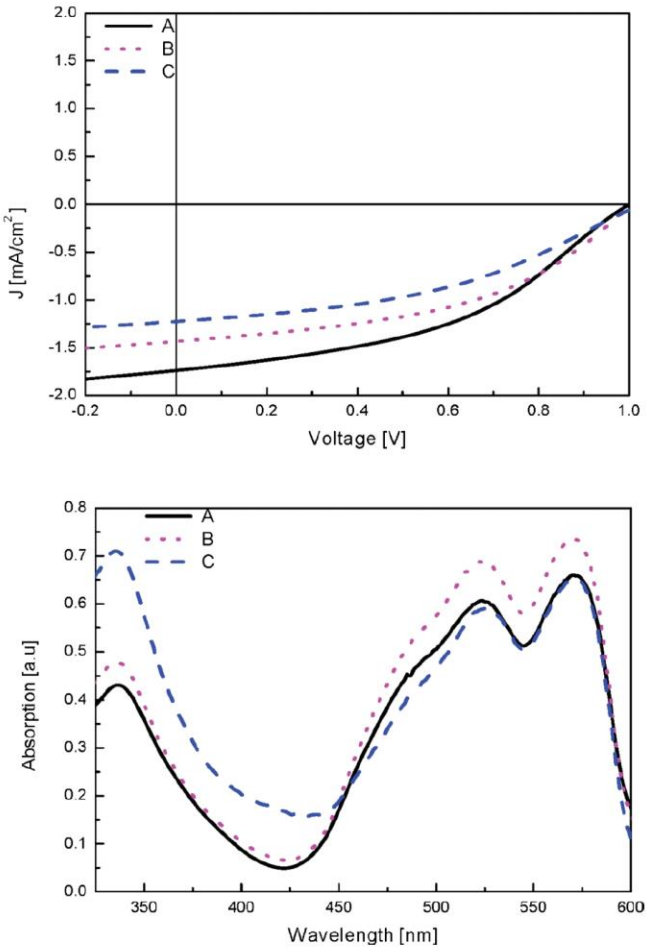

Fig. 5 *J*–*V* curves for devices A, B and C under white light illumination (top) and the corresponding absorption spectra (bottom).

its narrower bandgap. The highest incident photon-to-current conversion efficiencies (IPCE) are around 15% and coincide with the peak in the absorption of the cyanine dyes. For non-inverted device geometries the IPCE spectrum can show a dip at the absorption peak of the dye. This is related to the extremely high absorption coefficient of the dyes resulting in most of the light being absorbed in the first few nanometres of the dye layer, which in that case is at the donor–anode interface. For these inverted bi-layers however this phenomenon called antibatic behaviour does not occur since the light enters the donor layer at the donor–acceptor interface.[13]

The IPCE as a function of wavelength follows the absorption spectra over the range of the solar spectrum with contributions of both dye and fullerene.

White light *J*–*V* characteristics for the bi-layer at around 1 sun illumination are depicted in Fig. 7 and the main performance parameters are depicted in Table 2.

The achieved open circuit voltages (V_{oc}) (1.0 and 0.99 V) are especially high for organic solar cells. Previous reports of solar cells using cyanine dyes showed limited voltages of 0.6–0.7 V caused by the mismatch of the deep lying HOMO level of the dyes with the work function of PEDOT:PSS. The open circuit voltages we observed are even higher compared to devices using a vacuum dried polyaniline anode (V_{oc} = 0.72 V).[13] The difference of the V_{oc} and the bandgap (1.8 eV) is especially for

Table 1 Device performance using different PCBM and **D1** layer thicknesses. Best values are presented. For the power conversion efficiency (PCE) the corrected J_{sc} is used, calculated by integrating the IPCE spectrum over the AM1.5 solar spectrum

	PCBM [nm]	Dye [nm]	IPCE [%]	PE [%]	FF [%]	V_{oc} [V]	J_{sc} [mA cm^{-2}]	$J_{sc\ corrected}$[mA cm^{-2}]
A	45	30	15	0.6	0.43	1	1.7	1.5
B	50	40	13	0.59	0.46	1	1.42	1.28
C	70	30	10	0.45	0.41	1	1.2	1

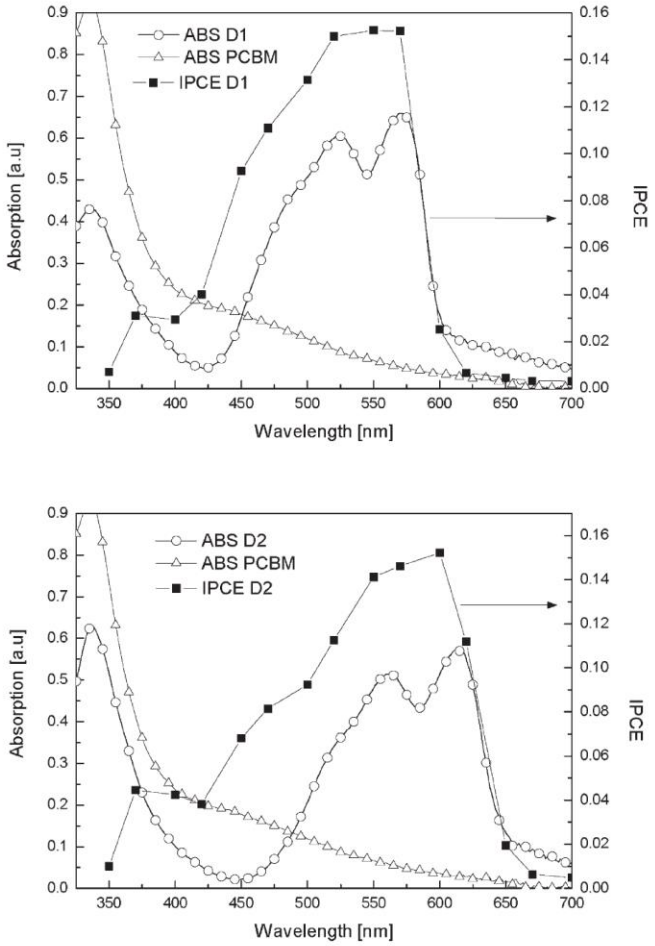

Fig. 6 Typical absorption spectrum (open symbols) and IPCE *versus* wavelength (solid squares) for the bi-layer solar cells, employing **D1** (top) and employing **D2** (bottom), additionally the absorption spectrum of a PCBM film is depicted.

the cell employing **D2** rather small at 0.8 eV. This is one of the smallest differences reported for organic solar cells and illustrates an almost optimal energy level alignment.[23,24] As **D1** absorbs at shorter wavelengths its energy gap is slightly larger and as such the energy difference between the V_{oc} and the band gap is around 1 eV. The short circuit current (J_{sc}) reaches 1.5 and 1.7 mA cm^{-2} for the devices using **D1** and **D2**, respectively where the narrower band gap of **D2** ensures a better overlap with the solar spectrum and hence facilitates higher currents.

We note that the devices presented in this paper are fabricated using commercially available starting materials which are used without further purifying. Especially for the cyanine dyes, higher purity starting materials are expected to increase the performance considerably by increasing the exciton diffusion lengths and carrier mobilities. For example it was shown by Fan *et al.*

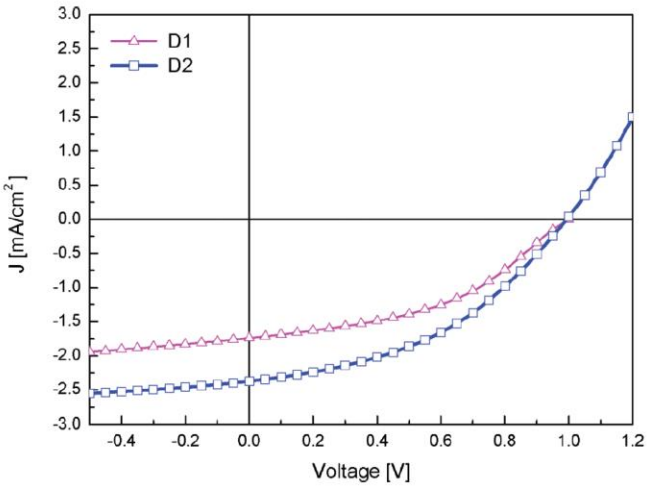

Fig. 7 *J–V* curves for the bi-layer solar cells with dyes **D1** and **D2** under white light illumination.

that EQEs of 60% can be reached using similar cyanine dyes in a bi-layer heterojunction with C_{60}.[13]

Conclusions

In summary solution processed bi-layer solar cells are demonstrated using small molecular weight materials. Meniscus coating was used to prepare the neat bi-layer devices as this technique allows for high quality pinhole-free films with very small material usage. Efficiencies of 0.6% are obtained with exceptionally high open circuit voltages of 1 volt demonstrating the optimal alignment of donor and acceptor energy levels.

Experimental details

Prepatterned ITO-covered glass substrates (*www.naranjosubstrates.com*) were extensively cleaned using detergent, demineralised water, and isopropyl alcohol, respectively, followed by UV-ozone treatment. The 30 nm ZnO layer was obtained by spin coating a precursor solution onto the cleaned substrates followed by an annealing step at 400 °C for 3 h. The precursor solution used was a solution containing zinc acetate dehydrate and acetic acid dissolved in ethanol : water (3 : 1). Acetic acid was added to avoid the formation of zinc hydroxide, $Zn(OH)_2$, and to enhance the film quality. A 50 nm layer of PCBM (SOLENME) was prepared by meniscus coating using a chlorobenzene solution (20 mg ml^{-1}) (technique described above) followed by the deposition of a 30 nm dye layer (FEW CHEMICALS) from a TFP solution (7 mg ml^{-1}) using the same technique. The samples were transferred to a nitrogen filled glove box (1 ppm O_2 and <1 ppm H_2O) where 30 nm MoO_3/70 nm silver top contact were thermally evaporated (<5 × 10^{-6} mbar).[14] Solar cells (active

Table 2 Main characteristics of the two types of bi-layer solar cells. Best values are presented. For the power conversion efficiency (PCE) the corrected J_{sc} is used, calculated by integrating the IPCE spectrum over the AM1.5 solar spectrum

Dye	PCBM [nm]	Dye [nm]	IPCE [%]	PE [%]	FF [%]	V_{oc} [V]	J_{sc} [mA cm^{-2}]	$J_{sc\ corrected}$[mA cm^{-2}]
D1	50	30	15	0.6	0.43	1	1.7	1.5
D2	50	30	15	0.7	0.42	0.99	2.4	1.7

area 9 mm^2) were illuminated by a white light halogen lamp in combination with interference filters for the EQE and *J–V* measurements (MiniSun simulator by ECN the Netherlands). An estimation of the short-circuit current density (J_{sc}) under standard test conditions was calculated by convolving the EQE spectrum with the AM1.5G reference spectrum, using the premise of a linear dependence of J_{sc} on light intensity. *J–V* characteristics of the solar cells were recorded using a Keithley 2400 SourceMeter. All characterisation was performed in a nitrogen filled glove box (1 ppm O_2 and <1 ppm H_2O).

Acknowledgements

This work has been supported by the European Union FP7 program (ORION, 229036), the Spanish Ministry of Science and Innovation (MICINN) (MAT2011-24594, CSD2007-00010) and the Generalitat Valenciana. The authors greatly acknowledge Alejandra Soriano, Jorge Ferrando and Eva Tormos for device preparation and testing, technical assistance and AFM analysis, respectively.

References

1 C. W. Tang, *Appl. Phys. Lett.*, 1986, **48**, 183.
2 R. Fitzner, E. Reinold, A. Mishra, E. Mena-Osteritz, H. Ziehlke, C. Koerner, K. Leo, M. Riede, M. Weil, O. Tsaryova, A. Weiss, C. Uhrich, M. Pfeiffer and P. Bauerle, *Adv. Funct. Mater.*, 2011, **21**, 897.
3 G. Dennler, M. Scharber and C. J. Brabec, *Adv. Mater.*, 2009, **21**, 1323.
4 P. Peumans, S. Uchida and S. R. Forrest, *Nature*, 2003, **425**, 158.
5 A. Ojala, H. Bürckstümmer, M. Stolte, R. Sens, H. Reichelt, P. Erk, J. Hwang, D. Hertel, K. Meerholz and F. Würthner, *Adv. Mater.*, 2011, **23**, 5398.
6 http://www.heliatek.com/news-19.
7 M. Riede, T. Mueller, W. Tress, R. Schueppel and K. Leo, *Nanotechnology*, 2008, **19**, 424001.
8 S. H. Park, A. Roy, S. Beaupre, S. Cho, N. Coates, J. S. Moon, D. Moses, M. Leclerc, K. Lee and A. J. Heeger, *Nat. Photonics*, 2009, **3**, 297–303.
9 G. Yang, Y. Yang, L. Yu, Y. Wu and G. Li, *Nat. Photonics*, 2009, **3**, 649–653.
10 Y. Liu, X. Wan, F. Wang, J. Zhou, G. Long, J. Tian and Y. Chen, *Adv. Mater.*, 2011, **23**, 5387.
11 B. Walker, C. Kim and T. Nguyen, *Chem. Mater.*, 2011, **23**, 470–482.
12 M. Lenes and H. J. Bolink, *ACS Appl. Mater. Interfaces*, 2010, **2**, 3664.
13 B. Fan, F. Araujo de Castro, B. T. Chu, J. Heier, D. Opris, R. Hany and F. Nuesch, *J. Mater. Chem.*, 2010, **20**, 2952–2955.
14 X. Tong, B. E. Lassiter and S. R. Forrest, *Org. Electron.*, 2010, **11**, 705–709.
15 B. Fan, R. Hany, J. Moser and F. Nuesch, *Org. Electron.*, 2008, **9**, 85–90.
16 A. Tada, Y. Geng, Q. Wei, K. Hashimoto and K. Tajima, *Nat. Mater.*, 2011, **10**, 450.
17 X. Ma, J. Hua, W. Wu, Y. Jin, F. Meng, W. Zhan and H. Tian, *Tetrahedron*, 2008, **64**, 345–350.
18 P. Bouit, D. Rauh, S. Neugebauer, J. L. Delgado, E. Di Piazza, S. Rigaut, O. Maury, C. Andraud, V. Dyakonov and N. Martin, *Org. Lett.*, 2009, **11**, 4806.
19 C. Villegas, E. Krokos, P. Bouit, J. L. Delgado, D. M. Guldi and N. Martin, *Energy Environ. Sci.*, 2011, **4**, 679.
20 J. Wang, W. Weng, M. Tsai, M. Lee, S. Horng, T. Perng, C. Kei, C. Yu and H. Meng, *J. Mater. Chem.*, 2010, **20**, 862.
21 C. S. Herrick, *Ind. Eng. Chem. Prod. Res. Dev.*, 1980, **19**, 314–316.
22 J. A. Britten, *Chem. Eng. Commun.*, 1993, **120**, 59–71.
23 D. Veldman, S. C. J. Meskers and R. A. J. Janssen, *Adv. Funct. Mater.*, 2009, **19**, 1939.
24 P. Heremans, D. Cheyns and B. P. Rand, *Acc. Chem. Res.*, 2009, **42**, 1740–1747.

ADVANCED ENERGY MATERIALS
www.advenergymat.de

Efficient, Cyanine Dye Based Bilayer Solar Cells

*Olga Malinkiewicz, Thais Grancha, Agustin Molina-Ontoria, Alejandra Soriano, Hicham Brine, and Henk J. Bolink**

Simple bilayer solar cells, using commercially available cationic cyanine dyes as donors and evaporated C_{60} layer as an acceptor are prepared. Cyanine dyes with absorption maxima of 578, 615 and 697 nm having either perchlorate or hexafluorophosphate counter-ions are evaluated. The perchlorate dye leads to cells with S-shape current-voltage curves; only the dyes with the hexafluorophosphate counter-ions lead to efficient solar cells. When the wide bandgap dyes are employed, S-shape current-voltage curves are obtained when the conductive polymer PEDOT:PSS is used as hole transport layer. Substitution of PEDOT:PSS with MoO_3 leads to cells with more rectangular current–voltage curves and high fill factors. Additionally, the cells using the MoO_3 layer for hole extraction lead to high open circuit voltages of 0.9 V. In the case that a low bandgap hexafluorophosphate dye is used with the HOMO above that of the PEDOT:PSS the cell performance is independent on the type of hole transport layer employed. Using this approach, bilayer solar cells are obtained with power efficiencies ranging from 1.8 to 2.9% depending on the particular dye employed. These are impressive numbers for bilayer solar cell that are partially solution processed in ambient conditions.

1. Introduction

Organic photovoltaic cells (OPVs) have attracted a lot of attention in the last years not least due to significant breakthroughs in device efficiencies.[1] Most of the best performing cells rely on bulk heterojuctions, optimized for maximum light absorption and efficient charge generation. Less attention has been paid to the much simpler planar heterojunctions in bilayer OPVs as first described by Tang.[2] Although bilayer cells have lower efficiencies as a consequence of the use of thinner active layers (determined by the limited exciton diffusion lengths), they still possess very interesting features which make them an excellent platform for the screening of new materials and for fundamental studies.[3] Thanks to the planar structure (one organic layer on top of another) the charges generated at the interface are spatially separated which means that holes are confined within the donor layer while the electrons are confined within the acceptor layer. Since recombination between free charges is practically eliminated it is possible to obtain information on physical phenomena in such cells.[3] Cyanine dyes are interesting molecules for use in photovoltaic applications, in particular in bilayer solar cells.[4] This is because they have very high absorption coefficients (~10^5 M^{-1} cm^{-1}) and their absorption spectra cover a wide range of wavelengths, from the blue to the near infrared.[5] Additionally, it was demonstrated that excitons generated in a thin film of cyanine dyes exhibit relatively long exciton diffusion lengths (aprox. 30 nm).[6] Hence, in principle, all excitons generated in a film with a thickness up to 30 nm can reach the interface. Furthermore, cyanine dyes are used in various applications and are therefore commercially available in high purity and quantities at low cost. In previously reported cyanine based solar cells, S-shaped current-voltage (I–V) curves were frequently reported.[4,7] The origin of the S-shaped I–V curves is not yet understood, but has been shown to be influenced by the type of counter-ion, partial oxidation, and the type of hole transporting material employed. Recently, an interesting hole injection/extraction material, MoO_3, has been successfully implemented as hole injection layer (HIL) in many OLEDs and recently also in some BHJ OPVs.[8] Additionally, it was shown that the MoO_3 layers can be obtained by solution processing.[9]

In this work we present planar heterojunctions using a solution processed cyanine dye donor layer and an evaporated fullerene layer. Also we demonstrate how the S-shape current density vs. voltage (J–V) curves can be avoided. Four cyanine dyes are used with different absorption spectra, three with a hexafluorophosphate (PF_6) and one with a perchlorate (ClO_4) counter-ion. The dye with the ClO_4 counter-ion leads to cells with low fill factors due to S-shaped J–V curves. Whereas the cells using the dyes having a PF_6 counter-ion have high fill factors and good device performances. The device performances can be increased when a MoO_3 hole transporting layer is used. This leads to an increase of the V_{oc} and the shape of the current density vs. voltage (J–V) curve which results in an increased fill factor. The best devices reach a power conversion efficiency (PCE) of 2.9%.

O. Malinkiewicz, T. Grancha, Dr. A. Soriano, H. Brine, Dr. H. J. Bolink
Instituto de Ciencia Molecular
Universidad de Valencia
C/Catedrático J. Beltrán 2
ES-46980 Paterna (Valencia), Spain
E-mail: henk.bolink@uv.es
Dr. A. Molina-Ontoria
Departamento de Química Orgánica
Facultad de Química
Universidad Complutense
28040 Madrid, Spain

DOI: 10.1002/aenm.201200764

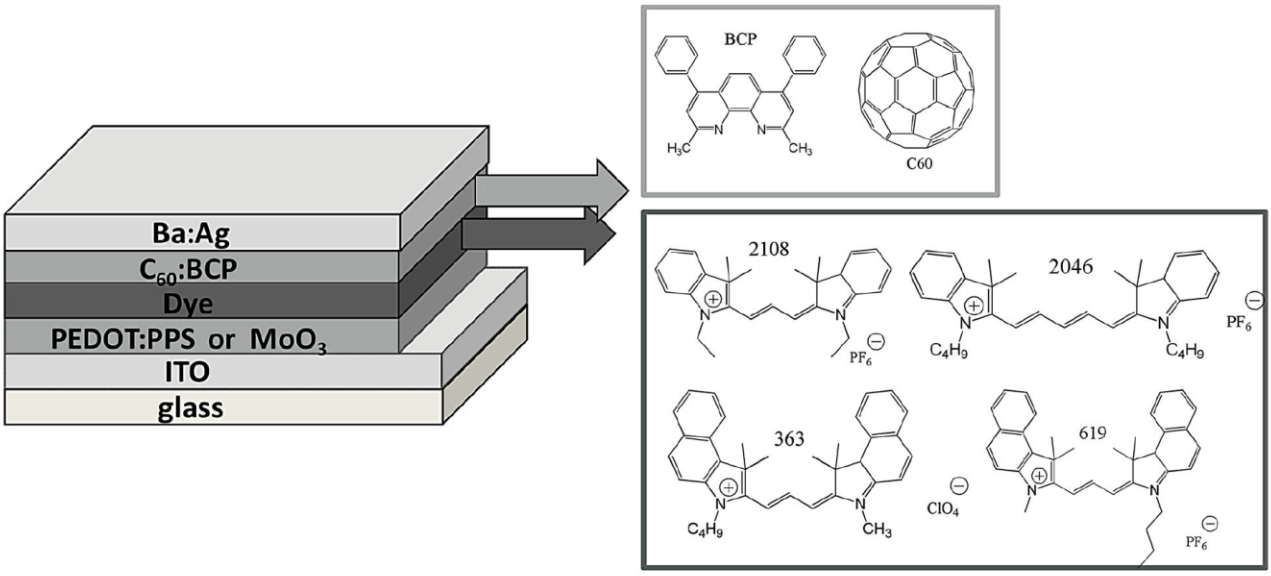

Figure 1. Schematic of the device layout and the chemical structures of the materials employed.

2. Results and Discussion

Four cyanine dyes were studied as donors: 1-ethyl-2-[3-[1-ethyl-3,3-dimethyl-1,3-dihydro-indol-2-ylidene]-propenyl]-3,3-dimethyl-3H-indolium hexafluorophosphate (**2108**), 3-butyl-1,1-dimethyl-2-[3-(1,1,3-trimethyl-1,3-dihydro-benzo[e] indol-2-ylidene)-propenyl]-1H-benzo[e]indolium hexafluorophosphate (**619**), 3-butyl-2-[3-(1,3-dihydro-1,3,3-trimethyl-2H-indol-2-ylidene)-propenyl]-1,1-dimethyl-1H-benzo[e]indolium perchlorate (**363**) and 1-butyl-2-[5-(1-butyl-1,3-dihydro-3,3-dimethyl-2H-indol-2-ylidene)-penta-1,3-dienyl]-3,3-dimethyl-3H-indolium hexafluorophosphate (**2046**) (**Figure 1**). The dye **2108** has been used before in this type of solar cells and the dyes **619** and **2046** have a similarly high extension coefficient but with a red shifted absorption spectrum. In addition to these hexafluorophosphate salts the perchlorate dye, **363** with the organic part similar to **619** was also evaluated.

Bilayer cells were prepared according to the layout shown in Figure 1. The dye layer is deposited on top of a hole transporting layer (HTL). This is either poly-(3,4-ethylenedioxythiophene)-poly-(styrenesulfonate), PEDOT:PSS (Clevios AI4083, from Hereaus) or MoO_3. The PEDOT:PSS layer was prepared by spincoating in ambient conditions. The MoO_3 was prepared by thermal evaporation in a high vacuum environment. Independently of this, HTL was employed the dye layer was prepared using spincoating from a chlorobenzene solution (7 mg/ml) in ambient conditions. The acceptor layer consisted of C_{60} which was thermally evaporated under a high vacuum. Prior to the deposition of the Ba/Ag cathode, a thin layer of (bathocuproine) BCP was evaporated. This layer of BCP is evaporated in between the C_{60} layer and the cathode to ensure a proper ohmic contact and hence an efficient charge extraction.[10] More detailed information regarding device preparation can be found in the Experimental Section.

The absorption spectra of 30 nm thin films of the dyes and C_{60} are depicted in **Figure 2**. Dye **2108** shows a maximum absorption at 578 nm, dye **619** and **363** both have a maximum absorbance at 615 nm and dye **2046** has the maximum at 697 nm. The absorption of the dyes **619**, **363** and **2046** is shifted towards longer wavelength with respect to that of dye **2108** which is due to an increase in the effective conjugation length of the dye. At similar film thicknesses the absorbance of the cyanine dyes in the visible part of the spectrum is approximately twice that of C_{60} as expected from their high extinction coefficients. However, due to the narrow width of the absorption spectra of the dyes the absorption of C_{60} at wavelengths below 500 nm is stronger than that of the dyes.

First we evaluated the 363 and 619 dyes that have a very similar organic cation, yet with a perchlorate and a hexafluorophosphate counterion, respectively. The effect of the counterion is not very well known but can play a significant role if it diffuses into the C_{60} layer. In **Figure 3**, the current density (J) to voltage

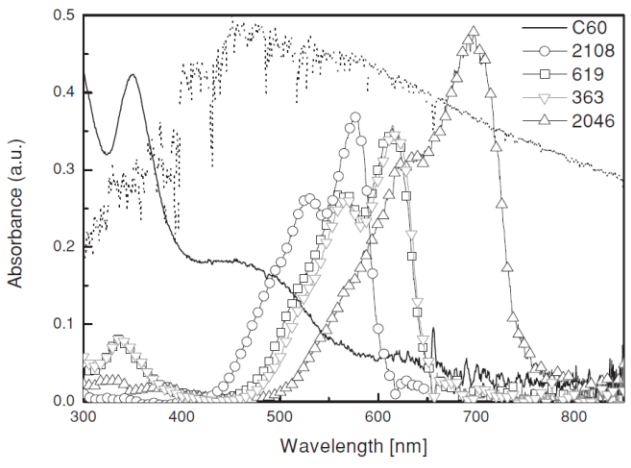

Figure 2. Absorption spectra of thin films of C_{60} (solid black line) and the cyanine dyes **2108**, **619**, **363** and **2046**. The dotted line represents the AM1.5 solar spectrum.

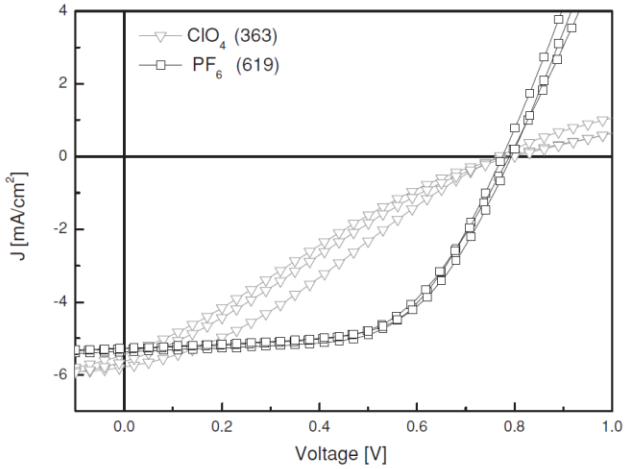

Figure 3. Current density vs voltage for cells using either dye **363** or **619** under an illumination of 1000 W/m^2 simulated AM1.5 solar light.

(V) characteristics are shown for cells using either the dye 363 or 619 under an illumination of 1000 W/m^2 simulated AM1.5 solar light. The J–V curve of cells using the ClO_4^- containing dye (363) has a very clear S-shape which leads to a very low fill factor. This is in sharp contrast with the J–V curve obtained from the devices employing the PF_6 dye (619), which has a rectangular shape, leading to a fill factor of 60%. The open circuit voltage (V_{oc}) and the short-circuit current (J_{sc}) are rather similar for both type of cells. Similar results were reported previously in two reports.[7] Notice also that the reproducibility of the results in these devices is rather good. This large change in performance is most likely not a result of a different absorbance or exciton formation process since the absorption spectra for both dyes are identical. The hole mobility in the dye layer is primarily determined by the organic cation of the dye, which, as mentioned, is the same in both cases. The type of counterion may influence the hole mobility as it may reorient to stabilize/trap a hole. This effect would be stronger for a more mobile counterion, such as the ClO_4^- ion. However, a more plausible explanation can be derived from a previous report by the group of Nuesch that mentions that ion migration from the dye layer to the acceptor layer can occur.[11] This leads to a strong interface dipole over the donor acceptor interface, which changes the energy off-set between donor LUMO and acceptor LUMO. Migration of ions is likely to depend strongly on the ion size, hence it is possible that the smaller ClO_4^- ions migrate more rapidly into the C_{60} layer, causing the poor photovoltaic performance. To identify the origin of this effect detailed studies are required.

In view of the results obtained the PF_6^- dyes (**619**, **2108** and **2046**) were selected to compare the effect of the hole injection material and the bandgap of the dye on the device performances. The incident photon-to-current conversion efficiencies (IPCE) for cells using the **619** dye with either an PEDOT:PSS or a MoO_3 HTL is depicted in **Figure 4**a. Figure 4b shows the typical J–V curves for both type of devices. The IPCE indicates that light absorption in the dye and C_{60} layer contribute both to the photovoltaic effect (Figure 4). This implies that the energy off-set between the lowest unoccupied molecular orbital (LUMO) of the dye is sufficiently above that of the LUMO of C_{60} and that the highest occupied molecular orbital (HOMO) of the C_{60} is sufficiently below that of the HOMO of the dye. The IPCE of the cells using PEDOT:PSS is slightly higher than that of the cells using MoO_3. This higher IPCE for the cells with PEDOT;PSS is reflected in a higher J_{sc} (see Figure 4 and **Table 1**). The reason for this difference may be related to a lower light transmission due to the absorbance of the MoO_3 layer. This was also observed for bulk-heterojunction solar cells using such layers.[9] The device absorption spectrum which contains the contribution from the C_{60} and the **619** dye shows a higher absorption in the wavelength range from 550 to 650 nm, demonstrating that the dye film is absorbing more light than the C_{60} film nm (Figure S5). Therefore, one might expect the IPCE to be higher in the wavelength range from 550 to 650 nm. The IPCEs of the PEDOT:PSS containing cells do show higher values in that wavelength range, yet those of the MoO_3-containing cells

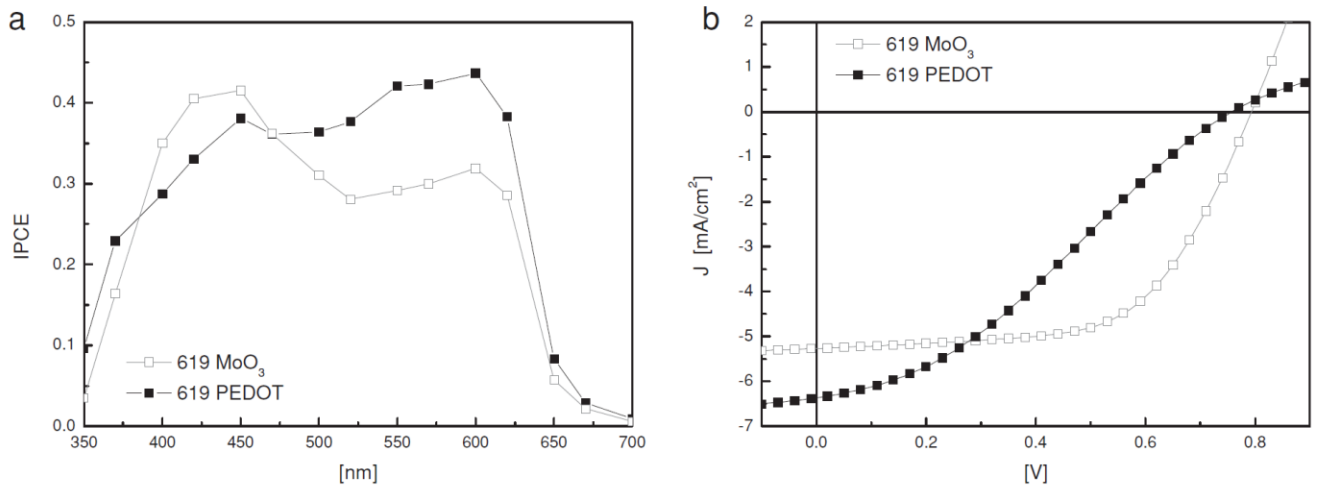

Figure 4. Left: IPCE of the solar cells based on dye **619** with a PEDOT:PSS (full squares) or a MoO_3 (open squares) anode. Right: Current density vs voltage for these two devices.

Table 1. Overview of the characteristics for the different cells described. Values displayed are average values from more than 10 cells. For an indication of the reproducibility of the cells see Figures (S1, S2 and S3) in the Supporting Information.

DYE	[nm]	HTL	[nm]	IPCE $_{max}$ [%]	PCE [%]	FF [%]	V_{OC} [V]	J_{SC} [mA/cm^2]
2108	30	MoO_3	30	41	2.4	55	0.92	4.6
2108[a)]	23	MoO_3	30	45	2.9	62	0.92	5.1
2108	30	PEDOT	70	54	1.9	44	0.77	5.7
0619	30	MoO_3	30	41	2.5	60	0.79	5.3
0619	30	PEDOT	70	44	1.4	30	0.76	6.3
0363	30	MoO_3	30	48	1.1	24	0.79	5.6
2046	30	MoO_3	20	35	1.8	50	0.62	5.8
2046	30	PEDOT	70	28	1.7	49	0.62	5.7

[a)]Best device.

do not. Hence in this case it appears that the lower IPCE is caused by an extraction barrier for holes when MoO_3 is used as the HTL (**Figure 5**). More striking is the different shape of the J–V curves. The MoO_3-containing cells show a rectangular curve leading to a fill factor of 60%. Whereas the cells using PEDOT:PSS have an S-shaped J–V curve. The S-shape for the PEDOT:PSS-containing devices is related to the lower build-in voltage for these devices. As shown by Uhrich et al., S-shape J–V curves are expected for bilayer solar cells when the build-in voltage is lower than the V_{oc}.[3] As shown in Figure 5 the energy level of the PEDOT:PSS layer is higher (less deep) than for the MoO_3 layer and therefore the built-in voltage is reduced when PEDOT:PSS is used. These results were also obtained for cells using dye **2108** (**Figure 6**). This implies that both dyes have a similar behaviour in the solar cells. The V_{oc} of the cells containing the MoO_3 layer is significantly higher (reaching 0.92 V) than what is obtained with the PEDOT:PSS layer. The higher V_{oc} for the cell based on this dye is in part due to the larger bandgap and to the larger built-in voltage when MoO_3 is used as the HTL. Also for these cells (like in those using dye **619**) the IPCE does not resemble the absorption spectrum of the device (Figure S6). The higher contribution of the dye layer to the device absorption is not reflected in a higher IPCE for the cells using the MoO_3 layer. When PEDOT:PSS is used as the HTL, a peak in the IPCE is observed in the wavelength range where the dye absorbs.

There is therefore a trade-off between an increase in the V_{oc} and the reduction of the J_{sc} when using MoO_3 as the HTL. Yet the good fill factors (FF) observed for the cells using MoO_3 leads to superior power conversion efficiencies (PCE) for these cells when compared with those using PEDOT:PSS as the HTL. Quite good PCE values are obtained for devices employing dyes with a PF_6 counterion and that use the MoO_3 as the HTL. They are very similar for both dyes, leading to average PCE values of 2.4 and 2.5% for cells using **2108** and **619**, respectively. Best devices showed even a sligthly higher value of 2.9%.

If the S-shape observed for the above described cells is indeed caused by an insufficient difference between the V_{oc} and the V_{bi}, when PEDOT:PSS is used as the HTL, it should be absent for cells using lower bandgap dyes. To verify this hypothesis, cells were prepared analogous to those mentioned above, yet using dye **2046**. Indeed, virtually no difference is observed in the J–V curves for cells using PEDOT:PSS or those using MoO_3 as the HTL (**Figure 7**). Both devices have very similar fill factors, 49 and 50%. Therefore, it appears plausible that the reason for the S-shapes observed for the cells uing the wider bandgap dyes is due to an insufficient V_{bi} when PEDOT:PSS is used as the HTL. The cells using **2046** also show more clearly the two distinct regions in the IPCE; one region due to the absorption in the fullerene layer (in the 400–500 nm range) and another due to the absorption in the dye layer (in the 550–750 range). This shows clearly that both layers contribute the photocurrent generation. The absoption spectrum of these devices (Figure S7) shows that the dye layer leads to an absorption that is almost twice as high as that

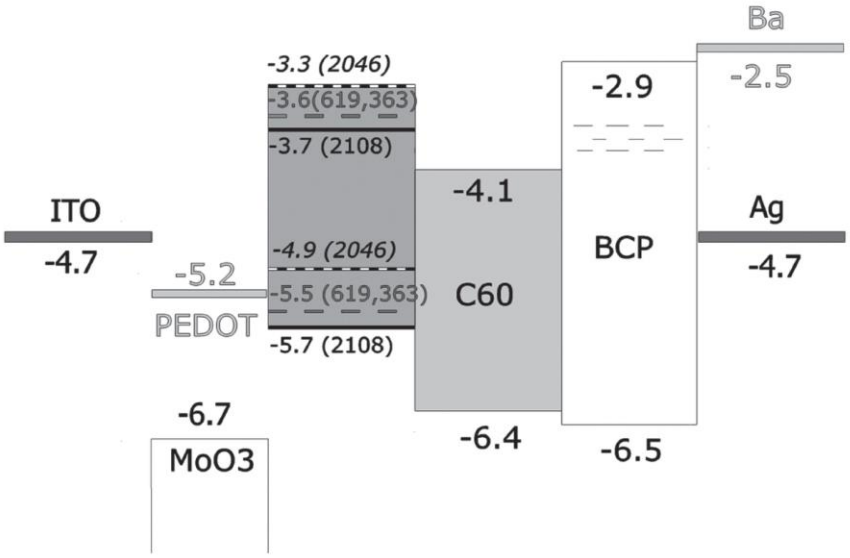

Figure 5. Energy levels of the different materials used in these solar cells.

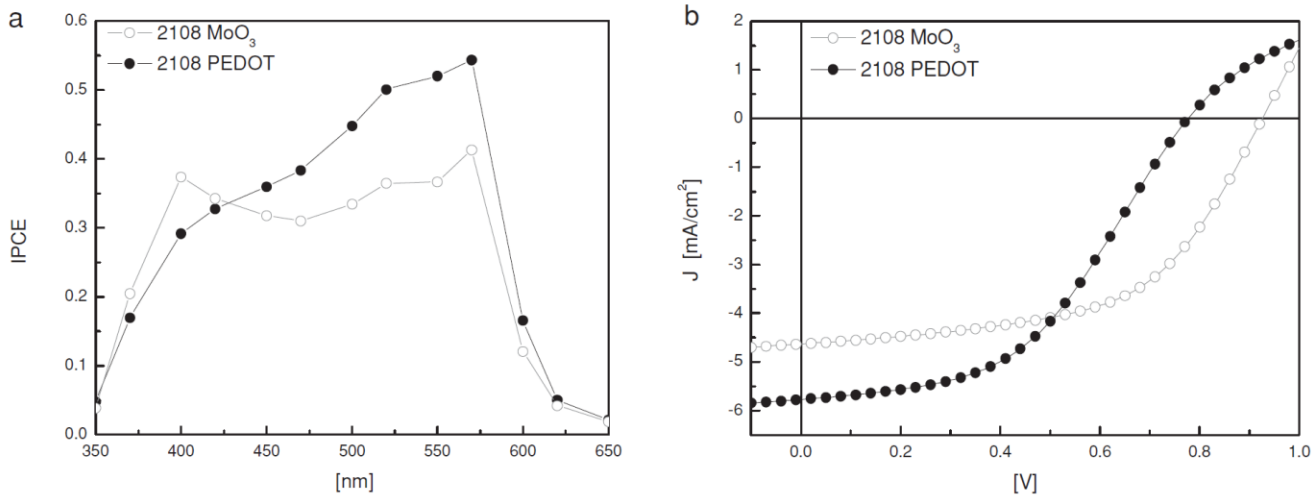

Figure 6. Left, IPCE of the solar cells based on dye **2108** with a PEDOT:PSS (full circles) or a MoO_3 (open circles) anode anode. Right, current density vs voltage for these two devices.

caused by the C_{60} layer. Yet, like in the previously described devices, the IPCE shows an approximately equal contribution from both layers. For this dye no difference is observed for PEDOT:PSS- or MoO_3-based devices, hence the extraction barrier for holes is the same in both cases. The lower IPCE in the wavelength region where the dye absorbs must therefore be related to a lower exciton diffusion/seperation in the dye layer compared to the C_{60} layer, or alternatively is caused by poorer charge carrier mobilities in the dye layer.

3. Conclusions

Simple bilayer solar cells, using commercially available cationic cyanine dyes as donors and evaporated C_{60} layer as an acceptor are prepared. Cyanine dyes with absorption maxima of 578, 615 and 697 nm having either perchlorate or hexafluorophosphate counter-ions were evaluated. Only the dyes with the hexafluorophosphate counter-ions lead to efficient solar cells. When the wide bandgap dyes are employed, S-shape current–voltage curves are obtained when the conductive polymer PEDOT:PSS is used as hole transport layer. Substitution of PEDOT:PSS with MoO_3 leads to cells with more rectangular current–voltage curves and high fill factors. Additionally, the cells using the MoO_3 layer for hole extraction lead to high open circuit voltages of 0.9 V. The performance of the cells employing the lower bandgap dye is independent on the type of hole transport layer employed. Using this approach, bilayer solar cells are obtained with power efficiencies ranging from 1.8 to 2.9% depending on the particular dye employed. These are impressive numbers for bilayer solar cells that are partially solution processed in ambient conditions.

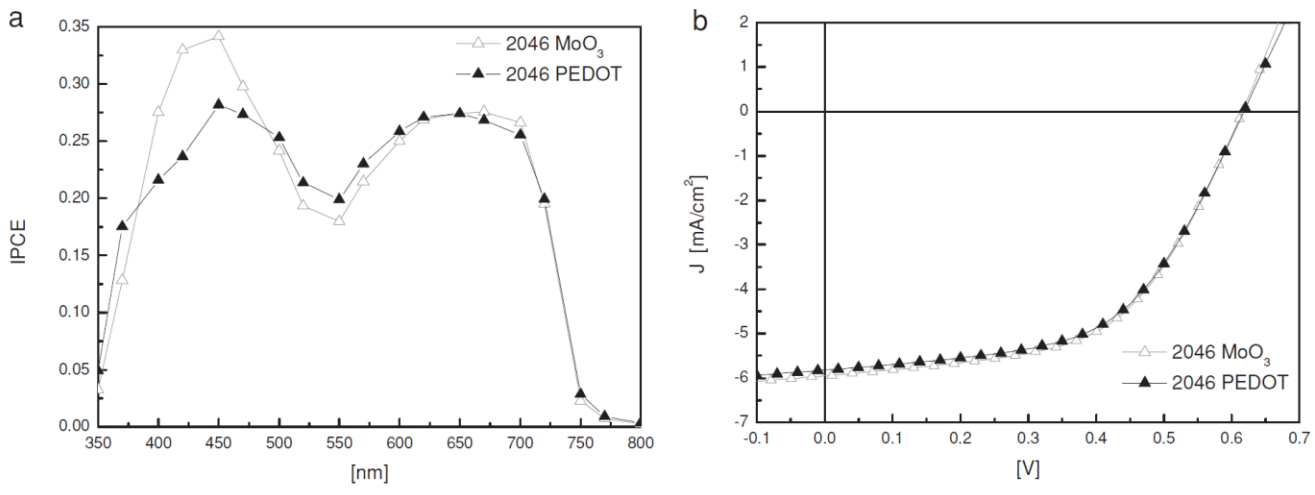

Figure 7. Left, IPCE of the solar cells based on dye **2108** with a PEDOT:PSS (full triangles) or a MoO_3 (open triangles) anode. Right, current density vs voltage for these two devices.

4. Experimental Section

Pre-patterned ITO-covered glass substrates (www.naranjosubstrates.com) where first pre-cleaned using a standard procedure involving a 5 min ultrasonication in detergent, deionized water and isopropanol respectively. UV-ozone treatment was applied for 15 min, after which the samples were immediately transferred in to the metal evaporator. 30nm layers of MoO_3 (ALDRICH) were there evaporated at 0.1 nm/s rate at 2×10^{-6} mbar. The thickness of molybdenum was both checked by profilometer and absorption spectra. In case of the samples without MoO_3 layer, 70nm of PEDOT:PSS (Clevios AI4083, from Hereaus) was spin-coated instead. The PEDOT:PSS was dried by 10 min annealing at 150°C in ambient atmosphere. Cyanine dyes, purchased from Few Chemicals were used as received and were spin coated (1000 rpm) from a chlorobenzene solution (7 mg/ml) in ambient atmosphere resulting in a layer thicknesses of around 30nm. After spin coating of the dye, the substrates were transferred to a nitrogen filled glove box (1 ppm O_2 and <0.1 ppm H_2O) for further processing. 30 nm layer of C_{60} (ALDRICH) and 10 nm of BCP (LUMTEC) were thermally evaporated in a molecular evaporator (7×10^{-7} mbar) followed by thermal evaporation of 5 nm barium and 70 nm silver in a separate vacuum system (2×10^{-6} mbar). Solar cells (with different active areas ranging from 9, 15, 35 to 95 mm^2) were illuminated by a white light halogen lamp in combination with interference filters for the EQE and J–V measurements (MiniSun simulator by ECN the Netherlands). An estimation of the short-circuit current density (J_{sc}) under standard test conditions was calculated by convolving the EQE spectrum with the AM1.5G reference spectrum, using the premise of a linear dependence of J_{sc} on light intensity. Current-voltage (J–V) characteristics were measured using a Keithley 2400 source measure unit. All characterisation was done in a nitrogen filled glove box (<0.1 ppm O_2 and <0.1 ppm H_2O) without exposure to ambient atmosphere. The reproducibility of the device performance is good as can be observed from Figure 3 and S1, S2 and S3 (see supporting information).

Supporting Information

Supporting Information is available from the Wiley Online Library or from the author.

Acknowledgements

This work has been supported by the European Union FP7 program (ORION, 229036), the Spanish Ministry of Science and Innovation (MICINN) (MAT2011-24594, CSD2007-00010) and the Generalitat Valenciana (Prometeo/2012/053).

Received: September 24, 2012
Published onlne:

[1] a) G. Dennler, M. Scharber, C. J. Brabec, *Adv. Mater.* **2009**, *21*, 1323; b) P. Heremans, D. Cheyns, B. P. Rand, *Acc. Chem. Res.* **2009**, *42*, 1740; c) M. A. Green, K. Emery, Y. Hishikawa, W. Warta, E. D. Dunlup, *Prog. Photovolt. Res. Appl.* **2012**, *20*, 12; d) G. Li, R. Zhu, Y. Yang, *Nature Photon.* **2012**, *6*, 153.

[2] C. W. Tang, *Appl. Phys. Lett.* **1986**, *48*, 183.

[3] C. Uhrich, D. Wynands, S. Olthof, M. K. Riede, K. Leo, S. Sonntag, B. Maenning, M. Pfeiffer, *J. Appl. Phys.* **2008**, *104*, 43107.

[4] a) F. Meng, K. Chen, H. Tian, L. Zuppiroli, F. Nuesch, *Appl. Phys. Lett.* **2003**, *82*, 3788; b) H. Bürckstümmer, N. M. Kronenberg, M. Gsänger, M. Stolte, K. Meerholz, F. Würthner, *J. Mater. Chem.* **2010**, *20*, 240; b) B. Fan, R. Hany, J. Moser, F. Nuesch, *Org. Electr.* **2008**, *9*, 85; c) X. Ma, J. Hua, W. Wu, Y. Jin, F. Meng, W. Zhan, H. Tian, *Tetrahedron* **2008**, *64*, 345; d) M. Lenes, H. J. Bolink, *ACS Appl. Mater. & Inter.* **2010**, *2*, 3664; e) O. Malinkiewicz, M. Lenes, H. Brine, H. J. Bolink, *RSC Adv.* **2012**, *2*, 3335.

[5] T. H. James, *The Theory of the Photographic Process*, Macmillan, Collier Macmillan, New York, London **1977**.

[6] R. Hany, B. Fan, F. Araujo de Castro, J. Heier, W. Kylberg, F. Nuesch, *Prog. Photovolt. Res. Appl.* **2011**, *19*, 851.

[7] a) B. Fan, F. A. Castro, J. Heier, R. Hany, F. Nuesch, *Org. Electr.* **2010**, *11*, 583; b) B. Fan, F. Araujo de Castro, B. T. Chu, J. Heier, D. Opris, R. Hany, F. Nuesch, *J. Mater. Chem* **2010**, *20*, 2952.

[8] a) V. Shrotriya, G. Li, Y. Yao, C.-W. Chu, Y. Yang, *Appl. Phys. Lett.* **2006**, *88*, 073508; b) S. Tokito, K. Noda, Y. Taga, *J. Phys. D: Appl. Phys.* **1996**, *29*; c) T. Matsushima, Y. Kinoshita, H. Murata, *Appl. Phys. Lett.* **2007**, *91*, 253504; d) H. Kanno, R. J. Holmes, Y. Sun, S. Kena-Cohen, S. R. Forrest, *Adv. Funct. Mater.* **2006**, *18*, 339; e) J. Meyer, A. Shu, M. Kröger, A. Kahn, *Appl. Phys. Lett.* **2010**, *96*, 133308; f) M. Sessolo, H. J. Bolink, *Adv. Mater.* **2011**, *23*, 1829.

[9] a) S. R. Hammond, J. Meyer, N. E. Widjonarko, P. F. Ndione, A. K. Sigdel, A. Garcia, A. Meidaner, M. T. Lloyd, A. Kahn, D. S. Ginley, J. J. Berry, D. C. Olson, *J. Mater. Chem 22*, 3249; b) K. Zilberberg, H. Gharbi, A. Behrendt, S. Trost, T. Riedl, *ACS Appl. Mater. Interfaces* **2012**, *4*, 1164; c) C. Girotto, E. Voroshazi, D. Cheyns, P. Heremans, B. P. Rand, *ACS Appl. Mater. Interfaces* **2011**, *3*, 3244.

[10] H. Gommans, B. Verreet, B. P. Rand, T. Muller, J. Poortmans, P. Heremans, J. Genoe, *Adv. Funct. Mater.* **2008**, *18*, 3686.

[11] H. Benmansour, F. A. Castro, M. Nagel, J. Heier, R. Hany, F. Nuesch, *Chimia* **2007**, *61*, 787.

PEROVSKITE SOLAR CELLS

PEROVSKITE SOLAR CELLS

1. Development of perovskite evaporation technique

The co-evaporation of different precursors was used in order to produce thin films of $CH_3NH_3PbI_3$ (MAPI) perovskite material[42]. This technique is for example widely used for fabricating OLED displays and OPV, where the active layers consist from more than one compound[43] (Alq_3 and NPB as examples). In the co-evaporation technique, the film thickness can be varied from few nanometers up to one micron with 5 nm precision, being mandatory to employ high vacuum conditions. The process of dual-source vapour deposition of lead iodide PbI_2 and organic methyl ammonium iodide CH_3NH_3I (MAI) was first described in the work of Masanao Era et al. in 1997[44]. Different elements are heated up to the point of either evaporation or sublimation. The evaporated atoms are condensed on a substrate which is located in the line-of-sight of the sources. The deposition rate is determined by the source area, source temperature and the distance between the source and the substrate. The condensed atoms arranges on the substrate due to the surface and bulk diffusion. In order to achieve a high degree of uniformity, the sample holder is rotating during the whole deposition process as it is schematically shown on Figure 10.

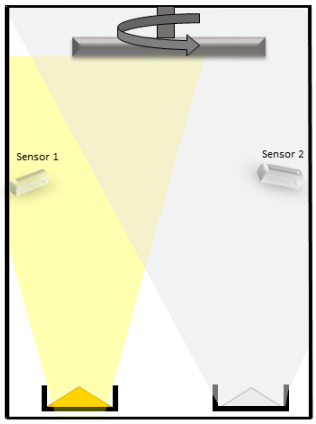

Figure 10. Scheme of the co-evaporation process

Co-evaporation of hybrid organic-inorganic perovskite was extensively studied and developed resulting in the formation of highly reproducible, crystalline and compact

perovskite layers. The use of this technique enabled the preparation of large area devices, achievement that was described as a "significant milestone in perovskite photovoltaic research" by Nature Photonics magazine[38].

Layered perovskites are crystalline materials, usually prepared by crystal growth from solution phase. In the solution method, appropriate amounts of perovskite precursors (e.g. metal halide PbI_2, SnI_2, etc. and the organic ammonium halide) are dissolved in organic solvents such as DMF and DMSO. The perovskite crystals are allowed to grow through evaporation of solvents. Because the crystal growth occurs spontaneously, a typical solution processing technique like spin-coating has difficulty in the precise control of the film thickness and film structure. Resultant crystalline layers from the solution methods, exhibit very high roughness and enable only the fabrication of small area devices due to poor layer uniformity. For large area processing, the preparation of high-quality crystalline material with a large grain size and high purity is required. In this sense, the best method would be associated to the growing of a single compact perovskite crystal. For the preparation of such high-quality single crystals, the crystal growth technique from the melt phase which has been well developed in the present semiconductor technology is preferable (e.g. silicon). Unfortunately, this strategy it is not applicable for layered perovskites due to their decomposition before melting. Additionally, it would be impossible to apply this technique on thermal fragile substrates, such as PET foils, due to the high processing temperatures. In the context of this Thesis, we set out to develop a self-organized growth method for layered perovskite films, denoted as vapour deposition method.

The main challenge in this process was the evaporation of the MAI precursor, which is a volatile organic salt that can decompose easier than the inorganic counterpart. Thus, it is a very difficult material to evaporate in a controlled way using a quartz sensor. Hence, we decided to set a chamber vacuum pressure by heating the MAI crucible at fixedconditions.

In this situation, we changed the evaporation rate of PbI_2 by adapting the source temperature from 250 to 260˚C. As PbI_2 is an inorganic material, its evaporation rate is easily controlled by a classic quartz sensor.

The resulting perovskite films were than analysed using X-ray diffraction (XRD) . In Figure 11, the diffraction patterns are shown for films as a function of PbI2 evaporation temperatures. The XRD measurement showed the tendency of the perovskite to decompose when the PbI2 was evaporated above 260˚C. This is evidenced by the appearance of the characteristic signal at 12 ˚ which can be assigned to PbI_2 as shown in figure 11.

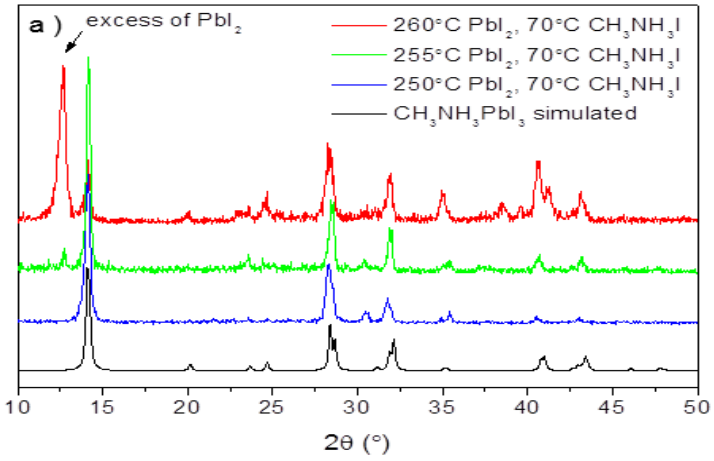

Figure 8. XRD-spectrum for perovskite obtained by a co-evaporation process carried at different temperatures[46].

This approach turned out to be successful ,allowing to set certain conditions that could be afterwards extended to successive processes. All the details about perovskite film fabrication from vapour phase are described in the method section of the publications inserted after this chapter. [42,46].

One of the critical issues that has to be considered in this process is the fact that perovskite is highly sensitive to water presence. Thus, the amine precursor has to be completely dry, otherwise, the trapped water can evaporate and disrupt the process.

The morphology of the obtained crystal perovskite layer was determined by AFM and SEM measurement and depicted in figure 12. The prepared layers exhibit high compactness with extremely low roughness and didn't require any post treatment in order to obtain good quality perovskite.

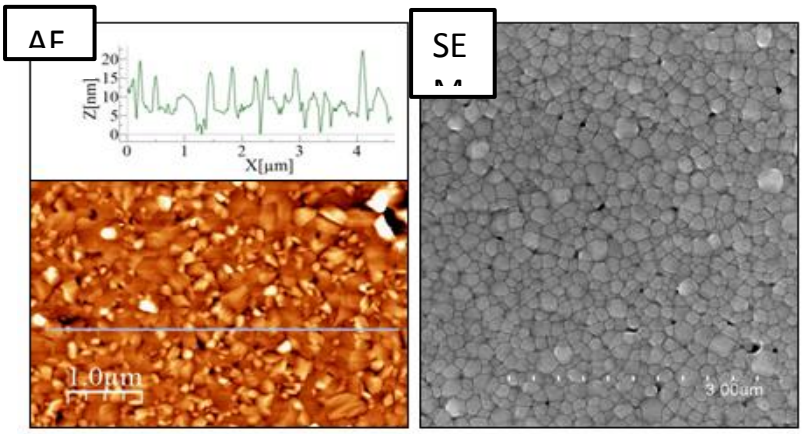

Figure 12. Atomic Force Microscopy and Scanning Electron Microscopy images of evaporated perovskite layers[46].

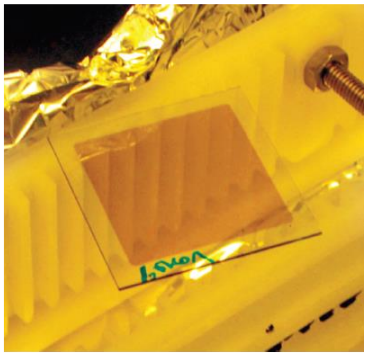

Figure13. One of the first evaporated perovskite layers, 50nm thickness.

Two possible growth mechanisms for the formation of layered perovskite structures via dual-source vapour deposition method were proposed in the work of Era et *al.* who was the first to achieve a high degree of crystallinity on the perovskite material via thermal evaporation[44]. In a first scenario, it was described a process in which the layered perovskite structure is formed already in vapour phase, subsequently deposited in the substrate by adhesion. On an alternative case, it was proposed that the growing of the layered perovskite takes place in the solid phase directly onto the substrate. The results of the experiments performed by M. Era et *al.* clearly

confirmed a process in which the perovskite structure is formed by the intercalation of organic ammonium iodide into the solid PbI_2 film already present in the substrate. Moreover, it is possible to consider that the self-organizing intercalation of CH_3NH_3I into the PbI_2 film promotes the rearrangement of the aggregated structure of PbI_2 and the formation of an oriented layered perovskite film in the dual vapour deposition of the two precursors. This technique was later successfully implemented by Oxford University, in prof. Henry Snaith group, to fabricate the sublimed perovskite based solar cells[45]. In this work, flat films of the mixed halide perovskite $CH_3NH_3PbI_{3-x}Cl_x$ were created by a dual-source vapour deposition from lead chloride ($PbCl_2$) and methylamonium iodide (CH_3NH_3I) which were evaporated simultaneously under high vacuum, onto the TiO_2-compact-layer-coated FTO substrates. This work was of great importance, because it was the first planar heterojunction thin-film perovskite architecture that has a solar-to-electrical power conversion efficiency (PCE) of over 15% with an open-circuit voltage of 1.07 V. This result showed that no mesoporous structure is necessary to build efficient devices, as well as presenting perovskites as excellent electron and hole conductors. Nevertheless, a TiO_2 electrode was still necessary to be used as a compact layer, limiting the fabrication of devices only to glass substrates. Additionally, samples needed to be heated after perovskite deposition as a post-treatment to enhance crystallization.

A distinct advantage of vapour deposition over solution processing is the ability to prepare layered multi-stacked thin films over large areas. The process of dual evaporation of perovskite is compatible with dry processing for the preparation of semiconductor films and devices in vacuum. Although ultimately an ‘all-perovskite’ multi-junction cell should be realizable, the perovskite cells have now achieved a performance that is sufficient to increase the absolute efficiency of high-efficiency crystalline silicon and copper indium gallium (di)selenide solar cells[49]. Additionally, because vapour deposition of the perovskite layers is entirely compatible with conventional processing methods for silicon wafer- based and thin-film solar cells, the

infrastructure is already in place to scale up this technology. Moreover, the band gap alignment of hybrid perovskite gives an opportunity to fabricate perovskite/silicon and perovskite/CIGS tandem cells with improved efficiency[50,51]. In this sense, the co-evaporation approach can potentially enable the fabrication of this kind of devices in one process, as vacuum deposition is commonly used in the field of thin-film photovoltaic technologies.

2. Devices

As shown in Chapter 3.2.1 smooth compact perovskite films can be prepared using the dual source evaporation method. The size of the crystal grains obtained in the evaporation process were different form one process to another, however, we found out that it has no impact on the process and the macroscopic properties of the device (such as power conversion efficiency). The simplest reason is that our crystals were grown from bottom to top (very elongated shape) in a monolithic configuration, (see SEM cross-section[56]) with the appearance of boundaries in between. Additionally, Yanfa Yan calculated that the discontinuities on the boundaries are not energetically attractive to trap the electrons and therefore, probably are not very important for the transport of charges in a solar cell[57].

a. Device architecture

All existing architectures used in the production of efficient perovskite based solar cells are based on the idea of sandwiching the intrinsic perovskite absorber between two layers, where one is a hole conductor (p-type layer) and a second is an electron conductor (n-type layer). This system was found to be very effective in generating a potential within the cell, which is necessary to pull out the charges generated inside the perovskite material after light absorption. Because the perovskite cells evolved from DSSC cells (see introduction part), the most frequently used n-type layer is TiO_2 which requires a high sintering temperature, eliminating the possibility of using fragile substrates like PET.

Initially, we tried to grow the perovskite on TiO_2 substrates to check the differences between the spin-coated and evaporated perovskite layer in a common DCCS architecture, as developed by H. Snaith group. However, this strategy was not successful, mainly due to the large hysteresis effect and low FF´s present in the devices even under the presence of a HTM layer. Some results illustrating the low performance of the first trials based on the conventional architecture for the device devices are depicted in figure 12. In this context, many different HTM's materials were tested without a positive impact on performances. Although most of these devices show a good external quantum efficiency (EQE), expressed as the ratio of electrical power over incident optical power as a function of illumination wavelenght , they exhibited a very low current density for the voltages corresponding to the working window of the solar cell. Only by applying high negative voltages it was possible to reach significant levels of current density. The EQE experiments are performed at much lower light intensities and at 0V, hence the carrier densities are much lower then under 1 sun equivalent illumination and the driving force for charge extraction is high (closed circuit condition with a large build in voltage).

This is a clear example of a charge extraction problem in the devices, which could be in principle associated to the application of the planar TiO_2 in our device architecture as having this material unfavourable electrical properties such as low electron mobility and conductivity[58]. It may also be related to the use of undoped hole transporters, as most hole transporters used in the TiO2 based devices are partially oxidized to improve the charge transport and extraction.

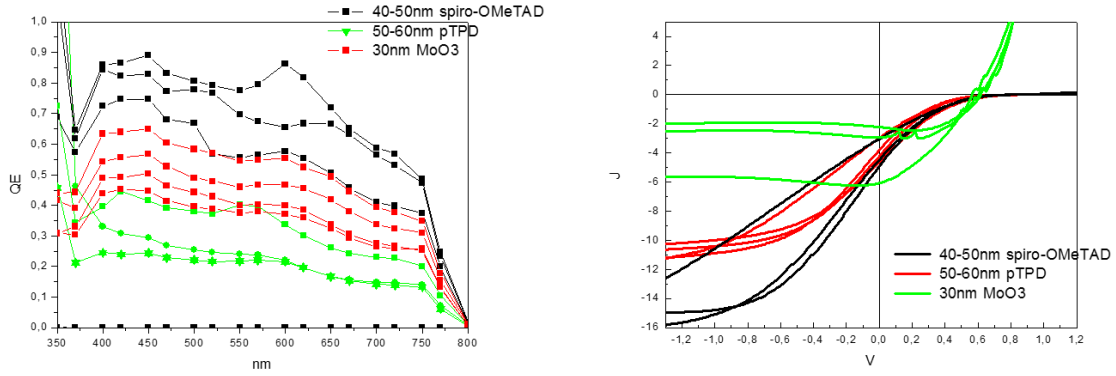

Figure 14. Characterization of perovskite solar cells based on device architecture: ITO/TiO2_planar/perovskite 300nm/HTM/Au.

In parallel we tried to use another architecture, not from DCCS but based on a typical OPV architecture (like the one described in the previous chapter), where the active absorber is placed onto a PEDOT layer. This strategy of employing only PEDOT as the electron blocking layer was not entirely successful. A negative impact of the physical properties of PEDOT in the device performance, such as too high conductivity, was discarded by the reported works in literature describing highly efficient perovskite solar cells based on this type of architecture[59]. Thus, the behaviour exhibited by our solar cells was in principle ascribed to two possible factors. From one part it could be due to a deficient thickness of the perovskite layer. On the other hand, it could be the result of an aggressive evaporation process of the metal electrode, leading to important defects in the device structure.

The breakthrough in this work came when a low-conductivity poly-TPD layer was inserted between the PEDOT and the perovskite layer in our device architecture. All the crystals were grown by evaporation on the amorphous poly-TPD polymer, which was used in our architecture as an electron blocking layer. Evaporation provided in this sense a great advantage with respect to spin coating, where the wetting of the poly-TPD by the perovskite precursor solution would be practically impossible. By employing poly-TPD the device showed a photovoltaic performance for the first time, with decent efficiencies and high FF and under the absence of

an electron transporting layer in our architecture. The work of L. Etgar et al. already demonstrated the good performance of hole conductor free solar cells, showing in this way that perovskite can act as a light harvester and as a good hole transporting material[60]. In this sense, our experiments suggested that perovskite can act as well as a good electron transporting material in the solar cell architecture.

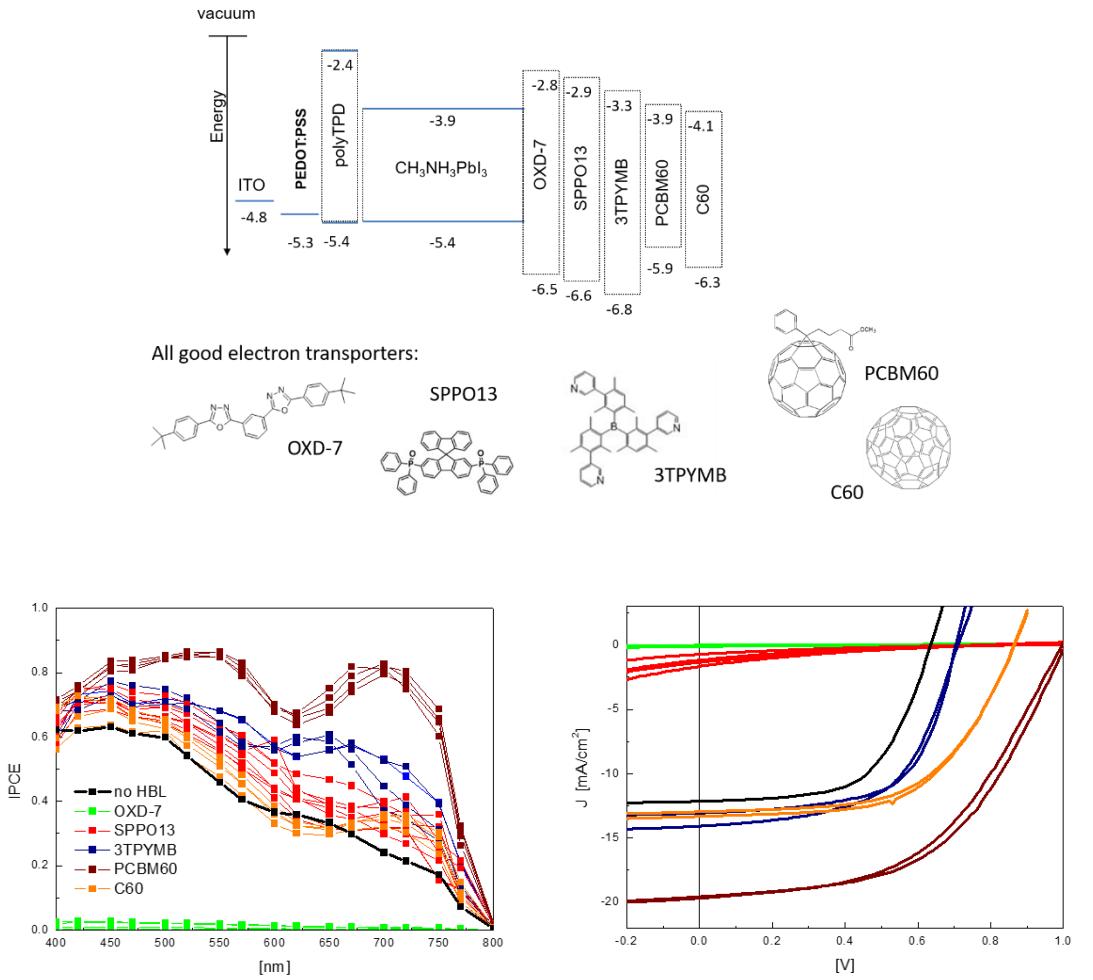

Figure 15. Influence of different hole and electron transport materials on the performance of the solar cells.

The final improvement in the architecture, leading to the highest efficient devices, was obtained by the choice of an effective n-type layer[42,61] (figure 15). In this context, the use of PCBM as the electron transport layer in this architecture was the first example of this kind in literature. The inclusion of a PCBM layer in the device lead to outstanding results in terms of performance. Additionally, our champion device was characterized in the facilities of EPFL with an absence

of hysteresis in the J-V curve (figure 16) from the first moment, supposing as well a very remarkable success. This highly positive effect, both in performance and hysteresis, can be understood as a result of a perovskite trap passivation induced by the presence of PCBM. In this context, the electron recombination at the perovskite surface reduces drastically the electron extraction efficiency. Thus, the PCBM layer onto the perovskite films can effectively passivate these electron traps and markedly reduce the interface charge recombination, which leads to an important improvement of the current densities and FF in the device as well as an elimination of the hysteresis problem[62].

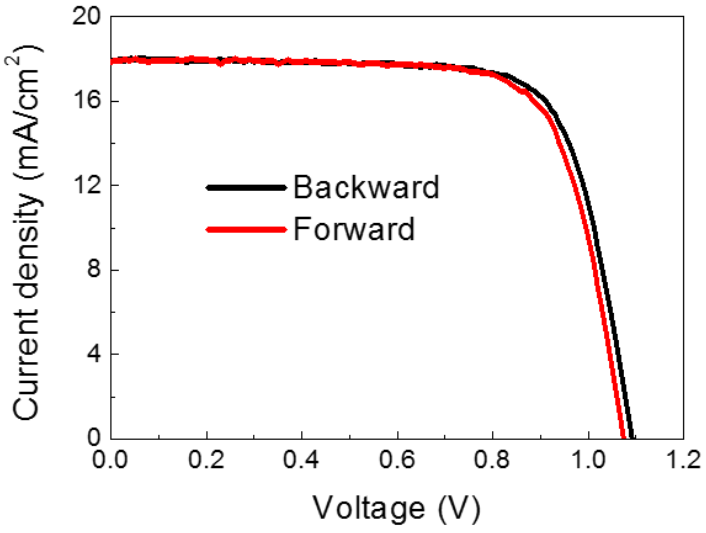

Figure 16. Champion device characterized in the facilities of EPFL showing absence of hysteresis.

By employing this architecture, it was possible to perform an exhaustive thickness optimization of the perovskite layer, determining a value of 300 nm as the most suitable for the device peroformance[63].

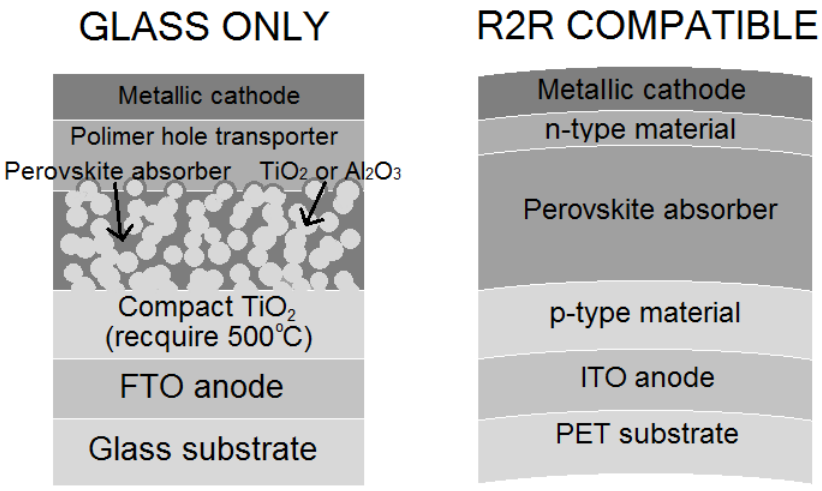

Figure 17 Device architectures

From all this work, it is very important to remark that the whole device architecture proposed was highly innovative and, what is more important, it was the first example in literature of an oxide-free architecture exceeding 10% efficiency. Indeed, in 2014 almost no group was applying this strategy, but nowadays it is becoming much more popular due to the many advantages with respect to the use of TiO_2 . Inverting the device architecture, with a substitution of a TiO_2 oxide layer by an organic fullerene, allows a low cost and room temperature processing using economically favourable materials, which is extremely attractive for the industry sector. As a particular example, it is the possibility of extending the fabrication of these devices to a roll-to-roll (R2R) production line when using polymeric flexible substrates, allowing the direct transfer of this technology from laboratory to industry (figure 17).

It is worthy to mention that in this configuration, the devices did not reach record efficiencies (typically an open-circuit voltage (V_{OC}) of 1.05 V, a short-circuit current density (J_{SC}) of 18.8 $mAcm^{-2}$, and a fill factor (FF) of 0.64, which lead to average PCE of 12.4%) but despite of that , they were highly reproducible and did not suffer from hysteresis effects that hamper many other perovskite architectures.

b. Large area devices:

The ability to make large-area devices reproducibly is critical in practice, however almost all the best-performing cells reported to date have areas of <0.1 cm^2. Additionally, the fabrication methods used nowadays (e.g. spin-coating) allow for obtaining relatively small area solar cells (< 0.5 cm^2). Because of the self-assembly, crystalline nature of halide perovskites, and results obtained by using spin-coating makes simply impossible to apply this technique in a larger scale. In this sense, the report of a 1cm^2 perovskite solar cell with an efficiency higher than 8% was referred as a "significant milestone in perovskite photovoltaic research" by Nature Photonics magazine.

c. Flexible and Semi-transparent cells:

Finally, it was also possible to implement perovskite-based semitransparent[47] and flexible[48] devices demonstrating the full potential of the developed technology and unique device architecture. Currently, all the research and development work in this field concerns on the perovskite deployment on rigid surfaces as glass. This removes one of the main advantage of the perovskites, i.e. their lightness and flexibility. The flexible and semi-transparent devices based on our unique architecture are exhaustively described in the correspondent references associated to this thesis (and copied completely after chapter 3)[47,48].

d. Radiative efficiency:

The radiative efficiency can be considered as a key figure of merit, which determines of how far a certain PV technology is from its upper limit of operation. Having this information makes possible the comparison of performances between different PV technologies. Under open circuit (V_{oc}) conditions, charges are not allowed to flow in the solar cell, thus they will recombine as a unique alternative. An ideal solar cell would be the one in which the flux of emitted photons, in open circuit conditions, is equal to the flux of absorbed photons. Under this

situation, the cell is considered to be in the "radiative limit", exhibiting the highest efficiency and V_{oc}. When comparing a methylamonium lead iodide perovskite cell with a model organic cell (bulk heterojunction of MDMO-PPV:PCBM), it has been observed a radiative efficiency of around 190 times higher for the former one with a much sharper band-to-band transition. This feature in the hybrid perovskite solar cell makes possible to reach V_{oc} values closer to the maximum value associated to the radiative limit. Thus, the high radiative efficiency detected for a methylamonium lead iodide perovskite situates this PV technology over other alternatives such as amorphous silicon, DSSC and CdTe, showing its enormous potential as renewable energy source[64].

3. Summary

In this thesis co-evaporation process was optimized resulting in excellent quality, compact and pinhole free perovskite layers, which were employed in simple, innovative architecture compatible with flexible substrates. It is metal oxide free, prepared using room temperature processing with average efficiencies of 12% (champion cell 15%). It uses a methylammonium lead iodide ($CH_3NH_3PbI_3$) perovskite layer sandwiched in between two thin organic charge transport layers polyarylamine (polyTPD, p-type material) and [6,6]-Phenyl C_{61}-butyric acid methylester (PCBM, n-type material)[42] . Combination of the excellent film control and reproducibility with simple device architecture allowed many interesting studies, including:

- the influence of different hole and electron transport materials[46] on the device performance,
- comparison of the electrodes with the different work functions[46],
- effect of the thickness of the perovskite absorber [71]
- radiative efficiency of the perovskite cells[64].

It was also possible to describe the effect of increasing cell area on the cell efficiency.

LETTERS
PUBLISHED ONLINE: 22 DECEMBER 2013 | DOI: 10.1038/NPHOTON.2013.341
nature photonics

Perovskite solar cells employing organic charge-transport layers

Olga Malinkiewicz[1], Aswani Yella[2], Yong Hui Lee[2], Guillermo Mínguez Espallargas[1], Michael Graetzel[2], Mohammad K. Nazeeruddin[2]* and Henk J. Bolink[1]*

Thin-film photovoltaics play an important role in the quest for clean renewable energy. Recently, methylammonium lead halide perovskites were identified as promising absorbers for solar cells[1]. In the three years since, the performance of perovskite-based solar cells has improved rapidly to reach efficiencies as high as 15%[1–10]. To date, all high-efficiency perovskite solar cells reported make use of a (mesoscopic) metal oxide, such as Al_2O_3, TiO_2 or ZrO_2, which requires a high-temperature sintering process. Here, we show that methylammonium lead iodide perovskite layers, when sandwiched between two thin organic charge-transporting layers, also lead to solar cells with high power-conversion efficiencies (12%). To ensure a high purity, the perovskite layers were prepared by sublimation in a high-vacuum chamber. This simple planar device structure and the room-temperature deposition processes are suitable for many conducting substrates, including plastic and textiles.

The hybrid organic–inorganic methylammonium lead halide perovskites, pioneered by Mitzi, are recognized for their excellent semiconducting properties[11,12]. Following the pioneering work of Miyasaka and co-workers[1], the ease with which these organic–inorganic hybrid perovskite materials can be prepared and processed from solution makes them attractive for photovoltaic applications[13]. In their studies, the methylammonium lead iodide perovskite was used as a sensitizer in liquid dye-sensitized solar cells and an efficiency of 3.8% was obtained. The low efficiency results from the solubility of the perovskite layer in the iodine/iodide redox electrolyte system. High efficiencies have been realized by replacing the liquid electrolyte with a solid hole-transporting material such as 2,2′,7,7′-tetrakis(*N*,*N*-di-*p*-methoxyphenylamine)-9,9′-spirobifluorene (spiro-MeOTAD), as reported by the groups of Snaith and Graetzel[2–9]. Interestingly, Lee *et al.*[6] showed that a mixed-halide perovskite on a mesoporous Al_2O_3 photoanode acts both as a light absorber and an electron conductor. Etgar *et al.*[8] reported that the pure methylammonium lead iodide perovskite also acts as an efficient hole conductor. Recently, Burschka *et al.*[4] published a high power-conversion efficiency of 15% for a solar cell in which the perovskite was deposited by a novel sequential deposition technique on a mesoporous TiO_2 film. Ball *et al.*[5] showed that a thick layer (350 nm) of the mixed-halide methylammonium lead perovskite ($CH_3NH_3PbI_{3-x}Cl_x$) leads to efficient solar cells (12%). They argue that the perovskite functions as the absorber and as the electron and hole transporter. Additionally, it was suggested that the excitons dissociate predominantly in the bulk and not at a donor–acceptor interface. The operating mechanism of planar perovskite solar cells, however, is not clear. For example, it was shown that the photoluminescence of a mixed-halide methylammonium lead perovskite was reduced strongly when either a hole- or an electron-transporting layer was deposited on top of it[14]. A similar effect, but less strong, was observed for thin films of the pure iodide methylammonium lead perovskite[14]. Hence, exciton dissociation may occur both in the bulk and at the perovskite interface. Currently, the dominant process is not established and may well depend on the exact nature of the perovskite film. Up to now, the highest efficiency was reported by Liu *et al.*, who used a thin metal oxide layer and a sublimed perovskite layer that leads to solar cells with an efficiency of 15.4%[9]. High material purity is essential for efficient charge-carrier transport and to prevent exciton quenching, as established in organic light-emitting diodes and organic photovoltaic (OPV) devices[15,16]. Therefore, in these devices vacuum sublimation is employed frequently to achieve high-purity layers. Solution-processed perovskites are generated *in situ* and therefore may contain imperfections and impurities. Purification of the perovskite layer is not possible as it decomposes on dissolving.

An inverted layout, similar to that employed in small molecular weight and polymeric solar cells, has also been described[17,18]. In these bilayer planar heterojunction devices, the perovskite layer was used as the electron donor in combination with an electron acceptor, in analogy to a frequently used OPV layout. The holes are extracted via the transparent conductor poly(3,4-ethylenedioxythiophene):poly(styrenesulfonic acid) (PEDOT:PSS). The device performances, however, were significantly inferior to those of devices that employ (mesoporous) metal oxides.

Here, we present an inverted thin-film solar cell based on a sublimed methylammonium lead iodide perovskite layer sandwiched between two very thin electron- and hole-blocking layers that consist of organic molecules. The organic materials were deposited using solution-based processes, whereas the $CH_3NH_3PbI_3$ perovskite and the metal contact were deposited using thermal evaporation under vacuum. These simple devices, free of metal oxide and prepared using room-temperature processing, reach efficiencies as high as 12% at 100 mW cm^{-2}, which demonstrate their potential for a wide variety of photovoltaic applications.

The $CH_3NH_3PbI_3$ perovskite thin film was prepared by coevaporation of the two starting compounds, CH_3NH_3I and PbI_2. Details of the experimental conditions are given in the Methods section. These films were characterized using grazing incidence X-ray diffraction (GIXRD). Initially, excess PbI_2 was present in the film, yet on optimizing the evaporation process, highly oriented pure $CH_3NH_3PbI_3$ films were obtained (see Fig 1a and Supplementary Fig. 1). The films adopt the typical tetragonal structure for $CH_3NH_3MX_3$ hybrid perovskites (M = Pb, Sn; X = Cl, Br, I) formed by a three-dimensional anionic framework of PbI_6 octahedra with the methylammonium cations in the interstitial space (see Fig. 1b)[19]. The roughness of the $CH_3NH_3PbI_3$ film was evaluated using atomic force microscopy (AFM) and an image of a typical

[1]Instituto de Ciencia Molecular, Universidad de Valencia, C/Catedrático J. Beltrán 2, 46980 Paterna (Valencia), Spain, [2]Laboratory of Photonics and Interfaces, Swiss Federal Institute of Technology (EPFL), Station 6, Lausanne, CH 1015, Switzerland. *e-mail: mdkhaja.nazeeruddin@epfl.ch; henk.bolink@uv.es

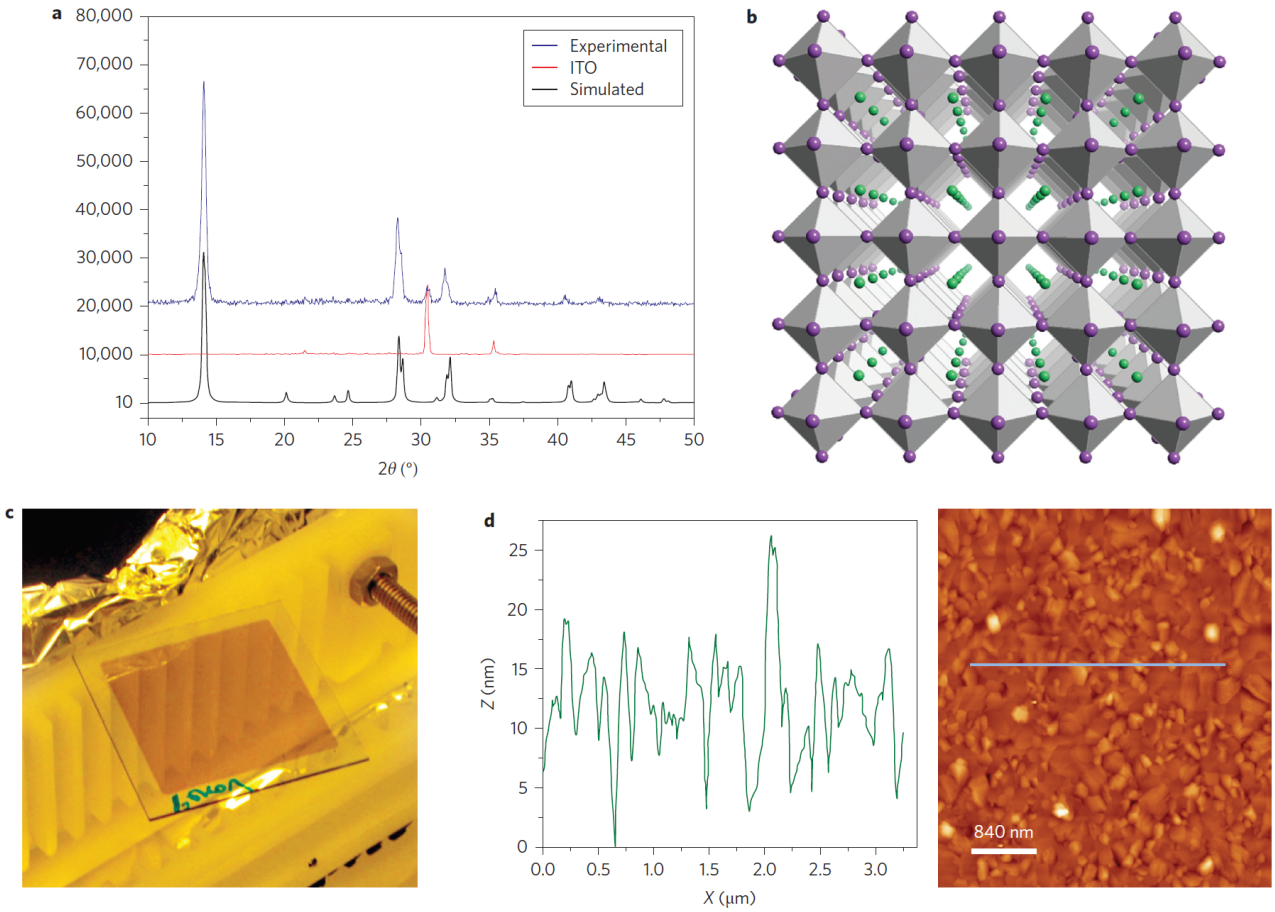

Figure 1 | Characteristics of the sublimed $CH_3NH_3PbI_3$ perovskite layer. a, GIXRD pattern with Cu $K\alpha_1$ radiation ($\lambda = 1.54056$ Å) of the sublimed thin film (blue), ITO substrate (red) and calculated for $CH_3NH_3PbI_3$ with preferred orientation along the (100) and (001) directions. **b**, Simulation of the crystal structure of $CH_3NH_3PbI_3$ perovskite. Pb atoms are placed at the centre of the grey octahedrons, lavender spheres represent iodine atoms and green spheres represent the methylammonium cations. **c**, Photograph of a 20-nm-thick film. **d**, AFM image and profile of a 60-nm-thick film.

scan is given in Fig. 1d, which demonstrates a smooth film with a root mean square roughness of 5 nm. Figure 1c is a photograph of a 20-nm-thick film.

As the $CH_3NH_3PbI_3$ layer is prepared via vacuum sublimation, it can be implemented easily in different device architectures. To demonstrate that the $CH_3NH_3PbI_3$ is capable of performing most of the roles required to obtain an efficient solar cell and to minimize the use of costly organic semiconductors, a simple device structure was chosen. In this structure, which is typical for both organic photovoltaic and light-emitting devices, a semitransparent organic conductor was used as the positive charge-collecting contact. The structure of the device is shown in Fig. 2a, and consists of a 70 nm PEDOT:PSS layer and a thin layer (<10 nm) of poly(*N*,*N*′-bis(4-butylphenyl)-*N*,*N*′-bis(phenyl)benzidine) (polyTPD) (Fig. 2c) as the electron-blocking layer. On top of this, the $CH_3NH_3PbI_3$ was evaporated thermally to a thickness of 285 nm followed by a thin layer (<10 nm) of (6,6)-phenyl C_{61}-butyric acid methyl ester (PCBM) as the hole-blocking layer (Fig. 2d)[20]. The device was completed by the evaporation of an Au top electrode (100 nm). Both the polyTPD and the PCBM layers were deposited using a meniscus-coating process to ensure high-quality films[21]. The thickness of the layers was established using absorbance measurements.

The relevant energy levels of the materials used to prepare the solar cell are depicted in Fig. 2b. The valence band (VB) and conduction band (CB) of the $CH_3NH_3PbI_3$ perovskite are −5.4 and −3.9 eV, versus vacuum, respectively[7]. On illuminating the device, excitons are generated in the $CH_3NH_3PbI_3$ perovskite layer. It was reported that excitons in $CH_3NH_3PbI_3$ perovskites are of the Wannier–Mott type, which implies that they may dissociate in the bulk of the perovskite layer[5,12]. Owing to the use of indium–tin oxide (ITO)/PEDOT:PSS as the hole-collecting contact and Au as the electron-collecting electrode, the built-in voltage of this device is small. Hence, to direct the flow of electrons and holes, thin hole-blocking and electron-blocking layers are incorporated adjacent to the perovskite layer. PolyTPD and PCBM were selected for this role as their highest occupied molecular orbital (HOMO) and lowest unoccupied molecular orbital (LUMO) levels, respectively, match well with the VB and CB of the perovskite, which allows for a good transport of holes towards the polyTPD and of electrons to the PCBM layer (Fig. 2b). As the LUMO of polyTPD is significantly closer to vacuum compared with that of the perovskite CB, polyTPD efficiently blocks the flow of electrons. The opposite process, the blocking of holes, occurs at the perovskite–PCBM interface because of the lower HOMO of PCBM compared with that of the perovskite VB. As mentioned above, exciton dissociation may also occur at the perovskite–polyTPD and perovskite–PCBM interfaces[14].

Figure 3a shows the current–voltage (J–V) characteristics of a typical small-area (0.09 cm^2) perovskite solar cell measured in the dark and under light intensities of 100, 50 and 10 mW cm^{-2}. The

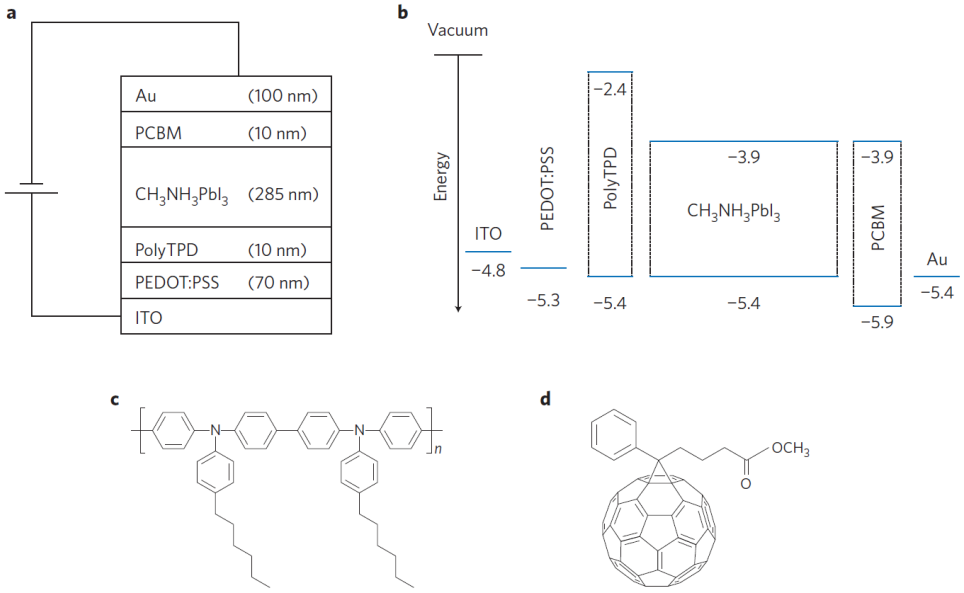

Figure 2 | Schematics of the device. a, Stacked layer structure. **b**, Schematic of the relative energy levels of each layer. **c**, Chemical structure of the polyarylamine (polyTPD). **d**, Chemical structure of PCBM.

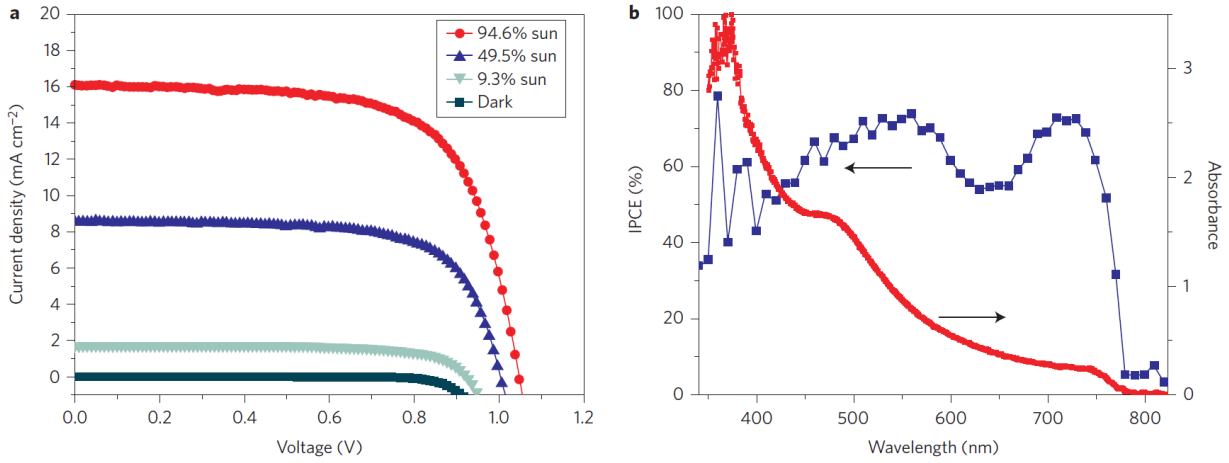

Figure 3 | Typical *J*–*V* and IPCE characteristics of the perovskite solar cell. a, Photocurrent density versus voltage at 100, 50 and 10 mW cm^{-2} and in the dark. **b**, IPCE spectrum and absorbance of a 285-nm-thick perovskite layer.

reproducibility from device to device was excellent, with less than 10% deviation. The short-circuit current density (J_{SC}), open-circuit voltage (V_{OC}) and fill factor (*FF*), respectively, are 16.12 mA cm^{-2}, 1.05 V and 0.67, which lead to a power-conversion efficiency of 12.04% measured at 100 mW cm^{-2}. At 50 and 10 mW cm^{-2} the device exhibited very similar efficiencies, 12.04% and 12.00%, respectively. The high open-circuit potential indicates that there are negligible surface and sub-bandgap states in the perovskite film. The device performance under 100 mW cm^{-2} is remarkable in view of the very thin perovskite film of 285 nm. A device with cells of larger area (0.98 cm^2) was also prepared and evaluated at 100 mW cm^{-2} (Supplementary Fig. 4). The J_{SC} and V_{OC} are very similar to the data obtained for the small-area cell (14.76 mA cm^{-2} and 1.05 V, respectively). The *FF*, however, is significantly lower (0.52), which is the main reason for the lower power-conversion efficiency (8.27%) for these larger cells.

The incident photon-to-current conversion efficiency (IPCE) spectra exhibit 74% (Fig. 3b) where the generation of photocurrent started at 790 nm, in agreement with the bandgap of the $CH_3NH_3PbI_3$. It is interesting that the IPCE spectra show a very steep onset, contrary to the IPCE spectra reported for TiO_2 and Al_2O_3 mesoscopic-based perovskite cells. A very similar IPCE spectrum as observed for our solar cells was reported for a solar cell based on a perovskite layer sandwiched between a C_{60}-modified TiO_2 layer and a layer of poly(3-hexylthiophene)[22]. As such, the steep onset may be related to the specific interaction of the perovskite with the fullerene molecules. The IPCE spectrum is almost flat, except for a dip at 630 nm that could result from the oxidized polyTPD acting as a filter or from reduced absorption of the perovskite. Integrating the overlap of the IPCE spectrum with the AM1.5G solar photon flux yields a current density of 16.40 mA cm^{-2}, which is in excellent agreement with the measured photocurrent density of

16.12 mA cm^{-2} at the standard solar AM1.5G intensity of 100 mW cm^{-2}, which confirms that the mismatch between the simulated sunlight and the AM1.5G standard is negligible. The absorbance of the $CH_3NH_3PbI_3$ film is similar to those reported previously for this material and increases with increasing layer thickness (Fig. 3b). The absorption extends over the complete visible spectrum up to 800 nm, with a local maximum around 500 nm (the scale of the graph in Fig. 3b is optical density).

Conclusion

An efficient solid-state, thin-film solar cell was obtained by sandwiching a sublimated $CH_3NH_3PbI_3$ perovskite layer between two thin organic charge-transporting layers that function as hole and electron blockers, respectively, and contacting it via an indium tin oxide (ITO)/PEDOT:PSS as the hole-extraction and an Au electron-extraction contact. The simple device architecture, which is an *n*-type oxide and scaffold free, coupled with easy room-temperature fabrication using economically favourable materials, high efficiency and high reproducibility rivals strongly the established thin-film photovoltaic technologies. The device power-conversion efficiency of 12% at 100 mW cm^{-2} is remarkable in view of the very thin (285 nm) perovskite film. The high J_{sc} of 16.12 mA cm^{-2} and the open-circuit potential of 1.05 V reveal that very few electrons and holes recombine, which demonstrates the effectiveness of the hole- and electron-blocking layers. We believe that this new class of perovskite solar cell using organic semiconductors to collect the charges will find widespread applications to rival photovoltaic solar cells based on thin films.

Note added in proof: During the revision of this paper, a highly relevant article to this topic was published: P. Docampo, J.M. Ball, M. Darwich, G.E. Eperon & H.J. Snaith, Efficient organometal trihalide perovskite planar-heterojunction solar cells on flexible polymer substrates. *Nature Commun.* **4**, 2761 (2013).

Methods

Materials. Photolithographically patterned ITO-covered glass substrates were purchased from NaranjoSubstrates. Aqueous dispersions of PEDOT:PSS (Clevios P VP Al 4083) were obtained from Heraeus Holding and used as received. Poly-TPD was purchased from ADS Dyesource. PbI_2 was purchased from Aldrich and used as is. CH_3NH_3I was prepared similarly to a previously published method[8]; in brief, CH_3NH_3I was synthesized by reacting 21.6 ml methylamine (40 wt% in water; Aldrich) and 30 ml hydroiodic acid (57 wt% in water; Aldrich) in a 250 ml round-bottomed flask at 0 °C for 2 h with stirring. The white precipitate was recovered by evaporation at 50 °C for 1 h. The product, CH_3NH_3I, was dissolved in ethanol, filtered, recrystallized from diethyl ether and dried at 60 °C in a vacuum oven for 24 h.

Device preparation. Devices were prepared on cleaned ITO substrates by spin coating a thin layer of PEDOT:PSS from the commercial aqueous dispersion (1,200 revolutions per minute for 30 s (Chemmat, 3 cm diameter), which resulted in a thickness of 70 nm). On top of this layer a thin film of polyTPD was deposited from a chlorobenzene solution (10 mg ml^{-1}) using a meniscus coater and a coating speed of 2.5 mm s^{-1}. Then the substrates were transferred to a vacuum chamber integrated into an inert glovebox (<0.1 ppm O_2 and <0.1 ppm H_2O; MBraun) and evacuated to a pressure of 1×10^{-6} mbar. Two ceramic crucibles were filled with CH_3NH_3I (freshly prepared) and PbI_2, which were heated to 70 °C and 250 °C, respectively. The film thickness was controlled by the PbI_2 evaporation at a rate of evaporation of 0.5 Å s^{-1} (see Supplementary Information for more details concerning the perovskite evaporation process). The PCBM layer was deposited using a chlorobenzene solution (10 mg ml^{-1}) in ambient conditions with a meniscus coater and a coating speed of 10 mm s^{-1}. The device was completed by the thermal evaporation of the top metal electrode under a base pressure of 2×10^{-6} mbar to a thickness of 100 nm. The solar cells (active area of 0.09 and 0.98 cm^2) were then encapsulated with a glass cover using an ultraviolet-curable epoxy sealant (Ossila E131 Encapsulation Epoxy), with an ultraviolet exposure of 5 min.

Characterization. GIXRD data were collected at room temperature in the 2θ range 5–50° on an Empyrean PANalytical powder diffractometer using Cu $K\alpha_1$ radiation. Typically, four repeated measurements were collected and merged into a single diffractogram. Pawley refinements[23] were performed using the TOPAS computer program[24] and revealed an excellent fit to a one-phase model with a tetragonal cell ($a = 8.80(2)$, $c = 12.57(2)$ Å) and space group *I*4/*mcm*. Additional peaks that correspond to the ITO substrate were also observed. The observed and calculated diffraction patterns for the refined crystal structures are shown in Supplementary Fig. 3.

Simulation of the crystal structure of $CH_3NH_3PbI_3$ perovskite was performed using, as a starting model, the isostructural Sn analogue (CCDC ref. code: ZZZBWS02), and modifying the cell parameters to those obtained in the Pawley refinement[25].

Absorption spectra were taken using a fibre-optics based Aventes Avaspec2048 spectrometer.

Current–voltage characteristics were recorded by applying an external potential bias to the cell and recording the generated photocurrent with a digital source meter (Keithley Model 2400). The light source was a 450 W xenon lamp (Oriel) equipped with a Schott K113 Tempax sunlight filter (Praezisions Glas & Optik) to match the emission spectrum of the lamp to the AM1.5G standard. A black mask was used in the photovoltaic studies to limit the active area of the device. Before each measurement, the exact light intensity was determined using a calibrated Si reference diode equipped with an infrared cut-off filter (KG-3, Schott). IPCE measurements were determined using a 300 W xenon light source (ILC Technology). A Gemini-180 double monochromator (Jobin Yvon) was used to select and increment the wavelength of the radiation that impinged on the cells. The monochromatic incident light was passed through a chopper run at 1 Hz frequency, and the on/off ratio was measured by an operational amplifier. IPCE spectra were recorded as functions of wavelength under a constant white-light bias of approximately 5 mW cm^{-2} supplied by an array of diodes that emitted white light. The excitation beam from a 300 W xenon lamp (ILC Technology) was focused through a Gemini-180 double monochromator (Jobin Yvon) and chopped at approximately 2 Hz. The signal was recorded using a Model SR830 DSP Lock-In Amplifier (Stanford Research Systems).

Received 16 September 2013; accepted 14 November 2013; published online 22 December 2013

References

1. Kojima, A., Teshima, K., Shirai, Y. & Miyasaka, T. Organometal halide perovskites as visible-light sensitizers for photovoltaic cells. *J. Am. Chem. Soc.* **131,** 6050–6051 (2009).
2. Kim, H.-S. *et al.* High efficiency solid-state sensitized solar cell-based on submicrometer rutile TiO_2 nanorod and $CH_3NH_3PbI_3$ perovskite sensitizer. *Nano Lett.* **13,** 2412–2417 (2013).
3. Heo, J. H. *et al.* Efficient inorganic–organic hybrid heterojunction solar cells containing perovskite compound and polymeric hole conductors. *Nature Photon.* **7,** 486–491 (2013).
4. Burschka, J. *et al.* Sequential deposition as a route to high-performance perovskite-sensitized solar cells. *Nature* **499,** 316–319 (2013).
5. Ball, J. M., Lee, M. M., Hey, A. & Snaith, H. J. Low-temperature processed meso-superstructured to thin-film perovskite solar cells. *Energy Environ. Sci.* **6,** 1739–1743 (2013).
6. Lee, M. M., Teuscher, J., Miyasaka, T., Murakami, T. N. & Snaith, H. J. Efficient hybrid solar cells based on meso-superstructured organometal halide perovskites. *Science* **338,** 643–647 (2012).
7. Kim, H-S. *et al.* Lead iodide perovskite sensitized all-solid-state submicron thin film mesoscopic solar cell with efficiency exceeding 9%. *Sci. Rep.* **2,** 591 (2012).
8. Etgar, L. *et al.* Mesoscopic $CH_3NH_3PbI_3/TiO_2$ heterojunction solar cells. *J. Am. Chem. Soc.* **134,** 17396–17399 (2012).
9. Liu, M., Johnston, M. B. & Snaith, H. J. Efficient planar heterojunction perovskite solar cells by vapour deposition. *Nature* **501,** 395–398 (2013).
10. Hodes, G. Perovskite-based solar cells. *Science* **342,** 317–318 (2013).
11. Kagan, C. R., Mitzi, D. B. & Dimitrakopoulos, C. D. Organic–inorganic hybrid materials as semiconducting channels in thin-film field-effect transistors. *Science* **286,** 945–947 (1999).
12. Tanaka, K. *et al.* Comparative study on the excitons in lead-halide-based perovskite-type crystals $CH_3NH_3PbBr_3$ and $CH_3NH_3PbI_3$. *Solid State Commun.* **127,** 619–623 (2003).
13. Snaith, H. J. Perovskites: the emergence of a new era for low-cost, high-efficiency solar cells. *J. Phys. Chem. Lett.* **4,** 3623–3630 (2013).
14. Stranks, S. D. *et al.* Electron-hole diffusion lengths exceeding 1 micrometer in an organometal trihalide perovskite absorber. *Science* **342,** 341–344 (2013).
15. Sasabe, H. & Kido, J. Development of high performance OLEDs for general lighting. *J. Mater. Chem. C* **1,** 1699–1707 (2013).
16. Riede, M., Mueller, T., Tress, W., Schueppel, R. & Leo, K. Small-molecule solar cells—status and perspectives. *Nanotechnology* **19,** 424001 (2008).
17. Jeng, J-Y. *et al.* $CH_3NH_3PbI_3$ perovskite/fullerene planar-heterojunction hybrid solar cells. *Adv. Mater.* **25,** 3727–3732 (2013).
18. Sun, S. *et al.* The origin of high efficiency in low-temperature solution-processable bilayer organometal halide hybrid solar cells. *Energy Environ. Sci.* http://dx.doi.org/10.1039/C3EE43161D (2014).
19. Mitzi, D. B. in *Progress in Inorganic Chemistry*, Vol. 48 (ed. Karin, K.D.) 1–121 (John Wiley, 2007).
20. Yu, G., Gao, J., Hummelen, J. C., Wudl, F. & Heeger, A. J. Polymer photovoltaic cells: enhanced efficiencies via a network of internal donor–acceptor heterojunctions. *Science* **270,** 1789–1791 (1995).

21. Malinkiewicz, O., Lenes, M., Brine, H. & Bolink, H. J. Meniscus coated high open-circuit voltage bi-layer solar cells. *RSC Adv.* **2,** 3335–3339 (2012).
22. Abrusci, A. *et al.* High-performance perovskite–polymer hybrid solar cells via electronic coupling with fullerene monolayers. *Nano Lett.* **13,** 3124–3128 (2013).
23. Pawley, G. S. Unit-cell refinement from powder diffraction scans. *J. Appl. Cryst.* **14,** 357–361 (1981).
24. TOPAS-Academic, Version 4.1, 2007, http://www.topas-academic.net (Coelho Software, Brisbane).
25. Takahashi, Y. *et al.* Charge-transport in tin-iodide perovskite $CH_3NH_3SnI_3$: origin of high conductivity. *Dalton Trans.* **40,** 5563–5568 (2011).

Acknowledgements

We thank A. Soriano-Portillo, J. Ferrando, A. K. Chandiran and E. Ortí for their assistance with the sample preparation and characterization, and careful proofreading of the manuscript. This work was supported by the European Community's Seventh Framework Programme (ORION, Grant 229036 and NANOMATCELL, Grant 308997), the Spanish Ministry of Economy and Competitiveness (MAT2011-24594), the Generalitat Valenciana (Prometeo/2012/053) and the Global Research Laboratory Program, Korea (GLOBASOL, Grant 309194).

Author contributions

O.M. designed, prepared and characterized the devices, A.Y. and Y.H.L. characterized the devices, G.M.E. supervised the X-ray characterization and interpretation, M.G. supervised the work and wrote the manuscript, M.K.N. initiated the research, provided key materials and wrote the manuscript, H.J.B initiated the research, designed the devices, supervised the work and wrote the manuscript.

Additional information

Supplementary information is available in the online version of the paper. Reprints and permissions information is available online at www.nature.com/reprints. Correspondence and requests for materials should be addressed to M.K.N. and H.J.B.

Competing financial interests

The authors declare no competing financial interests.

ADVANCED ENERGY MATERIALS
www.advenergymat.de

Metal-Oxide-Free Methylammonium Lead Iodide Perovskite-Based Solar Cells: the Influence of Organic Charge Transport Layers

*Olga Malinkiewicz, Cristina Roldán-Carmona, Alejandra Soriano, Enrico Bandiello, Luis Camacho, Mohammad Khaja Nazeeruddin, and Henk J. Bolink**

Metal-oxide-free methylammonium lead iodide perovskite-based solar cells are prepared using a dual-source thermal evaporation method. This method leads to high quality reproducible films with large crystal domain sizes allowing for an in depth study of the effect of perovskite film thickness and the nature of the electron and hole blocking layers on the device performance. The power conversion efficiency increases from 4.7% for a device with only an organic electron blocking layer to almost 15% when an organic hole blocking layer is also employed. In addition to the in depth study on small area cells, larger area cells (approx. 1 cm^{-2}) are prepared and exhibit efficiencies in excess of 10%.

1. Introduction

Thin-film photovoltaic devices hold great promise to reduce the dependencies on fossil energy.[1] Solid-state methylammonium lead halide perovskites solar cells are attracting much attention due to their ease of preparation, low cost and high efficiencies.[2] The hybrid organic-inorganic methylammonium lead iodide perovskites, pioneered by Mitzi, have been recognized for their excellent semiconducting properties.[3] After the seminal work of Miyasaka et al.,[4] tremendous progress in the performance of methylammonium lead iodide perovskite based solar cells has been obtained.[5] Most high efficiency perovskite solar cells reported until now use a (mesoscopic) metal oxide such as Al_2O_3, TiO_2 or ZrO_2 requiring a high temperature sintering process.[5b-e] Frequently in these devices, a rather thick and partially oxidized organic hole transport material is employed. Without the hole transport material power conversion efficiencies (PCEs) as high as 8% were achieved with metal oxide containing devices.[6] Flexible perovskite solar cells have also been described exhibiting efficiencies up to 10%,[5g,7] and showing compatibility with roll-to-roll processing.[7b,c] Some insights into the particular operational mechanism of these methylammonium lead halide perovskite-based solar cells have been recently obtained. Very long exciton diffusion lengths, in the range of several hundred nanometers, have been measured.[8] Recently, it was reported that these long diffusion lengths are caused by charge carrier recombination rates that defy the Langevin limit by four orders of magnitude.[9] These findings explain in part the report by Ball et al. who first showed that a thick layer (350 nm) of the mixed halide methylammonium lead perovskite ($CH_3NH_3PbI_{3-x}Cl_x$) leads to efficient solar cells (12%).[5c] This was confirmed by Liu et al., who showed that the mesostructure of the metal oxide is not required to prepare efficient (15.4%) perovskite based solar cells.[5e] Apart from the origin of the above mentioned large exciton, hole and electron diffusion lengths, it is also still not clear if the exciton dissociation occurs in the bulk film, at the interface or in both. It was shown that fluorescence quenching does occur at the interface of the perovskite layer and the hole and electron transporting layer, implying that exciton dissociation can occur at the interface.[8] Also very recently, the group of Cahen showed evidence for a p-i-n type mechanism obtained from electron beam induced current (EBIC) analysis.[10] This last report is in line with earlier reports on the low exciton binding energy in such perovskite materials.[5c] The studies mentioned above were carried out on perovskites with the same composition although prepared at different places using sometimes different procedures; it is possible that the exciton dissociation process depends on the exact nature of the film and the architecture of the device. It is important to unravel these as yet open questions to optimize the device architecture to push the efficiencies towards 20%. Recently, we reported on a metal oxide free $CH_3NH_3PbI_3$ perovskite solar cell in which the evaporated perovskite layer is sandwiched in between two thin organic electron and hole blocking layers.[5f] PCEs of 12% were

O. Malinkiewicz, C. Roldán-Carmona, Dr. A. Soriano, E. Bandiello, Dr. H. J. Bolink
Instituto de Ciencia Molecular Universidad de Valencia
C/ Catedrático J. Beltrán 2,
ES-46980, Paterna, Valencia, Spain
E-mail: henk.bolink@uv.es
C. Roldán-Carmona, Prof. L. Camacho
Department of Physical Chemistry
and Applied Thermodynamics
Campus Rabanales, Ed. C3, University of Cordoba
14014, Spain
Prof. M. K. Nazeeruddin
Laboratory of Photonics and Interfaces
Swiss Federal Institute of Technology (EPFL)
Station 6, Lausanne, CH 1015, Switzerland

DOI: 10.1002/aenm.201400345

achieved when the energy levels of the organic blocking layer were well aligned with the VB and CB of the perovskite.[5f]

In these metal-oxide-free devices the perovskite layer was prepared using dual source thermal evaporation in a high vacuum chamber. With this process very reproducible layers could be prepared with accurate control on the layer thickness. This allows for an in depth study of the effect of the perovskite layer thickness and the nature of the organic charge transport materials employed to block the electrons and holes. First devices only used an organic hole transporting/electron blocking layer that already lead to reasonable efficiencies when the perovskite layer thickness was optimized. With the addition of an organic electron transporting/hole blocking layer the device performance increased further, reaching 14.8% for the optimized device. We also show the importance of aligning the energy levels of the organic charge transporting materials with those of the perovskite layer.

2. Results and Discussion

2.1. Perovskite Film Formation and Characterization

The $CH_3NH_3PbI_3$ perovskite thin film was prepared by co-evaporation of the two starting compounds, CH_3NH_3I and PbI_2 in a similar way as reported previously.[5e,12] A schematic picture of the evaporation process is shown in **Figure 1**. Both starting materials were heated simultaneously to their corresponding sublimation temperatures forming a perovskite layer on the substrate situated above the crucibles, as it is shown in Figure 1. All the details about the evaporation process can be found in the experimental section. One of the main challenges for the successful perovskite film formation is the control over the CH_3NH_3I evaporation rate. Since the perovskite is formed by a dual evaporation process it is fundamental to know the evaporation rate of each material. For that purpose, the piezoelectric sensors that are located in the vacuum chamber need to be calibrated for each of these materials. This requires the determination of the thickness of different evaporated CH_3NH_3I and PbI_2 films. For CH_3NH_3I the calibration process turned out to be difficult due to the non-uniform layers and soft nature of the film which impeded accurate thickness measurements using a profilometer. To overcome these difficulties, the evaporation temperature for the CH_3NH_3I crucible was kept constant at 70 °C. The CH_3NH_3I:PbI_2 ratio was then controlled by changing the PbI_2 evaporation temperature. Hence, no inline control of the ratio was possible. Instead, the optimum conditions were determined by analyzing the evaporated perovskite films after preparation. This was done using grazing incidence X-ray diffraction (GIXRD). The results are shown in **Figure 2**a. As can be seen from Figure 2a higher temperatures of the PbI_2 crucible lead to an excess of the PbI_2 in the perovskite film. Upon decreasing the PbI_2 evaporation temperature, the excess of PbI_2 reduces and at an evaporation temperature of 250 °C the perovskite film has the correct stoichiometry. Once determined these conditions perovskite films with the same properties could be repeatedly prepared indicating that the above mentioned protocol is robust. The optimized films adopt the typical tetragonal structure for $CH_3NH_3MX_3$ hybrid perovskites (M = Pb, Sn; X = Cl, Br, I) formed by a three-dimensional anionic framework of PbI_6 octahedra with the methylammonium cations in the interstitial space (Supporting Information, Figure S1–S3). The roughness of the $CH_3NH_3PbI_3$ film was evaluated using atomic force microscopy (AFM). An image of a typical scan is given in Figure 2b, which demonstrates a smooth film with a root mean square (rms) roughness of 5 nm. The optimized film was also evaluated using scanning electron microscopy (SEM). The picture is shown in Figure 2c. The film presents a very compact surface consisting on an uniform grainy texture with an average grain size of 150 nm. Similar grain sizes were also obtained for the thicker films. The typical absorption spectrum of different $CH_3NH_3PbI_3$ perovskite film thicknesses is shown on **Figure 3**. The absorbance of light increases linearly with increasing perovskite layer thickness. It shows a broad band all over the visible spectrum with a local maximum centerd at 400 nm and a shoulder up to 800 nm, which corresponds to the 1.55 eV band gap for this material.

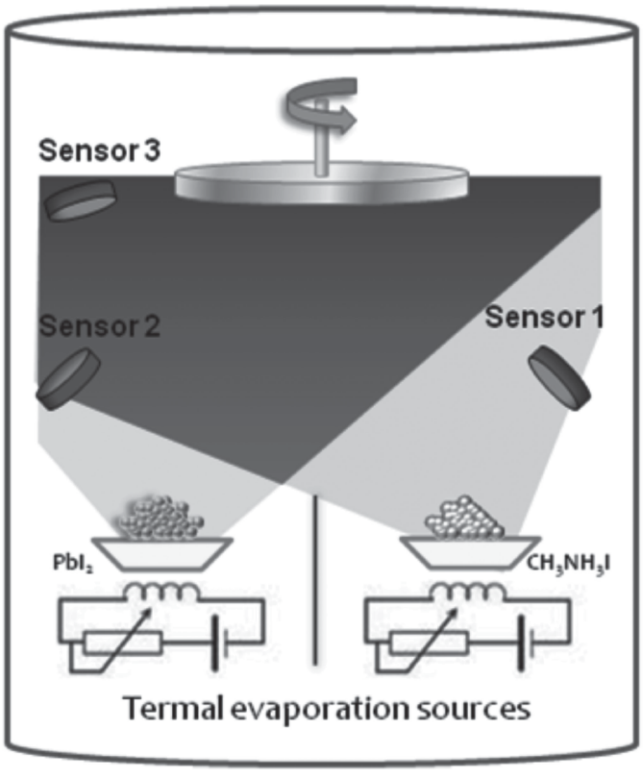

Figure 1. Schematic diagram of the dual evaporation process. CH_3NH_3I evaporates with a broader evaporating cone, affecting the reading of all the sensors.

2.2. Perovskite-Based Devices

One of the more robust layouts for sandwiching thin film devices is the one frequently used in the field of organic photovoltaic (OPV) and light-emitting diodes.[7b,11] In these devices, a conductive polymer composite poly(3,4-ethylenedioxythiophene):poly(styrenesulfonate) (PEDOT:PSS) is deposited on top of a transparent conductive electrode, most frequently indium tin oxide (ITO). In analogy with those devices, our first cells were fabricated by evaporating the perovskite film (200 nm) on top

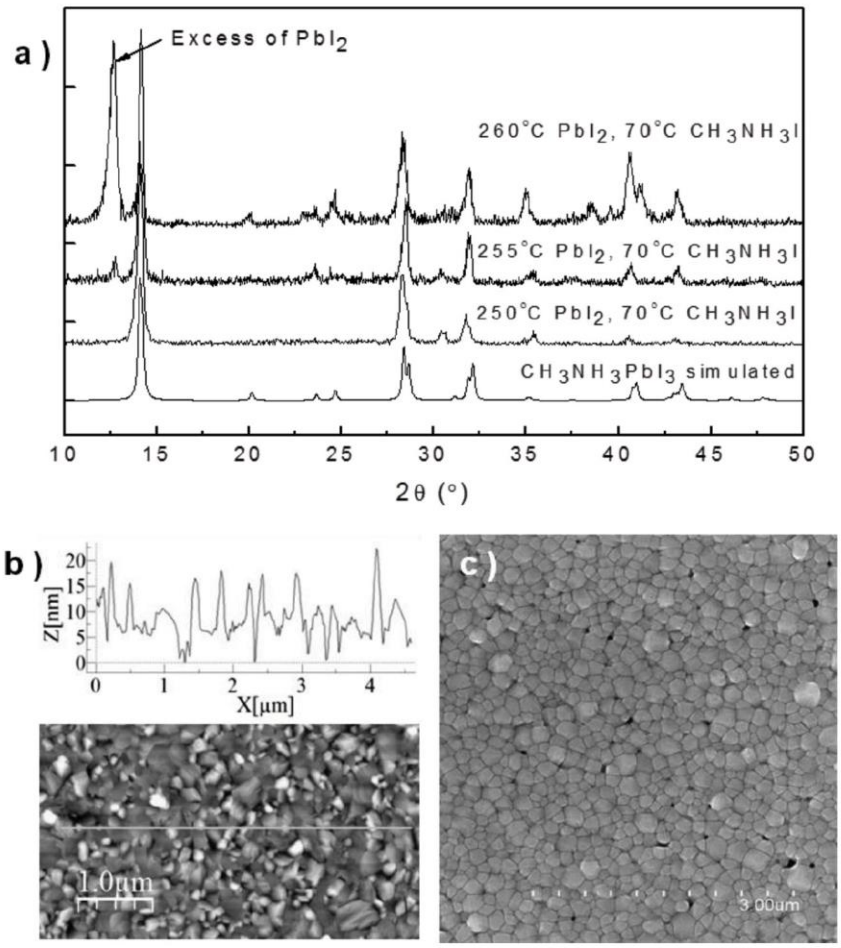

Figure 2. Characteristics of the sublimed $CH_3NH_3PbI_3$ perovskite layer. a) GIXRD pattern with Cu Kα1 radiation (λ = 1.54056 Å) of the $CH_3NH_3PbI_3$ film, films with excess of PbI_2 and calculated for $CH_3NH_3PbI_3$ with preferred orientation along the (100) and (001) directions. b) AFM image and profile of the 60 nm thick film. c) SEM image of a 60 nm thick film.

of a ITO/PEDOT:PSS substrate, followed by the deposition of a metallic cathode. Initially, several cathode materials were tested. Somewhat surprisingly Au electrodes led to more stable and better performing devices. For this reason all studies were performed using Au as the top electrode. For the best devices described in this manuscript we confirmed that the exchange of Au for an Ag cathode lead to similar efficiencies yet lower stabilities. Characterization of the solar cells was performed using two methods that are described in detail in the Supporting Information section. In all cases the characterization was performed within seconds of illuminating the cells (no light soaking was carried out) and no hysteresis was observed in the current density (J) versus voltage (V) scans. All the devices with the configuration ITO/PEDOT:PSS/$CH_3NH_3PbI_3$/Au had large ohmic conductivities indicative of the presence of shorts or of the relatively high conductivity of both materials. The conductivity of the used PEDOT:PSS grade is reported to be 2×10^{-3} to 2×10^{-4} S cm^{-1}.[13] The conductivity of the $CH_3NH_3PbI_3$ perovskite was determined to be around 0.15×10^{-4} S cm^{-1} which is in good agreement with previously reported value for this perovskite.[14] In line with the work of Jeng et al., who inserted a thin hole blocking layer in between the perovskite layer and the top contact here we evaluated the effect of a thin layer of an electron blocking layer.[15] Upon the insertion of a thin (20 nm) layer of the organic hole transporting polymer poly(4-butylphenyl-diphenyl-amine) (polyTPD) in between the ITO/PEDOT:PSS anode and the perovskite film (**Figure 4**) the solar cells no longer show the high ohmic currents. This is caused by the low conductivity of the polyTPD film (<2×10^{-8} S cm^{-1}). However, as the highest occupied molecular orbital (HOMO) of the polyTPD and the VB of the perovskite are very similar in energy, the hole extraction from the device in the presence of this additional layer is still rather efficient for thin layers of polyTPD.[16] However, due to the high energy level of the lowest unoccupied molecular orbital (LUMO) of the polyTPD (–2.4 eV),[17] the electrons that are generated and accumulated in the perovskite layer are blocked and are unable to reach the PEDOT:PSS anode.[18] This leads to a diffusion current of electrons towards the opposite electrode where they are extracted. Hence, in this device configuration a photocurrent is generated.

After showing the effect of inserting the polyTPD layer, the thickness of the perovskite layer was optimized. Figure 4 shows the performance of the devices prepared with different perovskite thicknesses ranging from 100 to 400 nm. As expected intuitively the IPCE increases with increasing film thickness due to the increased absorption of the sun light (Figure 4a). The IPCE spectrum resembles the shape of the absorption spectrum of the perovskite film and starts immediately at the bandgap close to 800 nm. In the wavelength region from 400 to 700 nm the IPCE increase linearly with increasing

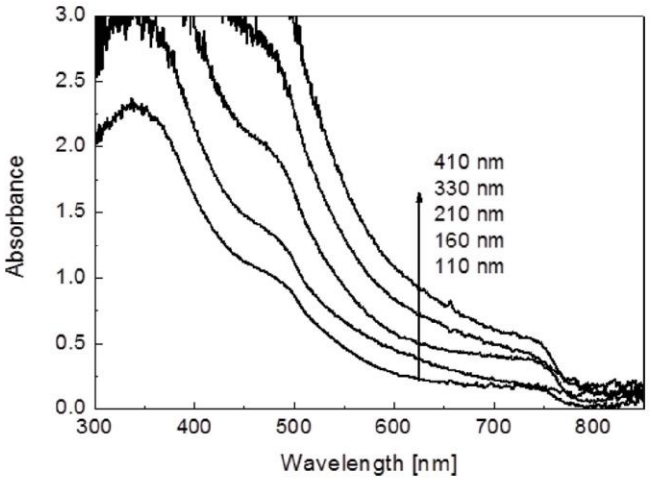

Figure 3. Absorance spectra of evaporated perovskite films with different thicknesses.

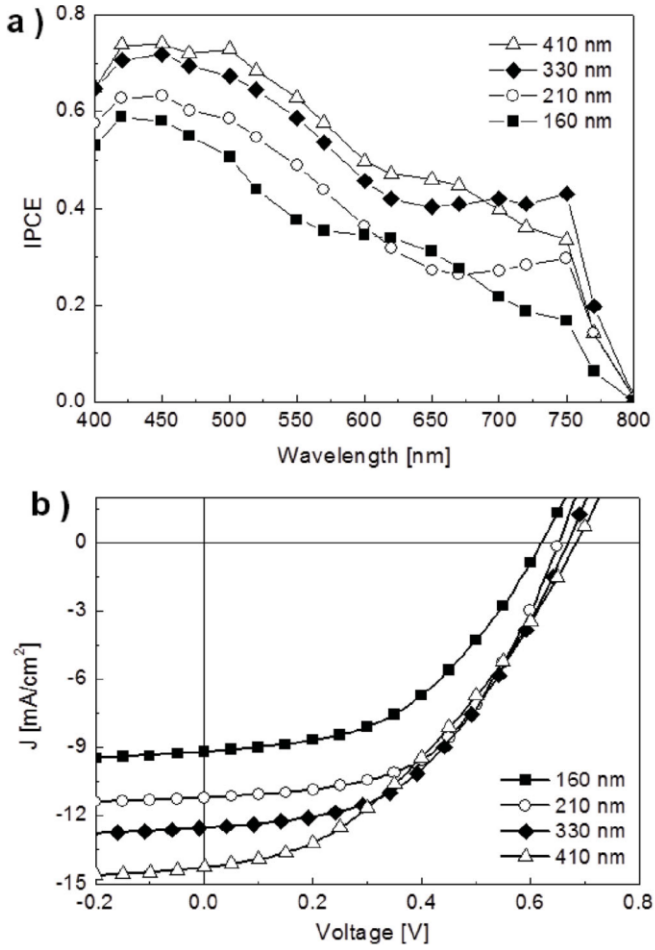

Figure 4. a) IPCE curves and b) *J–V* curves for devices with different evaporated perovskite thicknesses. The device configuration was ITO/PEDOT-PSS/polyTPD/$CH_3NH_3PbI_3$/Au.

perovskite layer thickness. Hence, the increased absorption leads to more excitons but importantly also to more free carriers. This is also observed from the *J* versus *V* scans (Figure 4b) where *J* scales linearly with the perovskite layer thickness especially around short-circuit conditions. These findings imply that with increasing absorption the number of free carriers increases and losses due to recombination appear to be small. This is in agreement with a recent finding in which the exciton recombination rates in methylaminium lead iodide perovskite was found to deviate strongly from the Langevin prediction.[9] In the wavelength region from 700 to 800 nm the increases in current appears to be more than linear with increasing perovskite film thickness (Figure 3). This may be due to optical effects, however, to verify this optical modelling must be performed on these stacks. Devices using thicker perovskite layers also lead to a slightly higher open circuit voltage (V_{oc}) as a result of the increased current densities. Unfortunately, however, with increasing perovskite layer thickness the shape of the *J–V* curves deviates from the ideal rectangular shape leading to a decrease in fill factor (FF) for these devices. Due to these effects the maximum efficiency is obtained for devices that employ perovskite layers with a thickness of 330 nm. The dependence of the key cell parameters on the perovskite layer thickness is represented in **Figure 5** and listed in **Table 1**. A peak PCE of 4.7% is obtained for this cell configuration. A similar optimum perovskite layer thickness was recently reported by Docampo et al. for metal oxide containing cells.[7a] Even though the performance of the optimized devices are quite good, they are significantly below those recently reported for similar metal oxide based thin film devices. The main difference between the above described devices and the record cells described in the literature is the presence of a metal oxide layer in between the perovskite and the electron collecting contact. Without going into detail about the different roles of the metal oxides employed, the valence band of the metal oxide is in all cases reported significantly below that of the perovskite. This implies that the metal oxide is a hole blocking layer in those devices. Hence, to increase the performance of the above described metal oxide free devices, the perovskite layer should be sandwiched in between the electron blocking polyTPD layer and an efficient hole blocking layer.

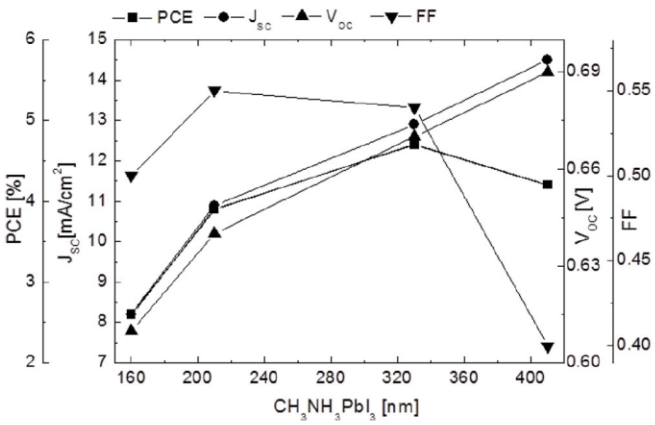

Figure 5. FF, J_{sc}, V_{oc} and PCE as a function of $CH_3NH_3PbI_3$ perovskite layer thickness for devices with the configuration ITO/PEDOT:PSS/polyTPD/$CH_3NH_3PbI_3$/Au.

2.3. Hole Blocking Layer

The hole blocking layer should consist of a material with a VB or HOMO energy level below the VB of the perovskite.[19] However, the hole blocking material must also allow the transport of the electrons implying that 1) it must be an electron transporter and 2) a careful match between the perovskite CB and the LUMO of the hole blocking material is required.[19] To demonstrate the importance of this second point two different materials were evaluated as hole blocking layer in our

Table 1. Overview of the ITO/PEDOT:PSS/polyTPD/$CH_3NH_3PbI_3$/Au device performance.

$CH_3NH_3PbI_3$ [nm]	J_{SC} [mA cm^{-2}]	V_{OC} [V]	FF [%]	PCE [%]
160	8.2 ± 0.5	0.61 ± 0.01	50 ± 3	2.6 ± 0.3
210	10.9 ± 0.22	0.64 ± 0.01	55 ± 3	3.9 ± 0.3
330	12.9 ± 0.5	0.67 ± 0.01	54 ± 5	4.7 ± 0.8
410	14.5 ± 0.5	0.69 ± 0.01	40 ± 1	4.2 ± 0.1

devices. [6,6]-phenyl-C_{61}-butyric acid methyl ester ($PCBM_{60}$) and tris(2,4,6-trimethyl-3-(pyridin-3-yl)phenyl)borane (3TPYMB). The chemical structures and the corresponding energy levels of these materials, taken from ref. [20,21] are depicted in **Figure 6**. Solar cells were prepared in a similar manner as described previously, using a perovskite layer thickness of 330 nm, yet now prior to the deposition of the top electrode the layer of either $PCBM_{60}$ or 3TPYMB was deposited using meniscus coating from a chlorobenzene solution.[22] For both hole blocking layers the thickness was kept constant at approximately 10 nm (for further details see the Experimental Section). As the last step the metallic cathode was thermally evaporated in a vacuum chamber. **Figure 7** shows the effect of each blocking layer on the IPCE and the *J–V* characteristic of the devices. The device parameters are listed in **Table 2**. The insertion of the hole blocking layers has a strong effect on both the IPCE and *J–V* curves. The insertion of the hole blocking layer consisting of 3TPYMB increases the current over most of the wavelength range with an additional peak around 650 nm (Figure 7a). The IPCE curve of the devices employing $PCBM_{60}$ as the hole blocking layer are very different. The presence of $PCBM_{60}$ leads to much higher IPCEs over the complete spectrum (450–800 nm). Especially intriguing are the high IPCE values in the lower energy range. The primary absorption of $PCBM_{60}$ is at 370 nm with only a very small absorption in the visible range of the spectrum. Moreover, the thickness of the hole blocking layers is only around 10 nm (see Supporting Information, Figure S4) and does not change the final absorption of the device. Hence, it appears unlikely that the increase in IPCE at lower energy in case of in the $PCBM_{60}$ layer is due to light absorption. These differences in IPCE shape when different HBLs are used are very interesting. One of the possible explanations for lower IPCE values in case of 3TPYMB blocking layer might be due to the barrier for electron extraction (a difference of 0.6 eV exist in between the perovskite CB and the LUMO of 3TPYMB). On the other hand for device employing $PCBM_{60}$ layer the dip around 625 nm warrants some more attention, because if it could be removed, this could lead to improved performance of the devices. Figure 7b shows the current voltage characteristics of the devices without and with the two different hole blocking layers. When 3TPYMB is used, both J_{sc} and V_{oc} increase with respect to the device without the blocking layer. The difference of 1.4 eV between the VB of the perovskite and the HOMO level of 3TPYMB, prevents the holes from reaching the Au electrode. As a result hole concentration at the perovskite-hole blocking layer increases leading to a diffusion gradient that directs the holes towards the polyTPD/PEDOT contact. This appears to be the reason for the increase in J_{sc} from 12.4 mA cm^{-2} to

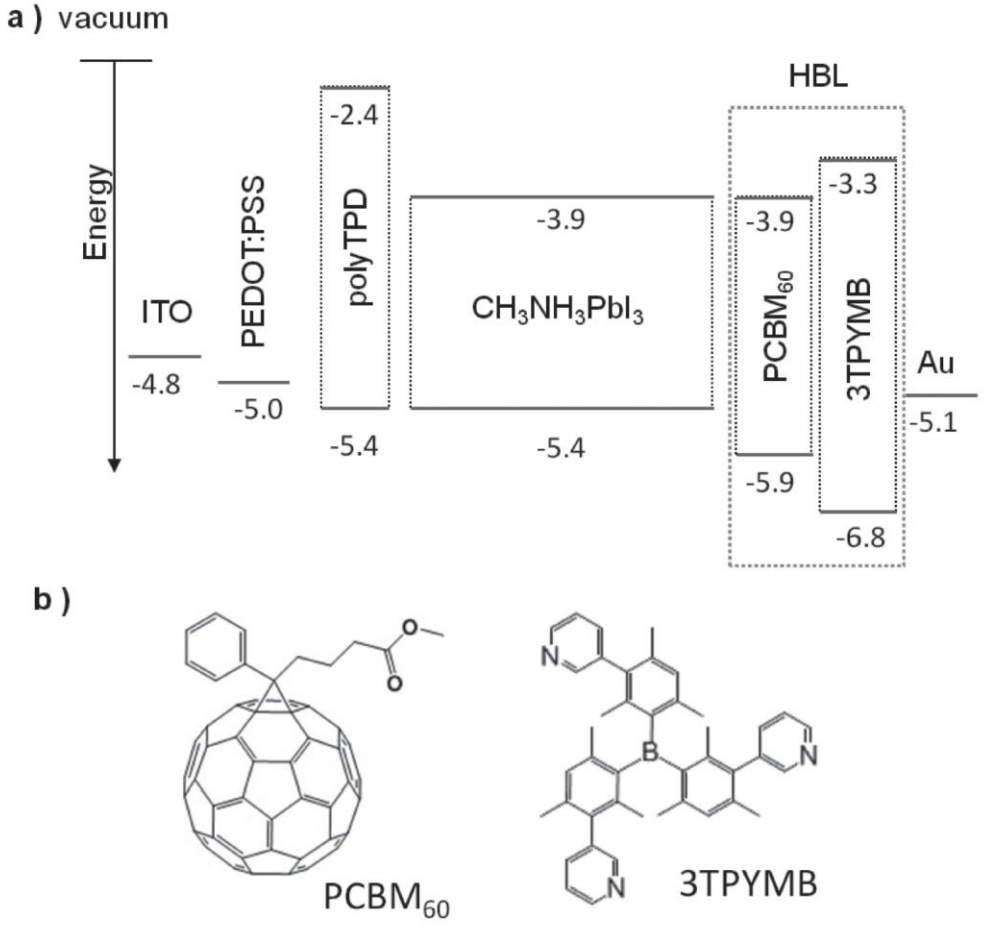

Figure 6. a) Solar cell configuration and energy level diagram for the different layers employed, based on the average literature values of HOMO–LUMO levels of the separate molecules (PEDOT:PSS,[18] polyTPD,[17] $CH_3NH_3PbI_3$,[19] $PCBM_{60}$,[18,20], 3TPYMB.[21] b) Chemical structures for the two hole blocking layers are also included.

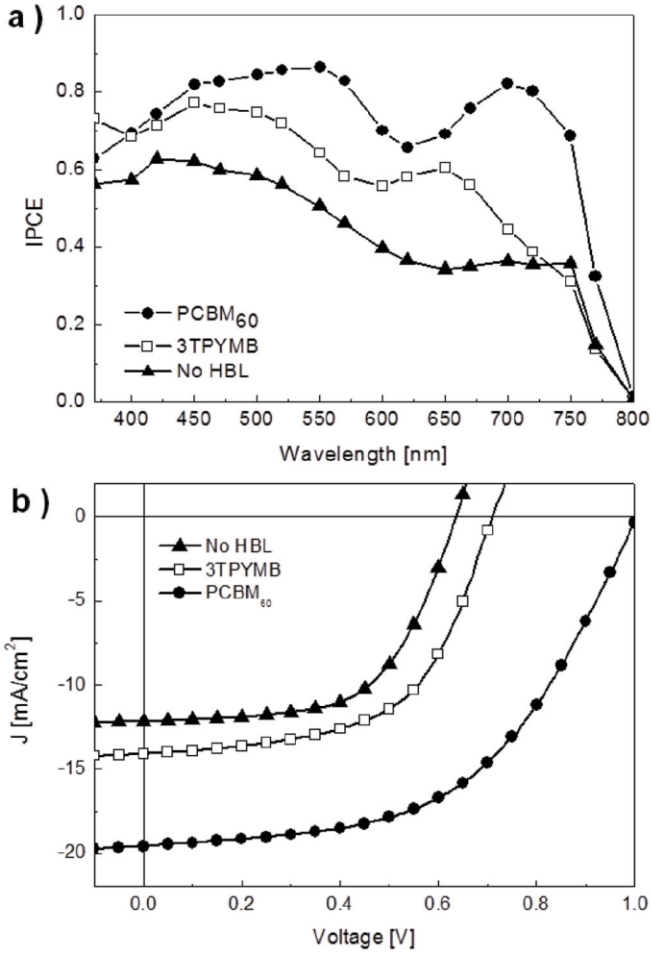

Figure 7. IPCE and *J–V* curves for the devices with the configuration ITO/PEDOT:PSS/polyTPD/$CH_3NH_3PbI_3$/HBL/Au with either, 3TPYMB (squares) or $PCBM_{60}$ (circles). Results of the device without the HBL is also included for clarity (triangles).

14.2 mA cm^{-2}. Another effect of the insertion of the 3TPYMB layer is a slight increase in the V_{oc} (0.1 V). Since the fill factor is not affected by the insertion of the hole blocking layer, the device PCE increases considerably from 4.6% to 5.5%. This increase is somewhat surprising perhaps as there still is an off-set between the CB of the perovskite and the LUMO of the 3TPYMB which should hamper the flow of electrons. There are a number of possible explanations for this observation: 1) it is possible that the thin layer of 3TPYMB contains pinholes or that in some places the gold diffuses into the layer leading to direct paths to the Au contact and 2) with two electron blocking contacts, the polyTPD on the anode side and the 3TPYMB on the cathode side, photogenerated electrons cannot escape. They either recombine with free holes, or accumulate at the interfaces. Accumulation of electrons at the interface leads to the generation of an interfacial field which leads to the effective decrease of the energy difference between the two materials. Hence, when the interfacial field is sufficient electrons can escape towards the gold electrode. This effect could explain the slightly higher V_{oc} observed. The insertion of the more suitable $PCBM_{60}$ hole blocking layer leads to an even larger improvement of the *J–V* characteristic. The LUMO of $PCBM_{60}$ matches well with the CB of the perovskite allowing for a good transport of electrons to the $PCBM_{60}$ layer yet there is an energy off set of 0.5 eV between the HOMO of the $PCBM_{60}$ and the VB of the perovskite. Hence, with this hole blocking layer no barrier for electron extraction is expected. As a result the J_{sc} almost doubles compared to the pristine device and the V_{oc} increases from 0.6 V to 1.06 V. The high open circuit potential indicates that there are negligible surface and sub band-gap states in the perovskite film. The fill factor for these devices is slightly lower than what is observed for the device without the hole blocking layer. Yet the insertion of the thin layer of $PCBM_{60}$ leads to a large improvement in the PCE from 4.6% to 10%, demonstrating the importance of selecting an adequate hole blocking material.

Table 2. Summary of the key parameters for the cells with and without hole blocking layers.

$CH_3NH_3PbI_3$ 330 [nm]	J_{SC} [mA cm^{-2}]	V_{OC} [V]	FF [%]	PCE [%]
No HBL	12.4	0.6	58	4.6
$PCBM_{60}$	19.5	1	52	10
3TPYMB	14.2	0.7	56	5.5

2.4. Device Optimization

Once the optimal architecture for these metal oxide free perovskite based solar cells has been established, the perovskite layer thickness was varied to find the best performing device. For this purpose, several devices with the following configuration ITO/PEDOT:PSS/polyTPD/$CH_3NH_3PbI_3$/$PCBM_{60}$/Au were prepared, with perovskite thicknesses varying from 200 nm to 400 nm. **Figure 8** shows the most important results which are summarized in **Table 3**. The maximum incident power efficiency increases with increasing perovskite layer thickness leading to peak efficiencies in excess of 85% (Figure 8a). The shape of the IPCE spectra changes with increasing perovskite layer thickness, especially in the region from 600 to 800 nm. The steep increase in IPCE just above the bandgap is only observed for devices with perovskite layer thicknesses in excess of 285 nm. The devices with thinner perovskite layers show a more gradual increase of the IPCE. The origin of this effect which was also observed, although less pronounced, in the devices without the hole blocking layer, is most likely related to the optical effects. Further optical modelling results is being carried out to quantify this. The typical values of the J_{sc} increases as well with increasing perovskite layer thickness as can be observed from the *J–V* curves (Figure 8b). A maximum J_{sc} = 21 mA cm^{-2} was observed for a device with the perovskite layer thickness of 340 nm (Table S2 in the Supporting Information). The devices with this layer thickness did not lead to the highest PCE value due to a significantly lower FF. Best devices were obtained with a pervoskite layer thickness of 285 nm. **Figure 9** depicts the key parameters of the solar cells as a function of the perovskite layer thickness. These values were obtained averaging the results for more than 40 different cells. The table with the data of all these devices is listed in the Supporting Information, Table S2. The good reproducibility of the data confirms the robustness of the preparation process. Devices with

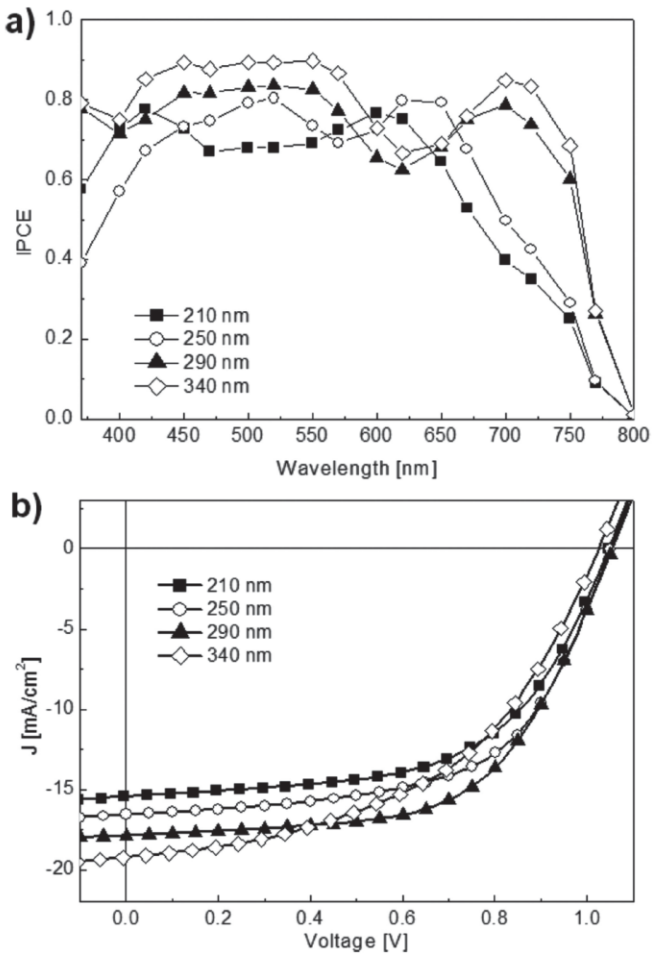

Figure 8. a) IPCE curves and b) *J–V* curves for devices with different perovskite layer thicknesses. The device configuration was ITO/PEDOT-PSS/polyTPD/$CH_3NH_3PbI_3$/$PCBM_{60}$/Au and perovskite thicknesses are shown in the legend.

active cell areas of 0.09 to 0.35 cm^2 were used for this study and no significant effect of the cell area on the cell performance was observed. What is clear from these data is that the current density increases with increasing layer thickness. This can be observed also from the IPCE curve in Figure 8a. Hence, when more light is absorbed, more excitons are generated which are separated and lead to more free charge carriers. The ease of extraction of these charge carriers however, decreases with increasing perovskite layer thickness, evidenced by the decrease in FF. The slope of the *J–V* curve around $V = 0$ V, is larger for the devices with the thicker perovskite layer. The build-in voltage in these devices with

Table 3. Summary of the ITO/PEDOT:PSS/polyTPD/$CH_3NH_3PbI_3$/$PCBM_{60}$/Au device performance.

$CH_3NH_3PbI_3$ [nm]	J_{SC} [mA cm^{-2}]	V_{OC} [V]	FF [%]	PCE [%]
210	15.4 ± 0.9	1.04 ± 0.01	55 ± 6	8.8 ± 1.0
250	16.7 ± 0.5	1.04 ± 0.01	61 ± 2	10.7 ± 0.6
285	17.6 ± 0.6	1.04 ± 0.01	62 ± 5	11.4 ± 1.1
340	19.3 ± 1.4	1.02 ± 0.01	49 ± 5	9.7 ± 1.3

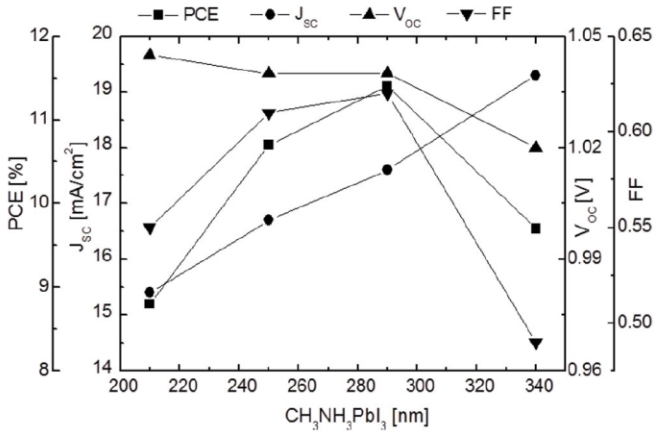

Figure 9. FF, J_{SC}, V_{OC} and PCE as a function of $CH_3NH_3PbI_3$ perovskite layer thickness for devices with the configuration ITO/PEDOT:PSS/polyTPD/$CH_3NH_3PbI_3$/$PCBM_{60}$/Au.

PEDOT:PSS and gold as the electrode is small, however, if slight doping of the hole and electron layers occurs the driving force for carrier flux may in fact be larger. With slightly negative driving voltages one effectively increases the driving force for carrier separation and it can be seen that the current density increases for the devices with the thicker perovskite layers. The opposite occurs at positive driving voltages, as this counteracts the internal field and hence the separation of charge carriers is hampered. This effect only becomes notable at thicknesses in excess of 300 nm. It is possible that this effect is related with the effective diffusion length of the electron and holes which was reported to be around 100 nm.[8] Yet some debate exists about the exact length. A recent study using electron beam induced current (EBIC) showed that electrons have a lower diffusion length than holes in $CH_3NH_3PbI_3$, effectively limiting the maximum thickness of the perovskite layer.[10] For the architecture selected and the pure iodine based perovskite layer prepared here the trade-off between increasing current density and decreasing fill factor is optimum around 285 nm.

2.5. Optimized Small and Large Area Devices

Using the architecture described above optimizations of the evaporation conditions of the perovskite layer (by controlling very carefully the ratios, and time intervals) were carried out for devices with an perovskite layer thickness of 300 nm. In addition to these small cell area devices, cells with a larger active area (0.95 cm^2) were also prepared. Both small and larger cell area devices were encapsulated with a glass cover slide and an UV curable epoxy resin. As such they were send for more accurate analysis to the Laboratory of Photonics and Interfaces of the Swiss Federal Institute of Technology (EPFL) in Lausanne Switzerland. Using their calibrated solar simulator slightly higher values for the J_{SC}, FF and PCE were obtained than compared to our analysis. Yet for the optimized small area device the main difference is the increase in fill factor. This leads to a peak PCE of 14.8% for small area cells and 10.9% for the larger area cells (**Figure 10**, **Table 4** and Supporting Information Figure S5,S6).

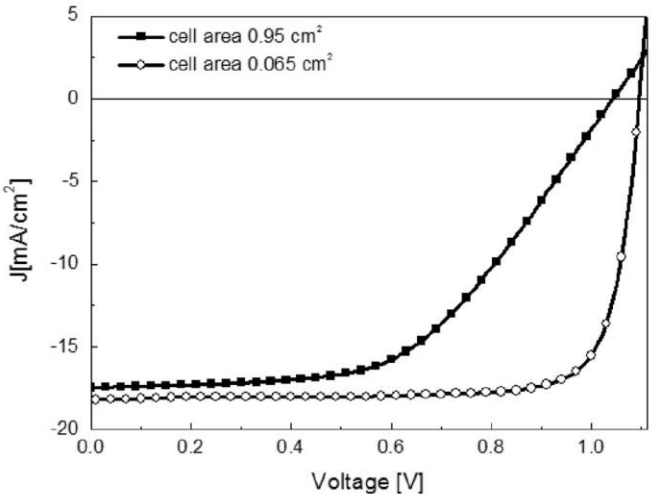

Figure 10. a) *J–V* curve for the large area optimized perovskite based device (full sqares). It is also included the *J–V* curve for the optimized device with small area (empty circles).

Table 4. Key performance parameters for the optimized small and large area cells.

$CH_3NH_3PbI_3$ 285 [nm]	J_{SC} [mA cm^{-2}]	V_{OC} [V]	FF [%]	PCE [%]
0.065 cm^2	18.2	1.09	75	14.8
0.95 cm^2	17.9	1.07	57	10.9

3. Conclusion

Thin films of methylammonium lead iodide perovskite prepared by co-evaporation of the two starting compounds, CH_3NH_3I and PbI_2, were integrated in different stacks to prepare thin film solar cells. We have demonstrated the importance of organic hole and electron blocking layers to increase the current density and open circuit voltage of the devices. When only an electron blocking layer was employed for a stack with a perovskite layer thickness of 330 nm the power conversion efficiency reached 4.7%. When in addition to the electron blocking layer a hole blocking layer was added the device performance increased significantly. The best results were obtained when a hole blocking material was used of which the LUMO matches the CB of the perovskite layer. This leads to a device with a power conversion efficiency of 12.9% for small area devices and 10.9% for devices with a cell area of 0.95 cm^2 .

4. Experimental Section

Materials: Photolithographically patterned ITO covered glass substrates were purchased from Naranjo-Substrates (www.naranjosubstrates.com). Aqueous dispersions of PEDOT:PSS (CLEVIOS PVP Al 4083) were obtained from Heraeus Holding GmbH and used as received. Poly-TPD was purchased from ADS Dyesource. PbI_2 was purchased from Aldrich and used as is, CH_3NH_3I was prepared similar to a previously published method,[24] in brief: CH_3NH_3I, was synthesized by reacting 21.6 mL methylamine (40 wt% in water, Aldrich) and 30 mL hydroiodic acid (57 wt% in water, Aldrich) in a 250 mL round-bottomed flask at 0 °C for 2 h with stirring. The white precipitate was recovered by evaporation at 50 °C for 1 h. The product, methylammonium iodide (CH_3NH_3I), was dissolved in ethanol, filtered and recrystallized from diethyl ether, and dried at 60 °C in a vacuum oven for 24 h.

Perovskite Evaporation Process and Perovskite Film Characterization: The sublimation of the perovskite was performed using an vacuum chamber of MBraun integrated in an inert glovebox (MBraun). Temperature controlled evaporation sources from Creaphys fitted with ceramic crucibles were employed to sublime the CH_3NH_3I and the PbI_2. The sources were directed upwards with an angle of approximately 90° with respect to the bottom of the evaporator. The substrates were placed at a distance of 20 cm from the top of the evaporation sources. A shutter was present below the substrate holder. Three quartz microbalance sensors were present in the chamber, two monitoring the rate of each evaporation source and a third one at the height of the substrate holder. After the ceramic crucibles were loaded with the CH_3NH_3I and the PbI_2 the chamber was evacuated to a base pressure of 1×10^{-6} mbar. Freshly synthesized CH_3NH_3I was used for each evaporation. After the base pressure was reached, the CH_3NH_3I crucible was heated to 70 °C. At this temperature, all three quartz sensors gave a signal. It was, however, impossible to calibrate the sensor by measuring the thickness of a deposited CH_3NH_3I film. Therefore, an alternative process was used. Upon stabilization of the sensor reading the crucible containing the PbI_2 was heated. Only at PbI_2 evaporation temperatures in excess of 200 °C dark brown films were obtained. The film thickness of the perovskite film was monitored using a quartz sensor at the height of the substrate holder. Perovskite films were prepared at different PbI_2 evaporation temperatures, changing temperature every 5 °C until optimum films were obtained at an evaporation temperature of the PbI_2 crucible of 250 °C.

Characterization GIXRD data were collected at room temperature in the 2θ range 5–50° on an Empyrean PANalytical powder diffractometer, using Cu Kα1 radiation. Typically four repeated measurements were collected and merged into a single diffractogram. Pawley refinements, were performed using the TOPAS computer program[25] and revealed an excellent fit to a one-phase model with a tetragonal cell (a = 8.80(2) Å, c = 12.57(2) Å) and space group I4/mcm. Additional peaks corresponding to the ITO substrate were also observed. The observed and calculated diffraction patterns for the refined crystal structures are shown in Supporting Information Figure S3. Simulation of the crystal structure of $CH_3NH_3PbI_3$ perovskite was performed using as starting model the isostructural Sn analogue (CCDC refcode: ZZZBWS02) modifying the cell parameters to those obtained in the Pawley refinement. Absorption spectra were taken using a fiber optics based Avantes Avaspec2048 Spectrometer.

Device Preparation and Characterization: Devices were prepared on cleaned ITO substrates, by spincoating a thin layer of PEDOT:PSS from the commercial aqueous dispersion (1200 rpm, 30 s result in 70 nm thickness). On top of this layer a thin film of polyTPD was deposited from a chlorobenzene solution (10 mg mL^{-1}) using a meniscus coater[22] and a coating speed of 2.5 mm s^{-1}. Then the substrates were transferred to a vacuum chamber integrated into a nitrogen-filled glovebox (MBraun, <0.1 ppm O_2 and <0.1 ppm H_2O) and evacuated to a pressure of 1×10^{-6} mbar. Two ceramic crucibles were filled with CH_3NH_3I (freshly prepared) and PbI_2 which were heated to 70 °C and 250 °C, respectively. The film thickness was controlled by the PbI_2 evaporation at a rate of evaporation of 0.5 Å s^{-1}. The $PCBM_{60}$ layer was deposited using a chlorobenzene solution of 10 mg mL^{-1} in ambient conditions using a meniscus coater and a coating speed of 10 mm/second. The device was completed by the thermal evaporation of the top metal electrode under a base pressure of 2×10^{-6} mbar to a thickness of 100 nm. The solar cells (active area from 0.09 to 0.98 cm^2) were then encapsulated with a glass cover using a UV curable epoxy sealant (Ossila E131 Encapsulation Epoxy), UV exposure 5 min.

Characterization of the solar cells was performed using two methods. For the majority of results presented here the devices were illuminated by a white light halogen lamp in combination with interference filters for the EQE and *J–V* measurements (MiniSun simulator by ECN the

Netherlands). An estimation of the J_{sc} under standard test conditions was calculated by convolving the EQE spectrum with the AM1.5G reference spectrum, using the premise of a linear dependence of J_{sc} on light intensity (Supporting Information Figure S5). *J–V* characteristics were measured using a Keithley 2400 source measure unit. The scan was performed with steps of 0.01 V starting from −0.2 V up to 1.1 V. The time delay between each point was set to 0.01 s. No hysteresis of the *J–V* scans was observed (Supporting Information Figure S6). All characterization was done in a nitrogen filled glove box (<0.1 ppm O_2 and <0.1 ppm H_2O) without exposure to ambient atmosphere. Only the best performing samples were encapsulated with a glass cover using a UV curable epoxy sealant (Ossila E131 Encapsulation Epoxy), UV exposure 5 min and shipped to the Laboratory of Photonics and Interfaces of the Swiss Federal Institute of Technology (EPFL) in Lausanne Switzerland for characterization. There the *J–V* characteristics of these encapsulated devices were recorded by applying an external potential bias to the cell while recording the generated photocurrent with a digital source meter (Keithley Model 2400). The light source was a 450 W xenon lamp (Oriel) equipped with a Schott K113 Tempax sunlight filter (Praezisions Glas & Optik GmbH) to match the emission spectrum of the lamp to the AM1.5G standard. A black mask was used in the photovoltaic studies to limit the active area of the device. Before each measurement, the exact light intensity was determined using a calibrated Si reference diode equipped with an infrared cut-off filter (KG-3, Schott).

Supporting Information

Supporting Information is available from the Wiley Online Library or from the author.

Acknowledgements

O.M. and C.R.-C. contributed equally to this work. The authors are grateful to Jorge Ferrando for technical assistance and Aswani Yella and Yonghui Lee for solar cell characterization. This work has been supported by the Spanish Ministry of Economy and Competitiveness (MINECO) (MAT2011–24594), the Generalitat Valenciana (Prometeo/2012/053). C.R. and L.C. would like to thank the MINECO for the financial support of this research in the framework of project CTQ2010–17481, the Junta de Andalucía (CICyE) for special financial support (P08-FQM-4011 and P10-FQM-6703). C.R. and E.B. thank the MECD (Spanish Ministry of Education, Culture, and Sport) and MINECO for an FPU and FPI grant, respectively.

Received: February 25, 2014
Revised: May 1, 2014
Published online:

[1] S. B. Darling, F. You, *RSC Adv.* **2013**, *3*, 17633.
[2] H. J. Snaith, *J. Phys. Chem. Lett.* **2013**, *4*, 3623.
[3] a) C. R. Kagan, D. B. Mitzi, C. D. Dimitrakopoulos, *Science* **1999**, *286*, 945; b) D. B. Mitzi, *J. Mater. Chem.* **2004**, *14*, 2355.
[4] A. Kojima, K. Teshima, Y. Shirai, T. Miyasaka, *J. Am. Chem. Soc.* **2009**, *131*, 6050.
[5] a) J.-H. Im, C.-R. Lee, J.-W. Lee, S.-W. Park, N.-G. Park, *Nanoscale* **2011**, *3*, 4088; b) M. M. Lee, J. Teuscher, T. Miyasaka, T. N. Murakami, H. J. Snaith, *Science* **2012**, *338*, 643; c) J. M. Ball, M. M. Lee, A. Hey, H. J. Snaith, *Energy Environ. Sci.* **2013**, *6*, 1739; d) J. Burschka, N. Pellet, S.-J. Moon, R. Humphry-Baker, P. Gao, M. K. Nazeeruddin, M. Gratzel, *Nature* **2013**, *499*, 316; e) M. Liu, M. B. Johnston, H. J. Snaith, *Nature* **2013**, *501*, 395; f) O. Malinkiewicz, A. Yella, Y. H. Lee, G. M. Espallargas, M. Graetzel, M. K. Nazeeruddin, H. J. Bolink, *Nat. Photonics* **2014**, *8*, 128; g) D. Liu, T. L. Kelly, *Nat. Photonics* **2014**, *8*, 133.
[6] W. A. Laban, L. Etgar, *Energy Environ. Sci.* **2013**, *6*, 3249.
[7] a) P. Docampo, J. M. Ball, M. Darwich, G. E. Eperon, H. J. Snaith, *Nat. Commun.* **2013**, *4*, 2761; b) C. Roldán-Carmona, O. Malinkiewicz, A. Soriano, G. Mínguez Espallargas, A. Garcia, P. Reinecke, T. Kroyer, M. I. Dar, M. K. Nazeeruddin, H. J. Bolink, *Energy Environ. Sci.* **2014**, *7*, 994; c) J. You, Z. Hong, Y. Yang, Q. Chen, M. Cai, T.-B. Song, C.-C. Chen, S. Lu, Y. Liu, H. Zhou, *ACS Nano* **2014**, *8*, 1674.
[8] a) G. Xing, N. Mathews, S. Sun, S. S. Lim, Y. M. Lam, M. Grätzel, S. Mhaisalkar, T. C. Sum, *Science* **2013**, *342*, 344; b) S. D. Stranks, G. E. Eperon, G. Grancini, C. Menelaou, M. J. P. Alcocer, T. Leijtens, L. M. Herz, A. Petrozza, H. J. Snaith, *Science* **2013**, *342*, 341.
[9] C. Wehrenfennig, G. E. Eperon, M. B. Johnston, H. J. Snaith, L. M. Herz, *Adv. Mater.* **2013**, *26*, 1584.
[10] E. Edri, S. Kirmayer, S. Mukhopadhyay, K. Gartsman, G. Hodes, D. Cahen, *Nat. Commun.* **2014**, *5*, 3461.
[11] G. L. Mauthner, K. Landfester, A. Kock, H. Bruckl, M. Kast, C. Stepper, E. J. W. List, *Org. Electron.* **2008**, *9*, 164.
[12] a) M. Era, T. Hattori, T. Taira, T. Tsutsui, *Chem. Mater.* **1997**, *9*, 8; b) D. B. Mitzi, *Chem. Mater.* **2001**, *13*, 3283.
[13] Conductive polymers, http://www.heraeus-clevios.com, (accessed June 2014).
[14] C. C. Stoumpos, C. D. Malliakas, M. G. Kanatzidis, *Inorg. Chem.* **2013**, *52*, 9019.
[15] J.-Y. Jeng, Y.-F. Chiang, M.-H. Lee, S.-R. Peng, T.-F. Guo, P. Chen, T.-C. Wen, *Adv. Mater.* **2013**, *25*, 3727.
[16] P. Schulz, E. Edri, S. Kirmayer, G. Hodes, D. Cahen, A. Kahn, *Energy Environ. Sci.* **2014**, *7*, 1377.
[17] Q. Sun, Y. A. Wang, L. S. Li, D. Wang, T. Zhu, J. Xu, C. Yang, Y. Li, *Nat. Photonics* **2007**, *1*, 717.
[18] S. Sun, T. Salim, N. Mathews, M. Duchamp, C. Boothroyd, G. Xing, T. C. Sum, Y.-M. Lam, *Energy Environ. Sci.* **2014**, *7*, 399.
[19] a) H.-S. Kim, C.-R. Lee, J.-H. Im, K.-B. Lee, T. Moehl, A. Marchioro, S.-J. Moon, R. Humphry-Baker, J.-H. Yum, J. E. Moser, M. Gratzel, N.-G. Park, *Sci. Rep.* **2012**, *2*, 591; b) J. H. Heo, S. H. Im, J. H. Noh, T. N. Mandal, C.-S. Lim, J. A. Chang, Y. H. Lee, H.-j. Kim, A. Sarkar, K. NazeeruddinMd, M. Gratzel, S. I. Seok, *Nat. Photonics* **2013**, *7*, 486.
[20] a) A. R. Kandada, G. Grancini, A. Petrozza, S. Perissinotto, D. Fazzi, S. S. Raavi, G. Lanzani, *Sci. Rep.* **2013**, *3*, 2073; b) C.-W. Chu, V. Shrotriya, G. Li, Y. Yang, *Appl. Phys. Lett.* **2006**, *88*, 153504; c) S. Sun, T. Salim, N. Mathews, M. Duchamp, C. Boothroyd, G. Xing, T. C. Sum, Y. M. Lam, *Energy Environ. Sci.* **2014**, *7*, 399.
[21] K. Goushi, K. Yoshida, K. Sato, C. Adachi, *Nat. Photonics* **2012**, *6*, 253.
[22] O. Malinkiewicz, M. Lenes, H. Brine, H. J. Bolink, *RSC Adv.* **2012**, *2*, 3335.
[23] E. Edri, S. Kirmayer, A. Henning, S. Mukhopadhyay, K. Gartsman, Y. Rosenwaks, G. Hodes, D. Cahen, *Nano Lett.* **2014**, *14*, 1000.
[24] L. Etgar, P. Gao, Z. Xue, Q. Peng, A. K. Chandiran, B. Liu, M. K. Nazeeruddin, M. Grätzel, *J. Am. Chem. Soc.* **2012**, *134*, 17396.
[25] V. TOPAS-Academic, http://www.topas-academic.net, Coelho Software, Brisbane, 2007.

GENERAL CONCLUSIONS

GENERAL CONCLUSIONS:

The first objective of the Thesis was to develop a lab-scale coating technique, for neat bilayer preparation from solution. Meniscus coating was successfully implemented in various neat bi-layer solar cells with fullerene acceptor and cyanine dye donor.

The second objective of the thesis, was to study the influence of the ions on the cyanine solar cell performance. It was demonstrated, that the mobile ions have large impact on the energetics of the solar cells.

The third objective of the Thesis was the development of an strategy for perovskite film preparation, which not only provides precise control of film thicknesses but also exhibits a good compatibility with dry processing. Co-evaporation process of $CH_3NH_3PbI_3$ perovskite was developed and optimized resulting in excellent quality, compact and pinhole free perovskite layers.

The final objective of this Thesis was the development of an oxide free perovskite device architecture, that shows no hysteresis and is compatible with flexible substrates. Evaporated perovskite layers were sandwiched in between two thin organic charge transport layers polyarylamine (polyTPD, p-type material) and [6,6]-Phenyl C_{61}-butyric acid methylester (PCBM, n-type material)[42] . This novel, oxide-free device architecture exhibit efficiencies as high as standard devices based on TiO_2 scaffold layer. Because device fabrication doesn't require high temperature sintering processes, it is fully compatible with flexible substrates. Excellent quality of perovskite films and lack of oxide layer lead to the absence of hysteresis effect. The work resulted in filling one patent application (patent application nr EP13183813), a number of publications and conference contributions.

OUTLOOK

OUTLOOK:

In a view of the low efficiencies obtained for cyanine dye based solar cells (comparing to for exp. perovskite cells) one can predict that it is very unlikely that they will ever play significant role in energy sector. Nevertheless the results from the study of those cells like for exp. ionic movements inside the device or the possible origins of the s-shape, can be directly transferred into perovskite filed. In general such a quick rise of the efficiencies of the perovskite solar cells wouldn't be possible without previous studies on organic and DSSC cells. Everthing that was developed by over a decade for the organic and DSSCs, significantly speed up the process of the evolution of the perovskite cells. Is not a coincidence that on NREL chart perovskite line appears to be almost a continuation of the organic and DSSCs line. Synthesis and study of different charge transport materials, as well as development and description of charge transport mechanism for organic and DSSC cells, all of this was adopted by perovskite field resulting in exciding 20% efficiency in a record time of only few years. This example clearly shows that there is still a niche (and a need) for a studying a new materials like cyanine dyes and their performance in organic solar cells. The knowledge gained on this simple systems can be later used for a better understanding of more complex systems like for exp. perovskite cells.

While promising to bring about the revolution in PV, the perovskite based solar technology is hindered by two essential limitations that need to be addressed, requiring considerable research effort, before perovskites can be deployed on the market: stability and lead content. The most commonly use methylamonium lead iodide perovskite with chemical formula $CH_3NH_3PbI_3$ has tendency to decompose into lead iodide and methylamonium iodide loosing optoelectronic properties mainly under humidity exposure. Additionally such degradation is accelerated by light illumination, oxygen presence and thermal treatment[65]. The issues of the degradation of perovskite and the stability of perovskite solar cells should be urgently addressed to achieve good reproducibility and long lifetimes with high conversion efficiency in order to transfer them

from the laboratory to industry and outdoor applications[66]. The promising strategy to overcome this problem is chemical composition manufacturing. Recently, mixed-cation formulations employing formamidinium (FA) and cesium (Cs) showed promising improvement in this field. Formamidinium cation due to its bigger size compare with methylamonium and cesium being inorganic element combined together significantly improved photo and moisture stability of perovskite films.[67] Solar cells employing the composition $Cs_{0.05}$ $(MA_{0.17}$ $FA_{0.83})_{0.95}Pb(I_{0.83}Br_{0.17})_3$ reached a stabilized power output of 21.1% with excellent long term stability under operational conditions during 250 hours [68]. On the other hand, perovskite stability can be provided by encapsulation. Introducing of additional layer with barrier properties (e.g. Al_2O_3) can effectively protect water-sensitive perovskite film lengthen device lifetime.

Regarding the low-cost technology it is questionable, if the long life time is necessary. After usage the cheap device can be easily replace by the new one. In this sense, there is only one limitation coming from environmental friendliness.

The methylammonium lead trihalide perovskite contains a significant weight fraction of lead, corresponding to around 0.35 g/m^2 for perovskite film thickness of 300nm. Although proper sealing and a return (recycling) after the end-of-the lifetime of the actual solar modules are foreseeable. It was proved that the lead from degraded devices can be recovered and used in a production of new perovskite based devices [69]. Another solution to overcome this problem is replacement of Pb which is by far preferred – in fact its use is problematic under current EU legislation and might be a bottleneck towards future commercialisation and public acceptance. Some trials has been already made towards lead free devices. First probe of lead replacement in hybrid perovskite light harvesting material was related to Tin (Sn). The devices based on methylamonium tin iodide reached the efficiencies of around 5,73%. However, tin perovskite is highly unstable due to the Sn^{2+} tendency to oxidize to Sn^{4+} [70]. Another disadvantage of this

approach is the fact that, in contrary to appearances tin-organic compounds are not inert for human health represents similar toxic level.

While everyone is focused on lead content there is another equally important thing. Large-area production of perovskite materials will require solution-based technology in order to be commercially viable. Current solution processing employs solvents that are not environmentally friendly and potentially hazardous for health like DMF (Dimethyloformamide) or toxic like chlorine-based ones. For large-scale production, their use is simply excluded.

LIST OF PUBLICATIONS

LIST OF PUBLICATIONS:

2014:

- **Radiative efficiency of lead iodide based perovskite solar cells**
  Kristofer Tvingstedt, **Olga Malinkiewicz**, Andreas Baumann, Carsten Deibel, Henry J. Snaith, Vladimir Dyakonov and Hendrik J. Bolink, Sci. Rep., 2014, 4, Article number: 6071 doi: 10.1038/srep06071

- **Thickness independent and efficient methylammonium lead iodide perovskite solar cells**
  Cristina Momblona, **Olga Malinkiewicz**, Cristina Roldán-Carmona, Alejandra Soriano, Lidon Gil-Escrig, Eran Edri and Hendrik J. Bolink, APL Mat., 2014, 2, 081504, DOI: http://dx.doi.org/10.1063/1.4890056

- **High efficiency single-junction semitransparent perovskite solar cells**
  Cristina Roldán-Carmona, **Olga Malinkiewicz**, Rafael Betancur, Giulia Longo, Cristina Momblona, Franklin Jaramillo, Luis Camacho and Hendrik J. Bolink, Energy Environ. Sci., 2014,7, 2968-2973, DOI: 10.1039/C4EE01389A

- **Effect of organic charge transport layers on the performance of perovskite based solar cells**
  Olga Malinkiewicz, Cristina Roldán-Carmona , Alejandra Soriano, Enrico Bandiello, Mohammad Khaja Nazeeruddin and Hendrik J. Bolink , Adv. Energy Mater., 4, 15, 1614-6840, DOI:10.1002/aenm.201400345

- **Flexible high efficiency perovskite solar cells**
  Cristina Roldán-Carmona, **Olga Malinkiewicz**, Alejandra Soriano, Guillermo Mínguez Espallargas, Ana Garcia, Patrick Reinecke, Thomas Kroyer, M. Ibrahim Dar, Mohammad Khaja Nazeeruddin and Hendrik J. Bolink, Energy Environ. Sci., 2014, 7, 994-997, DOI:10.1039/C3EE43619E

- **Nontemplate Synthesis of CH3NH3PbBr3 Perovskite Nanoparticles**
  Luciana C. Schmidt, Antonio Pertegás, Soranyel González-Carrero, **Olga Malinkiewicz**, Said Agouram, Guillermo Mínguez Espallargas, Hendrik J. Bolink, Raquel E. Galian, and Julia Pérez-Prieto, J. Am. Chem. Soc., 2014, 136 (3), 850–853, DOI: 10.1021/ja4109209

2013:

- **Perovskite solar cells employing organic charge-transport layers**
  Olga Malinkiewicz, Aswani Yella, Yong Hui Lee, Guillermo Mínguez Espallargas, Michael Graetzel, Mohammad K. Nazeeruddin and Hendrik J. Bolink, Nature Photon, 2013, 8, 128-132 , DOI:10.1038/nphoton.2013.341

- **Influence of the cyanine counter anions on a bi-layer solar cell performance**
  Olga Malinkiewicz, Thais Grancha, Martijn Lenes, Hicham Brine, Alejandra Soriano and Hendrik J. Bolink, MRS Proceedings, 1493, pp 275-280. DOI:10.1557/opl.2013.147

- **Solution-processed bi-layer polythiophene–fullerene organic solar cells**
  Toon Ghoos, **Olga Malinkiewicz,** Bert Conings, Laurence Lutsen, Dirk J. Vanderzande, Hendrik J. Bolink and Wouter Maes, RSC Adv., 2013, 3, 25197-25203, DOI:10.1039/C3RA43986K

- **Efficient, Cyanine Dye Based Bilayer Solar Cells**
  Olga Malinkiewicz, Thais Grancha, Agustin Molina-Ontoria, Alejandra Soriano, Hicham Brine and Hendrik J. Bolink, Adv. Energy Mater., 2013, 3, 472 , DOI: 10.1002/aenm.201200764

2012:

- **Meniscus coated high open-circuit voltage bi-layer solar cells**
  Olga Malinkiewicz, Martijn Lenes, Hicham Brine and H. J. Bolink, RSC Adv., 2012,2, 3335-3339,DOI:10.1039/C2RA20075A

Patent application:

" Inverted solar cell and process for producing the same " EP 2846371 A1 , Inventors: K M. K. Nazeeruddin, M. Graetzel, H. J. Bolink, **O. Malinkiewicz**, A. Soriano,

REFERENCES

REFERENCES

(1) Global Market Outlook For Photovoltaics 2014-2018.

(2) Sawin, J. L.; Seyboth, K.; Sverrisson, F.; Appavou, F.; Brown, A.; Epp, B.; Leidreiter, A.; Lins, C.; Murdock, H. E.; Musolino, E.; Petrichenko, K.; Farrell, T. C.; Krader, T. T.; Tsakiris, A.; Skeen, J.; Sovacool, B.; Sverrisson, F. *Renewables 2016. Global Status Report*; 2016.

(3) http://www.nrel.gov/ncpv/ ; Accesed on 28.07.2016.

(4) Søndergaard, R.; Hösel, M.; Angmo, D.; Larsen-Olsen, T. T.; Krebs, F. C. *Materials Today*. 2012, pp 36–49.

(5) McGehee, M. D.; Goh, C. In *AIP Conference Proceedings*; 2008; Vol. 1044, pp 322–330.

(6) E. Głowacki, N. S. Sariciftci, C. W. T. *Encyclopedia of Sustainability Science and Technology*; 2012; pp 7553–7584.

(7) Kearns, D.; Calvin, M. *J. Chem. Phys.* **1958**, *29* (4), 950.

(8) Morel, D. L.; Morel, D. L.; Stogryn, E. L.; Stogryn, E. L.; Ghosh, a K.; Ghosh, a K.; Feng, T.; Feng, T.; Purwin, P. E.; Purwin, P. E.; Shaw, R. F.; Shaw, R. F.; Fishman, C.; Fishman, C.; Bird, G. R.; Bird, G. R.; Piechowski, a P.; Piechowski, a P. *J. Phys. Chem.* **1984**, *88* (5), 923.

(9) Tang, C. W. *J. Chem. Phys.* **1975**, *62* (6), 2139.

(10) Corker, G. A.; Lundström, I. *J. Appl. Phys.* **1978**, *49* (2), 686.

(11) Tang, C. W. *Appl. Phys. Lett.* **1986**, *48* (2), 183.

(12) Wudl, N. S. S. L. S. A. J. H. F. *Science (80-.).* **2013**, *258*, 1474.

(13) Fan, B.; de Castro, F. A.; Heier, J.; Hany, R.; Nüesch, F. *Org. Electron. physics, Mater. Appl.* **2010**, *11*, 583.

(14) http://en.wikipedia.org/wiki/Cyanine.

(15) Fan, B.; Araujo de Castro, F.; Chu, B. T.-T.; Heier, J.; Opris, D.; Hany, R.; Nüesch, F. *Journal of Materials Chemistry*. 2010, p 2952.

(16) Pertegás, A.; Tordera, D.; Serrano-Pérez, J. J.; Ortí, E.; Bolink, H. J. *J. Am. Chem. Soc.* **2013**, *135*, 18008.

(17) http://de.lumiprobe.com/tech/cyanine-dyes.

(18) Bässler, H.; Köhler, A. *Top. Curr. Chem.* **2012**, *312*, 1.

(19) Nüesch, F.; Faes, A.; Zuppiroli, L.; Meng, F.; Chen, K.; Tian, H. In *Journal of Materials Science*; 2005; Vol. 40, pp 1353–1357.

(20) Benmansour, H.; Castro, F. A.; Nagel, M.; Heier, J.; Hany, R.; Nüesch, F. *CHIMIA International Journal for Chemistry*. 2007, pp 787–791.

(21) Nüesch, F.; Tornare, G.; Zuppiroli, L.; Meng, F.; Chen, K.; Tian, H. In *Solar Energy Materials and Solar Cells*; 2005; Vol. 87, pp 817–824.

(22) Lenes, M.; Bolink, H. J. *ACS Appl. Mater. Interfaces* **2010**, *2* (12), 3664.

(23) Tang, C. W. *Appl. Phys. Lett.* **1986**, *48* (2), 183.

(24) Krebs, F. C. *Solar Energy Materials and Solar Cells*. 2009, pp 394–412.

(25) Coropceanu, V.; Cornil, J.; Silva, D.; A, D.; Olivier, Y.; Silbey, R.; Bredas, J. L.; da Silva Filho, D. A.; Brédas, J.-L. J.-L.; Olivier, Y.; Silbey, R.; Brédas, J.-L. J.-L. *Chem. Rev.* **2007**, *107* (4), 926.

(26) Mitzi, D. B. *Journal of Materials Chemistry*. 2004, p 2355.

(27) Kojima, A.; Teshima, K.; Shirai, Y.; Miyasaka, T. *J. Am. Chem. Soc.* **2009**, *131*, 6050.

(28) Chung, I.; Lee, B.; He, J.; Chang, R. P. H.; Kanatzidis, M. G. *Nature*. 2012, pp 486–489.

(29) Lee, M. M.; Teuscher, J.; Miyasaka, T.; Murakami, T. N.; Snaith, H. J. *Science*. 2012, pp 643–647.

(30) Mitzi, D. B.; Chondroudis, K.; Kagan, C. R. *IBM Journal of Research and*

Development. 2001, pp 29–45.

(31) Mitzi, D. B. In *Progress in Inorganic Chemistry*; 1999; pp 1–121.

(32) Saliba, M.; Matsui, T.; Seo, J.-Y.; Domanski, K.; Correa-Baena, J.-P.; Mohammad K., N.; Zakeeruddin, S. M.; Tress, W.; Abate, A.; Hagfeldt, A.; Gratzel, M. *Energy Environ. Sci.* **2016**.

(33) Wei, Y. Synthesis and optical properties of self-assembled 2D layered organic-inorganic perovskites for optoelectronics- PhD Thesis, Ecole normale superieure de Cachan - ENS Cachan, 2012.

(34) Wan-Jian Yin; Shi, T.; Yan, Y. *Adv. Mater.* **2014**, *26* (27), 4653.

(35) Eperon, G. E.; Burlakov, V. M.; Docampo, P.; Goriely, A.; Snaith, H. J. *Adv. Funct. Mater.* **2014**, *24* (1), 151.

(36) Gao, P.; Nazeeruddin, M. K. *Energy Environ. Sci.* **2014**, *1* (c), 2448.

(37) Fan, R.; Huang, Y.; Wang, L.; Li, L.; Zheng, G.; Zhou, H. *Adv. Energy Mater.* **2016**, 1.

(38) Hodes, G.; Cahen, D. *Nat. Photonics* **2014**, *8* (2), 87.

(39) Nickel, F.; Sprau, C.; Klein, M. F. G.; Kapetana, P.; Christ, N.; Liu, X.; Klinkhammer, S.; Lemmer, U.; Colsmann, A. *Sol. Energy Mater. Sol. Cells* **2012**, *104*, 18.

(40) Park, B.; Han, M. *Opt. Express* **2009**, *17* (24), 21362.

(41) Parodi, M.; Batchelder, T.; Haaland, P.; and McKibben, J. *Semicond. Int.* **1996**, 101.

(42) Malinkiewicz, O.; Yella, A.; Lee, Y. H.; Espallargas, G. M. M.; Graetzel, M.; Nazeeruddin, M. K.; Bolink, H. J. *Nat. Photonics* **2014**, *8* (2), 128.

(43) Van Slyke, S. a.; Chen, C. H.; Tang, C. W. *Appl. Phys. Lett.* **1996**, *69* (15), 2160.

(44) Era, Masanao; Hattori Toshihiko; Taira, Takahiro; Tsutsui, T. *Chem. Mater.* **1997**, *9*, 8.

(45) Liu, M.; Johnston, M. B.; Snaith, H. J. *Nature* **2013**, *501* (7467), 395.

(46) Malinkiewicz, O.; Roldán-Carmona, C.; Soriano, A.; Bandiello, E.; Camacho, L.; Nazeeruddin, M. K.; Bolink, H. J. *Advanced Energy Materials*. 2014,.

(47) Roldan, C.; Malinkiewicz, O.; Betancur, R.; Longo, G.; Momblona, C.; Jaramillo, F.; Camacho, L.; Bolink, H. J. *Energy Environ. Sci.* **2014**, 2968.

(48) Roldán-Carmona, C.; Malinkiewicz, O.; Soriano, A.; Mínguez Espallargas, G.; Garcia, A.; Reinecke, P.; Kroyer, T.; Dar, M. I.; Nazeeruddin, M. K.; Bolink, H. J. *Energy Environ. Sci.* **2014**, *7* (3), 994.

(49) Beiley, Z. M.; McGehee, M. D. *Energy Environ. Sci.* **2012**, *5* (11), 9173.

(50) Löper, P.; Moon, S.-J.; Martín de Nicolas, S.; Niesen, B.; Ledinsky, M.; Nicolay, S.; Bailat, J.; Yum, J.-H.; De Wolf, S.; Ballif, C. *Phys. Chem. Chem. Phys.* **2015**, *17* (3), 1619.

(51) Bailie, C. D.; Christoforo, M. G.; Mailoa, J. P.; Bowring, A. R.; Unger, E. L.; Nguyen, W. H.; Burschka, J.; Pellet, N.; Lee, J. Z.; Grätzel, M.; Noufi, R.; Buonassisi, T.; Salleo, A.; McGehee, M. D. *Energy Environ. Sci.* **2015**, *8*, 956.

(52) Malinkiewicz, O.; Lenes, M.; Brine, H.; Bolink, H. J. *RSC Advances*. 2012, p 3335.

(53) Ghoos, T.; Malinkiewicz, O.; Conings, B.; Lutsen, L.; Vanderzande, D. J.; Bolink, H. J.; Maes, W. *RSC Adv.* **2013**, *3* (47), 25197.

(54) Malinkiewicz, O.; Grancha, T.; Molina-Ontoria, A.; Soriano, A.; Brine, H.; Bolink, H. J. *Adv. Energy Mater.* **2013**, *3* (4), 472.

(55) O. Malinkiewicz, T. Grancha, M. Lenes, H. Brine, A. Soriano, H. J. Bolink. *MRS Proceedings,*. **2013**, *1493*, 275.

(56) Momblona, C.; Malinkiewicz, O.; Roldán-Carmona, C.; Soriano, A.; Gil-Escrig, L.; Bandiello, E.; Scheepers, M.; Edri, E.; Bolink, H. J. *APL Mater.* **2014**, *2* (8).

(57) Yin, W. J.; Shi, T.; Yan, Y. *Adv. Mater.* **2014**, *26* (27), 4653.

(58) Chen, B.-X.; Rao, H.-S.; Li, W.-G.; Xu, Y.-F.; Chen, H.-Y.; Kuang, D.-B.; Su, C.-Y. *J. Mater. Chem. A* **2016**, *4* (15), 5647.

(59) Nie, W.; Tsai, H.; Asadpour, R.; Blancon, J.-C.; Neukirch, A. J.; Gupta, G.; Crochet, J.

J.; Chhowalla, M.; Tretiak, S.; Alam, M. A.; Wang, H.-L.; Mohite, A. D. *Science* **2015**, *347* (6221), 522.

(60) Laban, W. A.; Etgar, L. *Energy Environ. Sci.* **2013**, *6* (11), 3249.

(61) Malinkiewicz, O.; Roldán-Carmona, C.; Soriano, A.; Bandiello, E.; Camacho, L.; Nazeeruddin, M. K.; Bolink, H. J. *Adv. Energy Mater.* **2014**, *4* (15), 1614.

(62) Shao, Y.; Xiao, Z.; Bi, C.; Yuan, Y.; Huang, J. *Nat. Commun.* **2014**, *5*, 1.

(63) Momblona, C.; Malinkiewicz, O.; Roldán-Carmona, C.; Soriano, A.; Gil-Escrig, L.; Bandiello, E.; Scheepers, M.; Edri, E.; Bolink, H. J. *APL Mater.* **2014**, *2* (8), 0.

(64) Tvingstedt, K.; Malinkiewicz, O.; Baumann, A.; Deibel, C.; Snaith, H. J.; Dyakonov, V.; Bolink, H. J. *Nat. Sci. Reports* **2014**, *4*, 1.

(65) McMeekin, D. P.; Sadoughi, G.; Rehman, W.; Eperon, G. E.; Saliba, M.; Hörantner, M. T.; Haghighirad, A.; Sakai, N.; Korte, L.; Rech, B.; Johnston, M. B.; Herz, L. M.; Snaith, H. J. *Sci.* **2016**, *351* (6269), 151.

(66) Guangda Niu, a X. G. and L. W. *J. Mater. Chem. A* **2014**, *3*.

(67) Lee, J.-W.; Kim, D.-H.; Kim, H.-S.; Seo, S.-W.; Cho, S. M.; Park, N.-G. *Adv. Energy Mater.* **2015**, n/a.

(68) Saliba, M.; Nazeeruddin, K.; Zakeeruddin, S. M. *Energy Environ. Sci.* **2016**.

(69) Binek, A.; Petrus, M. L.; Huber, N.; Bristow, H.; Hu, Y.; Bein, T.; Docampo, P. **2016**, 6.

(70) Hao, F.; Stoumpos, C. C.; Cao, D. H.; Chang, R. P. H.; Kanatzidis, M. G. *Nat. Photonics* **2014**, *8* (6), 489.

(71) Momblona, C.; Malinkiewicz, O.; Roldán-Carmona, C.; Soriano, A.; Gil-Escrig, L.; Bandiello, E.; Scheepers, M.; Edri, E.; Bolink, H. J. *APL Mater.* **2014**, *2* (8), 081504.

ACKNOWLEDGEMENTS

ACKNOWLEDGEMENTS

I would like to thank to my supervisor, Dr. Henk Bolink, for giving me the opprotunity to work in his group where I have learn how to "do" and how to "apply" science. I would like to thank him for his kind support in any matter during all my Thesis. Working in his group was a privilege for me and one of the greatest experience in my whole academic career. I would like to thank also to my family, especially to my mother, for helping me with organizing my life when I was absorbed by work.